MICRO-EDM PROCESS FOR TOOL-BASED COMPOUND MICROMACHINING

ABU BAKAR MD ALI ASAD

NATIONAL UNIVERSITY OF SINGAPORE

2012

MICRO-EDM PROCESS FOR TOOL-BASED COMPOUND MICROMACHINING

ABU BAKAR MD ALI ASAD

(B.Eng. Mechanical Engineering, NUS)

A THESIS SUBMITTED

FOR THE DEGREE OF DOCTOR OF PHILOSOPHY

DEPARTMENT OF MECHANICAL ENGINEERING

NATIONAL UNIVERSITY OF SINGAPORE

2012

Acknowledgements

First of all, I express my heartiest gratitude and humbleness to the almighty ALLAH (S.W.T.) who is the most merciful and the most gracious for He blessed me with the opportunity, strength and the ability to complete my doctoral studies and subsequently write this thesis.

I would like to express my deepest appreciation and respect to my supervisors Prof Mustafizur Rahman and Prof Wong Yoke San for their exceptional guidance, continuous support and encouragement throughout the course of my graduate study. Without their valuable recommendations, ideas, advice, guidance and support the successful completion of this research work is unthinkable. A life is probably too short to learn properly the respect that they deserve for they have guarded me as a teacher, as a father and as a friend.

I received special guidance, support, generous sharing and encouragement from Dr. Takeshi Masaki of MASAKI GIKEN. I am blessed to have worked with a person like him with a very elegant way of thinking and problem solving skill; and a teacher to be called as a friend. I also want to thank Dr. Lim Han Seok (former faculty member of NUS) for his supervision. I want to extend my appreciation to the staff in the Advanced Manufacturing Laboratory and Microfabrication Lab, especially Mr Lim Soon Cheong, Mr Silva Kumar, Mr Tan Choon Huat, Mr Wong Chian Loong, Mr Yeo Nelson and others for their support during the experimentation and other lab matters.

I also take the pleasure to express my cordial appreciation for the support and the encouragement to all my lab mates and friends. In this regard, I would like to say special thanks to Arif, Ahsan, Tanveer, Minh Dang, Atiqur Rahman, Tarik Arafat, Sadiq, Sazid, Asma Perveen, Pervej, Muntakim, Masheed, Xu Wei, Zay Yar Thun, Choon Chye, Annaporani and Maria Low. I am indebted to my friend, Dr. Rabiul Alam (a senior PhD student of Prof Mustafizur Rahman), for his encouragement and motivation. I am also thankful to admin staff especially Ms Sharen, Ms Siew Fah and Ms Salmiah in Mechanical Engineering department for the support in the administration work throughout my studies.

I need to mention here the support, prayers and encouragement of my father, mother, sister, brother and my grandfather. The habit of exploration and way of learning new things taught by my father and grandfather will always serve me as the guiding light for my life. During the course of my doctoral degree the amount of support I received from my wife is not explainable in any words. I need to thank her for being so considerate during my tough days, for providing me the exact right mental support and covering me from most of my parental responsibilities. She molded this long and difficult journey of arriving at the other end into a joyous celebration; a rhythm of life to ride the ups and downs; even on the toughest days with positive consolation and remaining the happiest in life with the simplest things. Finally, I dedicate this thesis to my loving daughter, Yusra Tasnim Habiba, for still being happy with me even when every time I failed to keep my promise of taking her to the playground and ended up returning home late at night when it was her time to go to bed.

Table of Contents

Summary

At present components for MEMS and bio-MEMS are usually produced using semiconductor processing technologies, like photolithography on silicon substrate. In addition to their incompatible material properties for extreme applications like microsurgery, biotechnology, fluidics or high-temperature environments, these processes require special and extremely expensive facilities. Tool-based micromachining technologies such as micro-turning, micro-grinding, micro-EDM and micro-ECM have many advantages in productivity, efficiency, flexibility and cost effectiveness; but the capability of such micromachining around the lower boundary of micromachining range below 50μm has not been demonstrated extensively. Compound machining, which integrates conventional and non-conventional micromachining processes on the same machine tool, has several advantages over a single process. But, significant research work has not yet been conducted in exploring the capability of compound micromachining due to the unavailability of a suitable machining platform for performing several of such machining processes at the state-of-the-art benchmark. The primary objective of this project is to perform experimental study and development of successful micro-EDM based compound micromachining processes mostly between 5μm~50μm feature size range. This research work also aims to contribute to the fundamental understanding on the process physics of micro-EDM process.

A universal multi-process machine tool capable of performing compound micromachining processes has been evaluated using ISO standard evaluation techniques and cutting tests which substantiated the capability of the machine tool for performing conventional micromachining processes. Through theoretical analysis and

experimental evaluation of the micro-EDM process, the need for implementation of relaxation circuit (RC) power supply for very small discharge energy has been identified.

The theoretical analysis of micro-EDM process has been performed aiming to develop a model for the RLC network of RC type power supply employing micro-EDM plasma properties. Analytically it has been demonstrated that the capacitive plasma discharge for micro-EDM plasma can be modeled using the resistive component of the plasma. Using the proposed model, current waveform and discharge energy have been computed and shown to have good agreement with experimentally obtained current waveform. The proposed model provided significant insight for realizing changes in current waveform, and thus the final process outcome due to changes in process parameters, such as, input voltage, capacitance and inductance.

A new micro-EDM power supply using RC power supply has been developed to provide supply of very low discharge energy, down to ~37nJ at 60V supply voltage. With improvement in gap control capabilities and implementation of 3D micro-EDM milling sequence, a new method for straight electrode machining has been realized. These development activities have been based on the theoretical analysis of an RLC network, and an array of micromachining of shapes and features around 20μm has been demonstrated by micro-EDM milling and micro-EDM die-sinking process.

The developed platform has been utilized for the exploration of compound micromachining, where micro-EDM has a cardinal role due to its capability of machining with extremely low cutting force. Novel machining capabilities have been developed and demonstrated for compound machining of micro-slots and micro-shafts by combining micro-EDM, micro-turning and micro-milling processes.

List of Tables

List of Figures

List of Symbols

A – Cross-sectional area of the plasma

C – Capacitance of the RC power supply

C_0 – vacuum capacitance of a capacitor

c_p – Specific heat capacity

d – gap between two electrodes

d_w – Diamete of wire

e – Charge of electron.

E_d – Discharge energy in a spark

Hm – Energy of melting

Hv – Energy of vaporization

i – Discharge current

k_B – Botzmann's constant is denoted by

L – Inductance of the discharge line in RC power supply

l – Length of wire

L_m – Latent heat of fusion or melting

L_v – Latent heat of vaporization

m_e – Mass of electron

N_D – number of particles in a Debye sphere

n_e – Electron density in plasma

R – Resistor in the charging loop of RC power supply

$R2$ – Resistor for charging current detection

R_b – Plasma Resistance

R_d – Resistance of the discharge line in RC power supply

R_a – Average surface roughness

R_{max} – Peak-to-valley surface roughness

T – Temperature of plasma in Kelvin and

T_0 – Ambient temperature

T_b – Boiling or vaporization temperature

T_m – Melting point temperature

T_{off} – Pulse OFF time

T_{on} – Pulse ON time

V – Supply Voltage of power supply

V_g – Gap voltage

ν_m – *E*ffective electron-ion collision frequency for momentum transfer.

V_{ur} – Volume removal from a single discharge

ε_b – Plasma dielectric constant

ε_0 – Dielectric constant of vacuum

ω – Angular frequency of the oscillation in plasma

ω_{pe} – Electron Plasma Frequency

ρ - Density

ρ_b – Plasma Resistivity

$ln(\Lambda) \approx$ Coulomb logarithm correction factor

List of Abbreviations

AgW - Silver Tungsten

BEDG - Block electro-discharge grinding

CAM - Computer aided manufacturings

CNC - Computer numerical control

CuW - Copper tungsten

DC – Direct Current

ECM - Electro-chemical machining

EDG - Electro-discharge grinding

EDM - Electro-discharge machining

EWR - Electrode Wear Ratio

FEM - Finite element method

FIB - Focused ion beam

IC - Integrated circuit

KCL - Kirchhoff's current law

KVL - Kirchhoff's voltage law

MBEDG - Moving block electro-discharge grinding

MEMS - Micro-Electro-Mechanical Systems

MRR - Material removal rate

PCB - Printed circuit board

PCD - Plycrystalline diamond

SD - Standard deviation

SSE - Shape specification element

TCMMP - Tool-based Compound Micromachining Process

UMMT - Universal multi-process machine tool

UR - Unit Removal

W - Tungsetn

WC - Tungsten carbaide

WEDG - Wire electro-discharge grinding

WEDM - Wire electro-discharge machining

1 Introduction

A very senior software engineer colleague of the author from a semiconductor processing equipment company once commented being disgruntled with some biased decisions made by the process engineering team – "the most influential man in manufacturing is the process engineer; they are the only one and they are all in all". Though it was commented in a way to vent out frustration on the heated up argument on a technical issue that he had with a process engineer in the organization, there is an implication in his comment. Albeit manufacturing is not just about process engineering, but is multi-disciplinary in nature when dealing with the design, implementation, operation, and optimization of the process concerned. An equipment with very good mechanical structure and excellent control system void superior process capabilities will not be useful. But, at the same time an identified innovative process supported by fundamental study and driven by potential industrial application will not be realized if a pertinently designed equipment is not available to enable its implementation and in-depth study.

The aforementioned case also applies for tool-based compound micromachining processes (TCMMP). The process development will be hindered by the machine tool employed for machining having a wrong setup or the capability demonstrated at a dimensional range is not appropriate. Therefore, it is important to untwine the correct question and for TCMMP it should be: whether or not it can provide solutions to manufacturing problems otherwise not solved economically or even otherwise not possible at all. And the solution has to be at the required dimensional range and

supported by underlying physical principles given that a suitable platform exists for exploration of various TCMMPs. In particular this is very important to pay attention to the term 'required dimensional range' as that is expected and therefore, the answers should too match to that dimensional range which is often not the case. While machining of a 500µm diameter cylindrical rod is not particularly a problem with present day available technologies, this becomes a massive challenge when this is tried for a 50µm cylindrical rod. Therefore, demonstrations of capability of micromachining at upper or mid boundary of the dimensional range for micromachining domain are not acceptable as practically the challenges are lying at the lower boundary of micromachining domain below ~50µm dimensional range.

In order to answer the question asked above it is also important to provide a very brief overview on the nature of challenges for micromachining to happen at the lower boundary of micromachining domain. Micromachining is a relatively new arena of advanced manufacturing technology and there exists many magnificent process ideas for machining of parts and components with micrometer range geometry which are considered as the art of micromachining (Corbet et al., 2000; Dornfeld et al., 2006; Fang et al., 2006; Masuzawa 2000; Meeusen et al., 2003; Rahman et al., 2006; Schoth et al., 2005). At par, there exists enormous difficulties in translating these process ideas into profitable manufacturing reality which are the engineering of micromachining and demands optimization for a very complex set of mutually inversely dependent output parameters. The optimization process requires fragmenting the complex set of technical challenges into seemingly simple units following a systematic and rigorous approach which loops through the conventional development life cycle recurrently but it is not confined in a set of heuristic rules which could be

applied in every recurrent cycle. It involves understanding the process requirements, setting the criteria for mechanical system, mechanical design, fabrication and assembly of the mechanical structure, developing electronic circuits and control systems, developing intelligence in the system to control the physics behind the process and finally observing and empathizing to what the machine needs when it is not capable of controlling the underlying physics of the process.

The aforementioned essentially mean that for TCMMP the challenge is in the effective implementation which requires a synergistic development work and successful integration of practically four major areas (Figure 1.1) – (a) evaluation and characterization of a machining platform to assess suitability for micromachining; (b) in-depth understanding of process physics to leverage on the tuning of responsible parameters for an expected outcome – in the scope of this thesis it is micro-EDM process; (c) development of hardware and software guided by the understanding of process physics; and finally (d) exploration of TCMMP technologies on the platform.

The first section of this chapter focuses on the motivation behind this research effort followed by objective and the scope of this work. It concludes with a brief overview on the organization of this thesis.

1.1 Motivation

The drive for miniaturization and fabrication of components with a wide selection of materials will allow micro-systems technology to enhance health care, quality of life, to attain new technological breakthrough and to coat engineering applications with environment friendly and energy saving practices. The pervasive demands of

miniaturization across all engineering disciplines have imparted the challenge of fabrication of such components to the manufacturing engineers. In present day, state-of-the-art fabrication techniques refer to the fabrication of components and parts for Micro-Electro-Mechanical Systems (MEMS), sub miniature actuators and sensors, components for biomedical devices, high precision equipment, components for advanced communication technology, long micro-channels for lab-on-chips, shape memory alloy 'stents', fluidic graphite channels for fuel cell applications and many more (Corbett et al., 2000; Lang 1999; Madou 1997; Weck et al., 1997). The more recent trends indicate that the drive has gone beyond the little earlier challenge of precision and minuteness in dimension to a new level where components of same precision and even less visible dimensions are produced by machining on tough materials at lower cost.

Components for MEMS and most miniature applications are usually produced using semiconductor processing technologies, like photolithography on silicon substrate (Meeusen et al, 2003; Schoth et al, 2005). Applications related to micro-surgery, biotechnology, fluidics or high-temperature environments (Kuo et al., 2003) are examples of broad emerging need for fabrication of micro-parts with exquisite structure and strength dependent properties, on a par with size dependent properties, in which material properties of silicon often do not meet. Micro-structures produced by photolithography have the limitations of low aspect ratio and quasi-3D structure (Okuyama et al., 1998; Rajurkar et al., 2000). It is possible to fabricate high–aspect-ratio components with sub-micron structure by LIGA process (from the German: Lithographie Galvanformung und Abformung – a combination of lithography, electroplating and molding process) using the synchrotron radiation process and

focused ion beam machining process. However, present laboratory-scale and industrial fabrication techniques using LIGA require special and extremely expensive facilities like a synchrotron system and require machining of expensive masks which has imposed a hindrance on quick and economical fabrication of micro-parts. Furthermore, the dimensional ranges that such processes cover are sometimes not required which is illustrated in Figure 1.2. It can be observed from the illustration that tool-based micromachining has a unique place for performing micromachining operations at the lower boundary of micromachining range (between 5µm~50µm) to bridge the gap between mechanical machining, photolithography and LIGA process for dimensional range and aspect ratio (Rahman, A., et al., 2005, Rajurkar KP., et al., 2006).

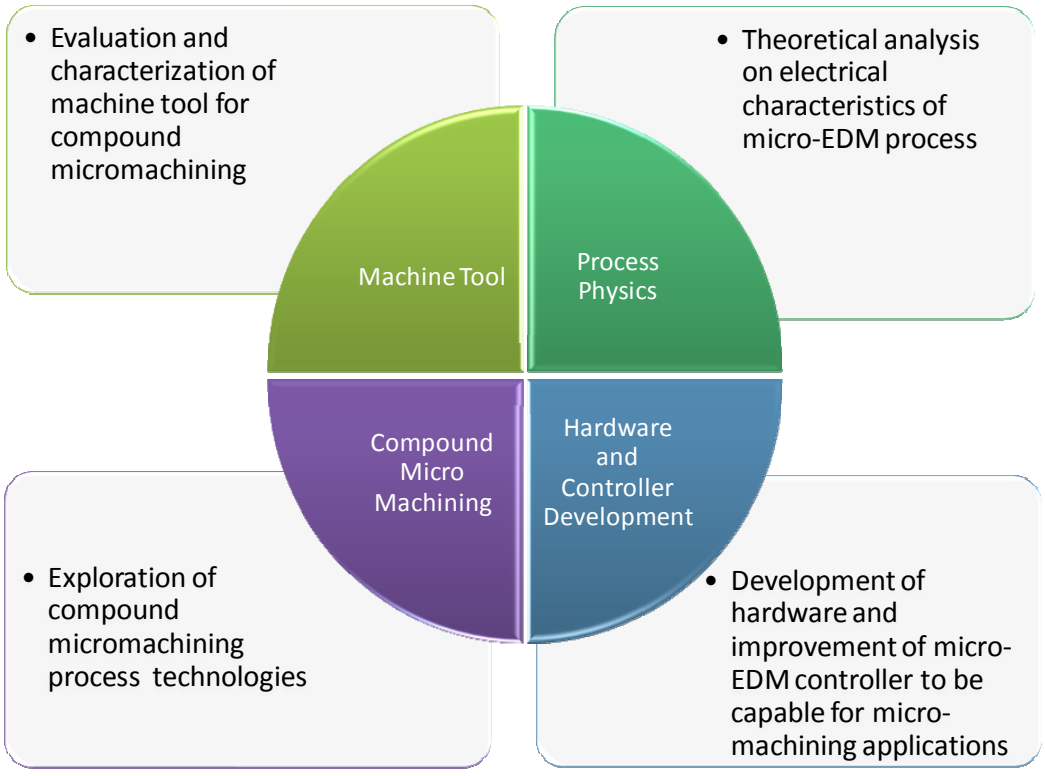

Figure 1.1 Synergistic research and development areas for successful compound micromachining.

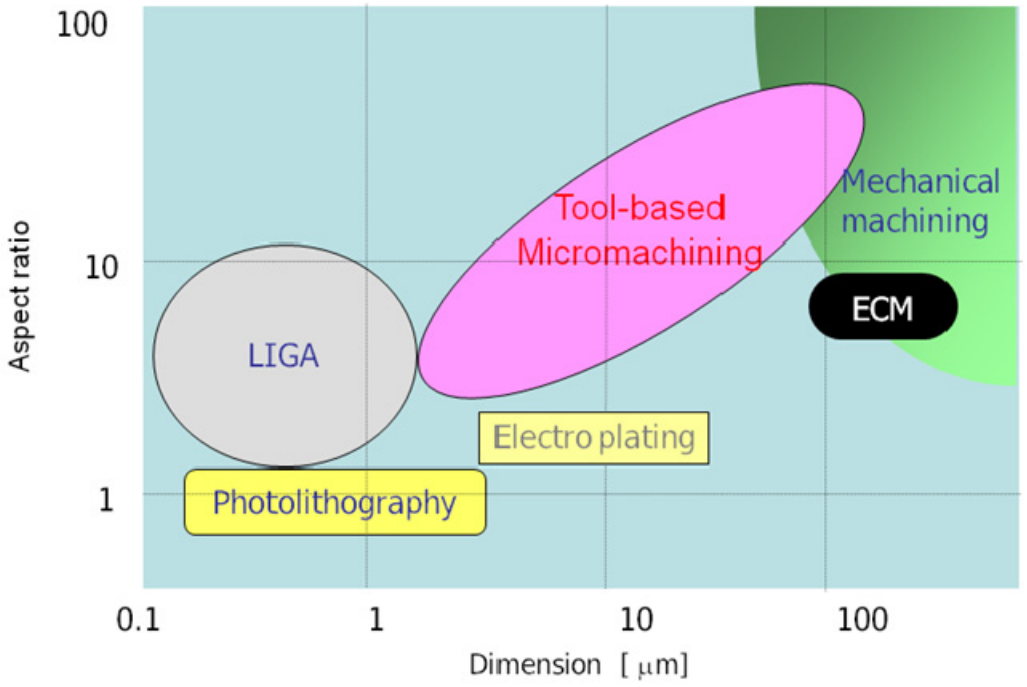

Figure 1.2 Illustration on dimensional range and aspect ratio of several machining processes.

Tool-based micromachining technologies, including micro-turning, micro-grinding, micro-EDM and micro-ECM, have many advantages in productivity, efficiency, flexibility and cost effectiveness and consequently have been applied to a variety of substrates and materials to fabricate micro-structures and transducers in addition to etching and LIGA (Fang et al., 2006; Gianchandani et al., 2006; Rahman et al, 2006; Schoth et al., 2005; Yu et al., 1998; Zhao et al., 2004). In many applications the workpiece is a final product while in other applications it might be the x-ray lithography mask or a mold for electroplating to create a micro-structure. Among the tool based micromachining techniques, micro-EDM, a non-conventional machining process, has been identified as a very promising technology for the machining of micro-components due to its non-contact machining capability. It involves almost

negligible amount of force interaction between the tool and workpiece and is capable of machining a wide range of conductive materials irrespective of toughness. The other techniques like micro-milling and micro-turning have the advantage of larger material removal rate (MRR) as well as the capability to machine non-conductive materials. However, despite the fact that their capability for making micro-scale products using tool-based micromachining has already been presented earlier, their disadvantages include high cost, low throughput and limitation in machining further smaller components in the current state of their technology.

A new concept of tool based micromachining is to utilize the complementary strengths of different material removal processes (conventional and non-conventional) within the same setup, where possible, for the machining of microstructures with high dimensional accuracy (Rahman, M., et al., 2007(a)). For example, material removal by micro-milling process has many advantages and it is fast as mentioned earlier. But it is limited by the lower limit of machinable feature size which is an order of magnitude larger compared to micro-EDM due to the presence of larger cutting force. On the other hand micro-EDM has the limitation of relatively high tool wear to workpiece removal ratio due to high tool wear rate and low machining speed. Moreover, usually the electrode for micro-EDM milling is prepared using other EDM based techniques like EDG (electro discharge grinding), which is also a slower process. For instance, in the machining of a micro plateau shaped structure, the bulk amount of material can be removed using conventional micro-milling process followed by micro-EDM milling process which can achieve the dimensional accuracy and finer range of feature size, and superior surface finish could be generated by applying micro-ECM process after

micro-EDM. The electrode too can be manufactured using micro-turning process which is also much faster compared to the EDG process.

Perhaps one of the main difficulties in TCMMP is the lack of availability of an appropriate machine tool that can be used for multiple tool-based micromachining processes and specially to utilize compound form of tool-based micromachining for machining of components at required scale. Most machine tools capable of micro-EDM are not designed to perform other machining processes like turning or milling on the same machine in a single setup. Attempts were made to perform TCMMP by modifying a machine tool suitable for one process to be adapted for another supportive compound process that performs at a less optimal level (e.g. modification of a micro-EDM machine for micro-milling) and while the capability was demonstrated, its potential would need further research to be better exploited for industrial applications. Further, such machine tools do not facilitate measurement of fabricated products on-machine which has the potential to be used as feedback and to compensate tool trajectory online. Another constrain is imposed by the precision required for such machining which conventional CNC machine tools cannot fulfill. Mechanical and thermal deformation, chatter vibration, tooling and its clamping usually constrain the making of small, super-precise parts with large, conventional machines. On the contrary, ultra-precision machines that provide high degree of motion accuracy are extremely expensive, require regular maintenance, and mostly do not include non-conventional process capabilities like micro-EDM. Moreover, both the ultra precision machines and conventional CNC machines occupy considerably large space and their power consumption is comparatively much higher relative to the contextual micro-parts. Furthermore, the present state of clamping techniques and fixturing poses a real

challenge on performing different machining processes on different machine tools on a micro-sized component. For instance, the commercial high precision clamping collets have clamping error of between 5 to 10µm and this can cause up to 50% error for the machining of a 20µm diameter micro-shaft which therefore limits the use of using multiple machines for TCMMP. Some attempts towards TCMMP have been done by developing machine tools or a dedicated process where the setup development occupies a considerable amount of effort and investment (Fleischer, J., et al., 2004; Morgan, JC., et al., 2006).

Hence, there is a need for a dedicated platform, here-in called as universal multi-process machine tool (UMMT), which enables multiple machining processes to be performed in micromachining domain on a single platform. This would ensure that the underlying equipment hardware is capable of providing the multiple-process needs for execution and realization of the art of micromachining. Besides making tool-based micromachining a feasible option for micromachining needs, in addition to significant contribution in accuracy, minimum achievable feature size and surface quality, it would also speed up the machining process by saving the re-clamping time and relieving from the handling needs during inter-process transfer of such miniaturized components. Secondly, research work needs to be undertaken towards the understanding of process physics to provide relevant background for modeling, measurement, identification of control parameters for precise process control of compound micromachining processes. Thirdly, hardware and software systems of the equipment guided by the understanding of process physics for performing micromachining at the appropriate dimensional range needs to be developed and implemented for processing real-time data processing and decision making. This is

particularly so for TCMMP as the quality of the output of a process can be monitored for any required correction before passing to the subsequent machining processes. Finally, the difficulties of micromachining using available techniques need to be understood and suitable compound processes identified to offer processing capabilities to overcome the difficulties and the weaknesses of single processes. An integrated approach in these areas (shown in the schematics of Figure 1.1) will provide for the required platform suitable for TCMMP to be implemented for solving the tool-based micromachining problems.

Therefore, efforts have been taken to fundamentally understand the electric properties of micro-EDM plasma and the interaction of plasma with the power supply, followed by hardware and software development for micro-EDM. On the developed platform research work has been conducted as an exploration of technologies to demonstrate the capability and potential of TCMMP for industrially-scalable applications.

1.2 Research Objectives

A big challenge in TCMMP is posed by the availability of a suitable machine tool that offers the multi-processing performance, as mentioned earlier. The requirement is indeed complex and demanding as the machine is expected to be capable of performing the different conventional and non-conventional micromachining processes without compromising their single-process performances. A common pitfall in the research and development of TCMMP is the use of a machine tool that is industrial gold standard for one of the multiple processes needed in the compound process but performs below average in one or more of the other multiple processes. A multi-process micromachining machine tool has been presented by Rahman et al. 2003,

which is capable of micromachining micro-components and is suitable for multiple processes. Further research and development work on this machine tool is required to set new benchmark in machining speed, feature size control, minimum achievable feature size and surface finish with focus on the micro-EDM process, as in this research micro-EDM process is considered as a major process to be compounded with the other tool-based processes. This project essentially targets at the experimental study and development of successful micro-EDM based compound micromachining mostly between 5μm~50μm feature size range. The research work also aims to contribute to the fundamental understanding on the physics of the micro-EDM process. The specific goals of this research are summarized below:

- To evaluate the UMMT for suitability of performing multi-process micromachining and to assess the performance of the machine tool to be used as a setup for implementing and performing various micromachining processes at a state-of-the-art level so that different processes could be compounded with much less effort.
- To perform fundamental analysis on the micro-EDM plasma characteristics and the interaction of micro-EDM plasma with the power supply. This will allow in-depth understanding of the requirement of micro-EDM power supply and the behavior of discharged energy to the workpiece at different settings.
- Design and development on the micro-EDM power supply guided by the fundamental analysis to provide superfine and ultra-short spark pulses with extremely short charging time for fine surface finish, reduced minimum achievable feature size and improved machining time.

- Implementation of gap control techniques for faster machining, 3D milling-EDM technique implementation and development of EDG based straight electrode machining technique.
- Verification of the process capability of the micro-EDM by performing characterization studies, including machining time, tool wear ratio and surface roughness, and further substantiation of the capability of micro-EDM setup by micromachining of high-aspect-ratio features which will ensure that the equipment is suitable for development of novel TCMMPs.
- Utilizing the setup developed, novel TCMMPs will be explored to demonstrate machining of micro-components at the lower boundary of micromachining domain in order highlight the true potential of such compound techniques.

1.3 Organization of the Thesis

This thesis comprises seven chapters. Chapter 1 starts with a prologue to give an overview to the nature of the problems, followed by the motivation behind this research endeavor, and finally the objective of this research work. This chapter also outlines the organization of this dissertation.

Chapter 2 assesses and reviews the literatures on the state-of-the-art micromachining technologies for machining and manufacturing of micro-features followed by the discussion on the present limitations of tool-based micromachining technologies. The chapter also provides a review on related literatures on TCMMP and highlights the advantages of these techniques. It ends with a discussion on the gap of the previous research works and the necessity of current work to develop a dedicated platform for TCMMP in order to demonstrate the capability of TCMMPs.

Chapter 3 starts with describing the UMMT as an experimental setup followed by experimental evaluation of UMMT by performing experiments in order to justify the required development works in micro-EDM hardware and software for successful demonstration of TCMMP.

Chapter 4 provides an in-depth fundamental analysis on micro-EDM electric characteristics employing plasma property with an objective to model the electric properties of micro-EDM plasma for an RC power supply circuit and to understand the role of the three components *R*, *L*, and *C* present in the power supply circuit in order to obtain optimal value of these parameters. The first section defines an electric equivalent network of micro-EDM plasma and the components of this electric network are evaluated in second section of the chapter. The third section provides an analysis of the power supply electric network and plasma network and proposes a set of equations as a model which is validated in the fourth section of the chapter. The final section discusses on the observations made from the current waveform generated by the proposed model.

In chapter 5, the design and development of RC power supply is presented based on the preceding fundamental analysis and experimental study. The second section of the chapter discusses on the implementation of jump based gap control which improves the previous gap control technique implemented on the machine. The third section presents the implementation of 3D micro-EDM milling technique for machining 3D features and shapes. In the fourth section a new technique for machining of straight electrode is presented followed by characterization experiments to better understand

the developed system which is essential for performing micromachining of complex shapes and features using micro-EDM. The final section presents a set of micromachining examples to demonstrate the machining capability resulting from the development of a suitable UMMT and synergistic combination of complementary processes.

Chapter 6 presents the exploration of TCMMP using on-machine fabrication of high-aspect-ratio microelectrodes that demonstrates a series of combination of processes employing 'micro-EDM + micro-Turning + micro-EDM; for drilling of deep holes and fine features. The second section presents a 'micro-EDM + micro-grinding' technique for machining on glass and 'micro-EDM + micro-milling' technique for milling of 30μm slots on PZT substrate using PCD micro-tools.

Finally this dissertation concludes with the Chapter 7 providing a summary of the contributions and ends with suggesting the potential advancement areas for future research work.

2 State-of-the-art of Micromachining Technologies

This chapter assesses and reviews the current science and technology and state-of-the-art capabilities for machining and manufacturing of micro-features. In the first section of this chapter an introduction on currently available and practiced micromachining technologies are summarized. The second section focuses on the science as well as the present state of tool-based micromachining, such as micro-milling, micro-turning, micro-drilling, micro-grinding, micro-EDM, and presents challenges in different micromachining technologies. The third section reviews research works done in TCMMP, which is comparatively a new direction of research efforts and is getting attention only recently as ordinary micromachining techniques face physical limitation with shrinking feature size.

2.1 Introduction

Micromachining is a general term used to indicate a collective form of all the process technologies used for machining of microstructures and microsystems. 1 to 500μm has been adopted as the formal dimensional range of micromachining by the Scientific Technical Committee of the Physical and Chemical Machining Processes of CIRP (Masuzawa, T., 2000). Most of the technologies that have been utilized in micromachining are existing technologies adapted to operate in micrometer dimensions or adopted from microelectronic fabrication processes. Microfabrication for industries like aerospace, automotive, precision engineering etc. are mostly done using mechanical tool-based micromachining and there have been significant advances

in the fabrication techniques, metrology and equipment technology (Chae et al. 2005, Dornfield et al. 2006).

However, the past two decades have evidenced tremendous research and development specially focused on fabrication techniques for MEMS. MEMS is the integration of mechanical elements, sensors, actuators and electronics on a common silicon substrate through the utilization of microfabrication technology. The electronic components in a MEMS package are mostly fabricated using integrated circuit (IC) fabrication processes and the micromechanical components are fabricated using specialized technologies unique to silicon micromachining processes that selectively etch away parts of the silicon wafer or add new structural layers to form the mechanical and electromechanical devices (Xuan et al., 2006). The manufacturing resources for silicon ICs are quite impressive, representing decades of research and billions of dollars worth of investment in developing manufacturing techniques and equipment and the existence of the very sizeable integrated circuit fabrication infrastructure. MEMS manufacturing leverages much of this extensive technological base, but has developed a distinct set of fabrication technologies which when combined with conventional IC manufacturing processes enable MEMS to be realized.

However, as has been mentioned in introduction, the majorities of these methods are limited to a few silicon-based materials, essentially planar geometries and therefore significant amount of design constraints and thus broad commercialization of MEMS based products has been hindered. Advent of miniaturization and new technologies have demanded micromachining of any shapes including true 3D structures on almost every material such as metals, plastics and semiconductors which are required for the

moving parts and guiding structures (Rahman, M., et al., 2007(b)). Micro-mold cavities are also required for mass-production of micro-components by injection molding and the machining of micro-mold cavities require very precise machining of 3D structures on hard to machine workpiece materials. There exist other requirements such as micro-scale fuel cells, micro-scale pumps and micro-fluidic systems (Liu et al., 2004; Weck et al., 1997). Over the years, tool-based micromachining methods have been applied to address some of the challenges mentioned above on a variety of substrates to fabricate microstructures and transducers; and gained additional advantage of low setup and manufacturing cost. The workpiece may be a final product or mold for LIGA based electroplating to create a microstructure or photomask for X-ray based lithography (Friedrich et al., 1997; Friedrich et al., 1998; Li, T et al., 2005; Maluf, N., 2002; Rahman, A., et al., 2005) or even could be continued from other processes like LIGA towards a final product through tool-based micromachining for better throughput (Takahata, K., et al., 2002).

2.2 Tool-based Micromachining Technologies

Through the 1990s, Masuzawa highlighted the need for the development of micromachining processes (Masuzawa, T et al., 1997) and drew attention towards the need of tool-based micromachining. In his opinion, in precision machining it is important to recognize what directly determines the shape of the products in the machining process and based on shape specification element (SSE) he categorized the micromachining processes into two basic groups one having SSE as the tool and the other one having mask as the SSE. He drew attention towards the fact that processes having mask as SSE are basically two dimensional in nature and have limitations in generating an actual three dimensional shapes. He also emphasized that, even though

very small unit removal (UR) requirement for precision engineering is mainly catered by mask based micromachining technology which could reach atomic level dimension, URs of tool-based micromachining processes are acceptable in many practical applications; and they could even be preferred due to their low setup and maintenance cost. Through his extraordinary research efforts, tool-based micromachining technologies received significant attention and acceptance in the scientific community (Masuzawa, T, 2000; Masuzawa, T et al., 1997; Masuzawa, T et al., 1985; Yu, Z. Y., et al., 1998). His initial research work in collaboration with Masaki, T., (Masaki, T. et al., 1990(a); Masaki, T et al., 1990(b); Masaki, T et al., 1989) and Sato, T., (Sato, T et al., 1985) from Matsushita Research Institute Tokyo, formed the foundation of micromachining with a main focus on micro-EDM process. Table 2.1 shows some of Masuzawa's pioneering research work and citation report according to Scopus – citation database (as of June 2, 2012) and growing research interest in this area is clearly visible through the number of citations received in last five years.

Table 2.1 Citation report of pioneering research work in tool-based micromachining

Title	Year of Publication	Total Citations	Citations in last 5 years
Wire Electro-Discharge Grinding for Micro-Machining (Masuzawa - 1985)	1985	250	135
State of the Art of Micromachining (Masuzawa - 2000)	2000	243	183
Micro-EDM for three-dimensional cavities – Development of uniform wear method (Yu ZY - 1998)	1998	124	79
Three-Dimensional Micromachining by Machine Tools (Masuzawa - 1997)	1997	113	62

2.2.1 Micro-milling

Milling is one of the most universal operations of machining processes. Extensive research on physical characteristics of milling process, tool failure analysis as well as process planning has been done (Fang, FZ., et al., 2006). In the adoption of the milling process for micromachining applications, the amount of UR needs to be reduced (Masuzawa et al., 1997). One issue in reducing UR for micro-milling is that

microcutting occurs in a small region which contains only a few layers of molecules and can be discrete in nature rather than continuous, as is assumed in conventional continuum mechanics. Molecular dynamics based simulation has been utilized to solve this problem and several recent results demonstrate that the microcutting processes are capable of reducing the UR to as small as 1nm (Shimada et al., 2001; Shimada et al., 1993; Ikawa et al., 1992). Recent development in ultraprecision machine tool technology provided excellent positioning accuracy as well as repeatability which is a significant step forward for successful implementation of micro-milling process in industrial applications for small UR.

Unfortunately, even though micro-milling is a scale-down adoption of the milling process for micromachining applications and has the theoretical capability of UR as small as 1nm, practically there exists significant challenges in realizing micro-milling, especially when the diameter of the end-mills are down to 0.1mm or smaller. Owing to the comparatively smaller and weaker size of micro-milling cutters and the fact that only a tiny portion of the tool involved in cutting at a particular instance of the process, tool failure due to tool run-out has been reported as one of the major problems (Bao et al., 2000; Fang et al., 2003; Friedrich et al., 1997; Masuzawa 2000; Sato et al., 1989; Tansel et al., 1998; Zaman et al., 2006) in micro-milling.

Recent research efforts include design of tool geometry to reduce cutting force in order to avoid tool breakage. Figure 2.1 shows some of the tool shapes being researched (Fang et al., 2003) and a FEM on relative rigidity demonstrated that the (d) and (e) types tools are 12 and 8 times, respectively, more rigid than the conventional (a) type tools of 100μm diameter having two-flutes. FEM studies demonstrated that 3 times larger cutting force is required for occurring chipping and breakage in (d) and (e) type

tools compared to (a) type tools. In micro-end-milling operation, the tool run-out to tool diameter ratio becomes very big compared to conventional end-milling operation. As a result, only one side of the tool performs the machining operation at any point of time while the other edge does not touch the workpiece at all and this generates significant amount of directional force variation on the tool. With such a small tool dimension, even if the cutting force is as small as few tens of mN, chipping and breakage of the tool tip occurs.

Another major concern is the limited availability of micro-milling tools below 50μm diameter. Even though commercially 25μm milling tools are available (Chern, GL., et al., 2007) at present, high tool cost, unreliable tool life and early tool failure can damage the workpiece; thus could be rendered unacceptable for precision applications. Schaller et al. 1999, have demonstrated that self made end mills with diameters ranging from 35μm to 120μm could be ground to cut microstructure grooves. Another rather common custom fabricated micro-milling tool machining process besides mechanical method is to employ focused ion beam (FIB) machining technique, as this process has gained popularity for machining of very small probe tips for biomedical use and micro-scalpels with extremely sharp cutting edges (Friedrich, CR., 2002; Friedrich, CR., et al., 1997; Vasile MJ., et al., 1996). It has been demonstrated that FIB could be used to shape a variety of cutting tools with diameter from 15μm to 100μm with 40nm cutting edge radius using a wide range of tool materials like single crystal diamond, tungsten carbide and high speed steel (Adams DP., et al., 2001; Picard, YN., et al., 2003). Figure 2.2 (Adams DP., et al., 2001) shows such tools with 2, 4 and 6 cutting facets fabricated using FIB. Even though, FIB process is capable of fabricating very fine custom micro-milling tool – the utilization of FIB technology demands a

vacuum background and thus involves more expensive and complicated equipment, setup and operating cost. In addition to that, FIB process could not be performed in-situ and thus it does not eliminate clamping error.

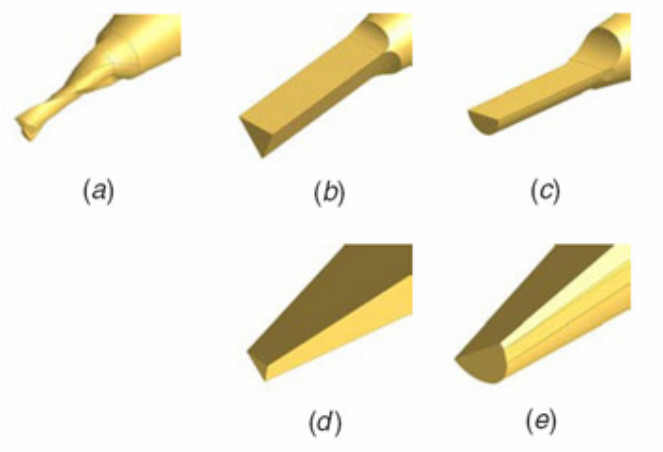

Figure 2.1 Various types of end-mills in micromachining. (a) Two-flute end-mills, (b) Δ-type end-mills with a straight body,(c) D-type end-mills with a straight body, (d) Δ-type end-mills with a tapered body and (e) D-type end-mills with a tapered body (Fang F. Z., et al., 2003).

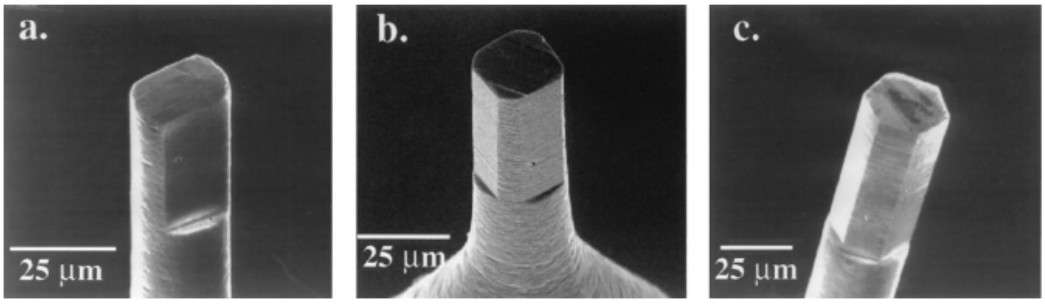

Figure 2.2 Micro end-mills made by focused ion beam sputtering having 2(a), 4(b), and 6 (c) cutting edges (Adams DP., et al., 2001).

2.2.2 Micro-turning

The present state of micro-turning process is very similar to conventional turning process on a lathe which has been extended to provide better precision and accuracy in machining process. Similar to micro-milling process, micro-turning has the capability to produce 3D structures on micro-scale (Rahman, A., et al., 2005). There are two

major types of micro-turning – cylindrical shaft turning for machining of micro-pins and face turning for machining of microgrooves, that has been reported for micromachining applications (Rahman, A., et al., 2005; Gao, W. et al., 2003). Micro-turning for machining of micro-pins is possible but it is more difficult to realize due to the deformation of the fine workpiece which is very similar to the deflection of micro-endmilling cutter as could be seen in Figure 2.3 (a). However the situation is even more critical for micro-turning as often the micro-turning workpiece is much weaker than the tool in micro-milling (Masuzawa, 2000) and thus the major drawback of micro-turning process is that the machining force influences machining accuracy and the limit of machinable size. Significant work has been done to develop different cutting paths and schemes to reduce the effect of cutting force on the fine shaft. A micropin of around 350μm diameter (Figure 2.3 (b)) with intricate shape and kinks has been fabricated (Rahman, A., et al., 2005; Rahman, A., et al., 2006). But, it is very difficult to achieve a straight shaft below 100μm diameter and in many cases, the workpiece is either broken, or starts to wobble due to excessive radial cutting force on the micro-shaft. Figure 2.4 shows one such micro-shaft machined using the conventional micro-turning process. The shaft was deformed plastically with very rough surface finish from plastic side flow caused by the strain gradient-induced strengthening due to the constant radial force during turning at a slower feedrate (Liu. K, et al, 2006). When a faster feedrate is applied, the shaft breaks easily as the radial force increases to an excessive level.

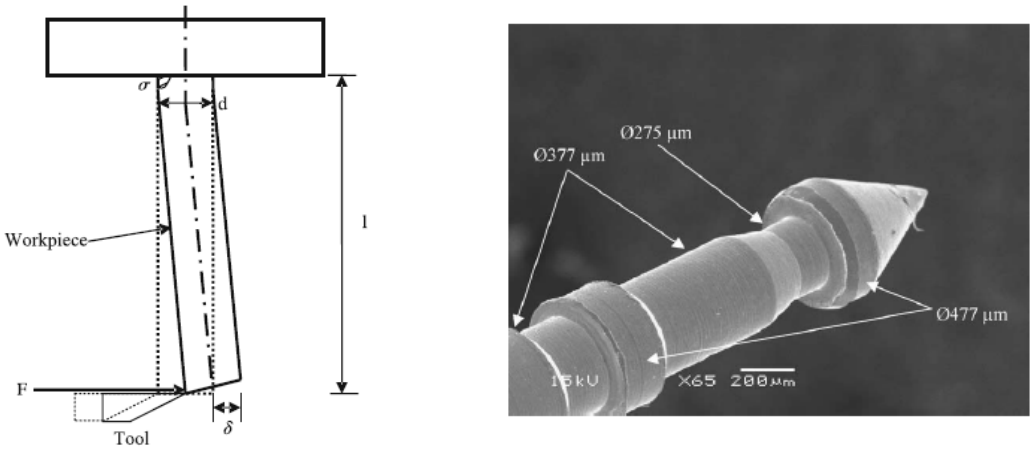

Figure 2.3 (a) Workpiece deflection in micro-turning, (b) SEM image of compound shaped micropin (Rahman, A., et al., 2006).

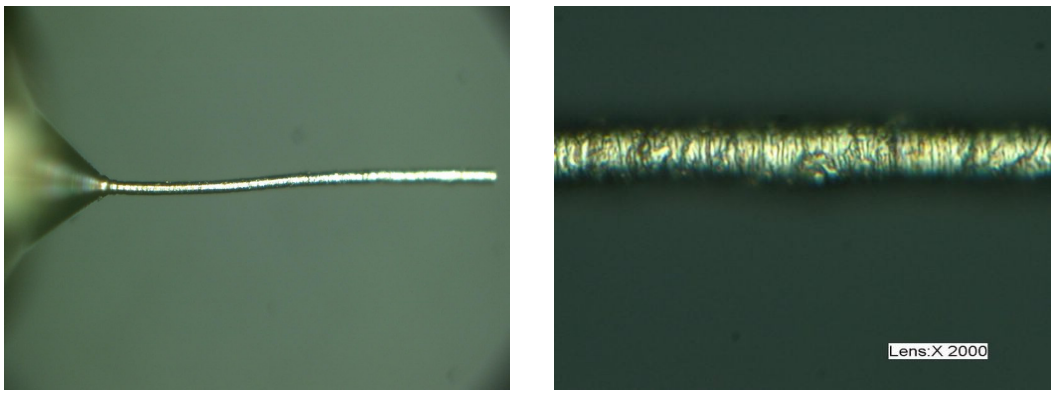

Figure 2.4 Plastic flow and rough surface generated during micro-turning of brass.

In face turning, research has been conducted for many years on diamond turning and this has found wide applications in machining of various components such as micro-lenses, lens arrays and parts for measurement references, for example, surface encoder for multi axis position accuracy measurement (Brinksmeier, E., et al., 2001; Gao, W. et al., 2003; Pramanik, A., et al., 2003). Diamond turning has been generally coupled with the term ultra precision machining as single point diamond turning is probably one of the few processes achieving mirror surface finish. Finish of less than 10nm and form error of less than 1µm can be obtained when machined using an ultraprecision

machine tool capable of moving in high accuracy at nanometeric precision (Rahman, M, et al., 2007(b)). It is also possible to fabricate micro-parts using conventional ultraprecision turning. After cutting micro-steps on the surface of a plate, micro-parts can be cut out by other methods such as WEDM as shown in Figure 2.5 (Masuzawa 2000; Brinksmeier, E., et al., 2001). Another important area of micro-turning is to support micro-grooving and micro-threading needs required for the fabrication of micro-fluidic sensors, micro-inductors and micro-actuators. But the major difficulty is in availability of such tools. Literature suggests that FIB can be a potential technique for machining of such tools (Vasile, MJ., et al., 1999; Adams, DP., et al., 2000), but as has been mentioned earlier, these processes require extensive investment and maintenance cost.

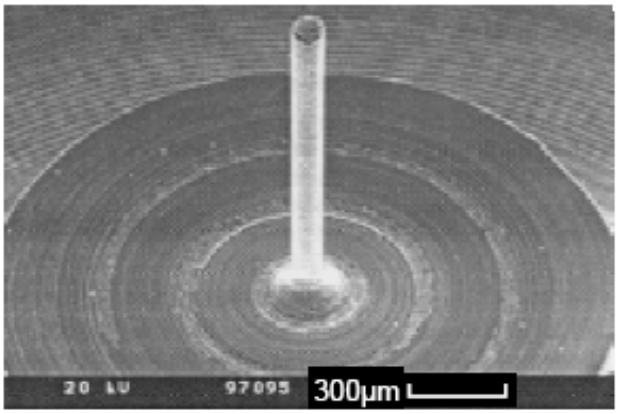

Figure 2.5 A micro-lapping tool made by micro-turning (Masuzawa 2000).

2.2.3 Mechanical Micro-drilling

Micro-drilling has been widely used in various applications such as PCBs, ink-jet printer nozzles in semiconductor industry, orifices for biomedical devices, cooling vents for gas turbine blades and diesel fuel injector spray holes. There also exist few parallel machining techniques of micro-holes, for instance, micro-EDM, micro-ECM, laser ablation in addition to mechanical micro-drilling. Mechanical micro-drilling has several advantages over other techniques (Chyan, HC., et al., 1998; Masuzawa 2000).

In mechanical micro-drilling the electrical properties of the workpiece do not influence the process and therefore, most metal and plastics, including their composites, can be machined easily. One typical example is the drilling of holes in PCB which is laminated with composite material consisting of copper foils, resin and glass fiber cloth (Watanabe, H., et al., 2008). Another advantage is unlike stochastic processes such as micro-EDM, machining time in mechanical micro-drilling can be controlled easily because the process is stable when an appropriate feedrate per rotation is set. On the other hand mechanical micro-drilling faces a lot of challenges as the high-aspect-ratio micro-drill bits are fairly weak and should be used with care in order to drill holes accurately and to prevent drill breakage. The drill point is the most important part of the drill which penetrates into the material of the workpiece during the machining process. The geometry of the drill tip is such that the normal rake and clearance angles and velocity of the cutting edge vary with the distance from the center of the drill. Even small variations in the geometry of symmetry errors can have a very strong influence on the performance of the drill. For example, if the tip relief angle is too small, excessive heat is generated resulting in an increase wear rate. Conversely, too large an angle can cause chipping or breaking of the cutting edge. Thus one very important requirement for successful micro-drilling is to minimize tool run-out and clamping error. Another important requirement is the straightness of the product and the axes of the machine tool (Masuzawa, 2000). Machined holes are often inclined because the already-machined part of the hole influences on the orientation of the drill. In order to avoid inclination, correct positioning is necessary when the drill tip begins to cut the workpiece. If the tip position shifts by even a small distance from the target center of the hole, the drill bends to follow a certain angle guided by the hole which the drill itself produces. Also there are difficulties in machining very hard or brittle

materials as the drill bit may break or crack might be generated in the workpiece. The above mentioned issues seriously affect the reliability and accuracy of the drilled holes. Fang et al., (Fang, F. Z., et al., 2006; Yang, Z., et al., 2002) has reported a micro-hole drilling on brass using high speed steel drill with a diameter of 50μm and due to the weak tool tip and off-set between the drill center and the rotational center, the fabricated hole has a diameter of 85μm which is much bigger than the drill diameter.

2.2.4 Micro-grinding

Grinding has been widely applied for machining pins and grooves with small dimensions due to the fact that UR of grinding is small and cutting is realized by the interaction of micrometer sized abrasive grains with the micro-grains of workpiece surface. With appropriate micro-grinding tools, machining of 2D or 3D micro-cavities in a system similar to mechanical- or EDM-milling is feasible and the advantage of this process is the capability of machining brittle and non-conductive materials which the former processes are not capable of. Another potential advantage micro-grinding can have is the ability to produce mirror surface on micro-components. However, in the field of micromachining, one of the technological problems in trying to realize micro-grinding is the fact that the tool must be made up of an abrasive and a matrix. When the tool size is very small, the grain size cannot be ignored, and this leads to certain difficulties in forming the precise shape of the grinding tool. Very small grain sizes are essential for micromachining and the tool too needs to be small. On the other hand, another difficulty is posed by the fact that the cutting force in grinding process is considerably high which can easily damage the micro-sized features in micromachining.

Onikura et al. (2000) proposed ultrasonic vibration grinding to reduce this limitation in fabricating micro-cylindrical tools and flat micro-drills of ultra fine grain cemented carbides. By adding ultrasonic vibration to the grinding process, they were able to produce high-aspect-ratio tools such as an 11μm diameter with a length of 160μm. Ohmori et al. (2003), fabricated micro-tools using micro-grinding, and investigated the surface quality of the tools since the surface quality is closely related to machining performance, part quality, and tool rupture strength. They claimed that surface characteristics of the prepared micro-tools were controllable at the nanometer level by controlling and optimizing the machining process conditions. They produced a micro-tool having an extremely precise shape, measuring 2μm in diameter at the tip with an extremely large aspect ratio. But, realization of conventional micro-grinding using micro-sized tools for machining of micro-features has not been successfully realized so far other than with the aid of TCMMP which has been discussed in section 2.3.3.

2.2.5 Micro-EDM

Micro-EDM is a material removal process employing discharges between a workpiece and a micro-scale electrode in a dielectric fluid. Discharges occur when the electric field between the electrode and workpiece exceeds a critical value and the dielectric breaks down. Either increasing the electric potential or reducing the separation distance between the electrode and workpiece may cause the field to exceed the critical value. Energy from each discharge melts a microscopic amount of material, which is subsequently flushed away after the voltage drops and the discharge collapses (Ho, KH., et al., 2003; Alting, L., et al., 2003; Pham, DT., et al., 2004).

Even though micro-EDM is based on the same physical principle of spark erosion it is not merely an adoption of EDM process for machining at micron level. There are

significant differences in the size of the tool used, machining method of micro-sized tools, the power supply of discharge energy, movement resolution of machine tool's axes, gap control, flushing techniques, and also in the processing techniques (Wong, 2003; Masuzawa, 2000). For example, the terms micro-EDM milling, Wire Electro-Discharge Grinding (WEDG), repetitive pattern transfer which forms a considerable amount of the basis of micro-EDM process but specific to micro-EDM process alone and not required for conventional EDM process.

The literature has shown significant contributions to micro-EDM going back 40 years. In 1968, Kurafuji and Masuzawa (1968), demonstrated the first application of micro-EDM. Through the years, micro-EDM has been developed into a versatile tool for fabricating a variety of micro-mechanical components, molds for plastic injection molding, sensors, micro-pumps, micro-nozzles, micro-grippers (Ansel et al., 2002; Kuo et al., 2004; Kuo et al., 2003; Masaki et al., 1990(a); Masuzawa et al., 1994; Meeusen et al, 2003; Michel et al., 2000; Yu et al., 1998). Micro-EDM is suitable for these and similar applications because of its remarkable advantage of low machining force as molten or vaporized material can be removed without direct contact. This property provides advantages to both the tool and the workpiece as probable deformation by machining force is avoided. Another very important advantage of the micro-EDM process is the capability of repetitive pattern transfer which is illustrated in Figure 2.6. The repetitive pattern transfer process, which Masaki et al. (2006) called as micro-EDM^n, is capable of fabricating very complex micro-structures by series of pattern transfer cycles.

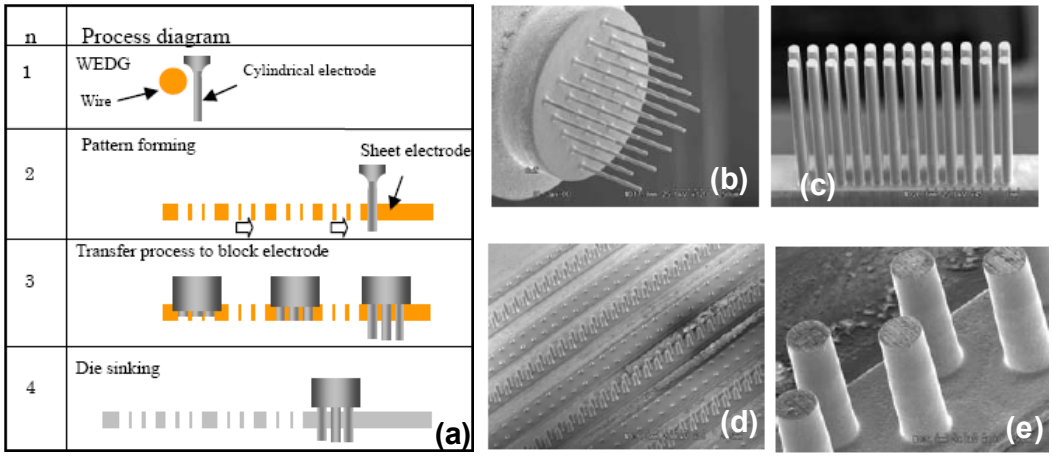

Figure 2.6 (a) Procedure of micro-EDM^n (b)Multi electrode, 14.3µm dia. Material - CuW, (c)Micro pin mold, Material - WC (d)Micro taper pin mold, Material - STAVAX (e) close-up of – (d) (Masaki, T., et al., 2006).

Current micro-EDM technologies used for manufacturing micro-features can be categorized into four major types (Pham, DT., et al., 2004): (a) micro-wire EDM, where a wire of diameter down to 0.02mm is used to cut through a conductive workpiece, (b) die-sinking micro-EDM, where an electrode with micro-features is employed to produce its inverted image in the workpiece, (c) micro-EDM drilling, where micro-electrodes of diameters down to 5µm are used to drill micro-holes in the workpiece, and (d) micro-EDM milling, where micro-electrodes are employed to produce 3D cavities by adopting a movement strategy similar to that in milling. There exists another important variant of the micro-EDM process practically very similar to of WEDM with apparent grinding-like setup and is known as EDG. Masuzawa et al. (1985) was the first to propose a variant of EDG using running wire (WEDG). The workpiece electrode is machined by feeding downwards against a traveling sacrificial wire. This process has been extended to the use of sacrificial block and sacrificial disk for EDG process (Lim, HS., et al., 2003; Alting, L., et al., 2003; Ravi N. et al., 2002) and has found extensive applications in tool fabrication (Morgan, CJ., et al., 2006).

Despite the number of publications extolling the improved capabilities of micro-EDM, they are still not widely used and industrial acceptance of micro-EDM is considerably slow given its immense potential. This is mainly due to the fact that available machine tools and process characteristics are still not sufficiently reliable. Until recently, micro-EDM has tended to be performed using conventional EDM machines modified to accommodate the micromachining requirements (Pham, DT., et al., 2004) and due to this lack of focused development for micro-EDM process, in addition to its stochastic nature, there exist significant number of challenges which are summarized in Figure 2.7. Among the many problematic areas the major problem is posed by the micro-EDM process characteristics and the interaction between the power supply and spark characteristics as this determines the process parameters. Therefore, most of the micro-EDM process parameters are obtained by experimental methods and because of the stochastic thermal nature of micro-EDM process it is difficult to explain the effects of process parameters well (Pham, DT., et al., 2004).

Among the problematic areas, micro-EDM process related issues are inherent to the process itself along with the advantages of micro-EDM and thus are practically impossible to eliminate with the available technology and process knowledge. High electrode wear and low MRR are two such major challenges. Electrode wear, which results from each discharge removing some material from the tool electrode, degrades the geometric accuracy of machined features. The relative electrode wear ratio is not constant across different workpiece materials and different geometric features. Due to this issue, it can be very difficult to provide CAM support for micro-EDM process. However, this effect can be minimized when making micro-pockets with the Uniform Wear Method, presented by Yu et al. (1998) but this method further compromise the

MRR. On the other hand due to rather comparatively larger size of the smallest possible UR – even though there is almost no cutting force involved in machining there is an early limit to minimally achievable feature size (Kawakami, et al., 2005; Kunieda, M. et al., 2005).

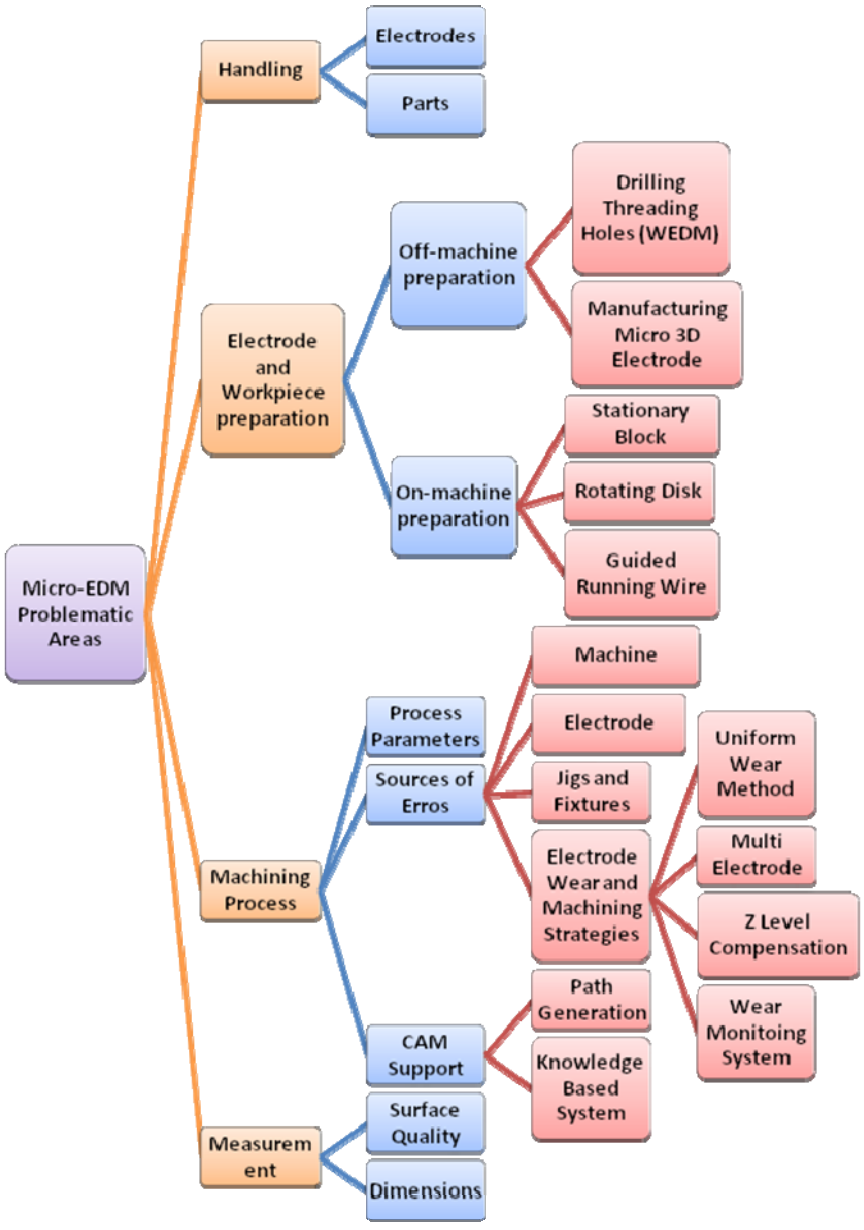

Figure 2.7 Problematic areas in micro-EDM (adapted from Pham, DT., et al., 2004).

2.3 Tool-based Compound Micromachining Processes (TCMMP)

Even though compound micromachining could be traced back to 1985 when Masuzawa et al. (1985) first proposed the WEDG process, TCMMP did not receive much attention until recently other than in the form of WEDG process and therefore TCMMP is considered rather new development in micromachining area. There exist many research efforts in compound micromachining where two processes were combined to increase production efficiency or production quality (Aspinwall, DK., 2001; Kitagawa, T., et al., 1990; Jia, ZX., et al., 1997; Koshy, P., et al., 1996) but not much research efforts were taken to transfer those ideas into the micromachining domain. Compound micromachining is yet to be formally defined by the scientific community due the process being rather new and search of databases returns less than 30 unique articles in total (this is excluding compound process of WEDG followed by micro-EDM drilling/micro-EDM milling)

. For defining the scope of this research work, discussion on TCMMP will be limited to processes which are synergism of at least more than one constituent processes where all the processes are involved in material removal either at the same time (e.g. electro chemical discharge grinding) or sequentially (e.g. micro-EDM followed by laser ablation). The material removal requires to be either from the final workpiece or via an intermediate workpiece but are performed in a single setup for machining of feature size ranging from 1μm~500μm.

2.3.1 Electrode machining for micro-EDM by TCMMP

The most commonly used TCMMP is the combination of WEDG and micro-EDM which has a wide application in machining of fine rods to be used for micro-drilling

which was first proposed by Masuzawa et al. (1985). WEDG employs a single wire guide to confine the wire tension within the discharge area between the rod to be machined and the front edge of the wire and to minimize the wire vibration. Therefore, it is possible to electrically grind a micro-sized rod (Masaki, T., et al., 1990(b); Masuzawa et al., 1997) with high accuracy, good repeatability and satisfactory straightness. Other advantages of WEDG include the ability to machine a rod with a large aspect ratio, irrespective of hardness of the material to be machined while maintaining the concentricity of the rod.

Lim, HS., et al. (2002) proposed a new compound micromachining technique on a specially designed multi-process machine tool whereby they used micro-turning process to fabricate very thin microshafts to be used as electrodes as opposed to the conventional WEDG technique and performed micro-EDM machining using this electrode. Using this technique they reduced the electrode machining time significantly facilitating micro-EDM drilling of holes with different diameters. This TCMMP has another additional advantage in that it does not require much operator's intervention and can mostly be automated due to a lesser likelihood of error compared to WEDG.

Localized electrochemical deposition method is suitable for electrochemical deposition in a predetermined and controlled area and was presented as one simple, inexpensive and damage-free ways to fabricate complex shape electrodes for micro-EDM process by Hunter et al. (1997). Later on, to further establish the capability of this process El-Giar (El-Giar et al., 2000; El-Giar et al., 1997) demonstrated the machining of micro-meter scale copper structures for micromachining applications from different substrates in acidic sulfate solutions by the process of LECD.

2.3.2 Microcutting tool machining using WEDG

Using the wire electro-discharge grinding (WEDG) process, successful machining of tiny electrodes has been reported (Kawakami, T., et al., 2005). This method was extended for machining of tungsten carbide micro-milling tools of diameter as small as 31μm (Chern, G. L., et al., 2007) as shown in Figure 2.8. The geometry of the fabricated micro-tool was designed to carry out a micromachining operation which is essentially a combination of micro-milling and grinding processes. The micro-EDMed surface of the micro-tool contains numerous tiny craters and asperities, arising from the micro-discharges, and these offer tiny cutting edges and can be well suited to perform machining operation similar to the grit abrasives on micro-tools in micro-drilling (Lee DG, et al., 2003). In addition to being cheap, this method has the capability to be performed in-situ and thus clamping error could be minimized, while there exists much scope to improve repeatability and precision. Figure 2.8(b) shows the three thin-walled structure of thickness 80μm, 31μm and 5μm. They observed severe deformation on the 5μm wall which they explained that was caused by machine tool vibration and lateral bending occurred by cutting forces during the machining operation.

Another process was proposed by Fleischer, J., et al. (2004), where they compounded WEDG and micro-milling. They demonstrated a promising way to produce micro-milling tools in tungsten carbide of diameter less than 100μm using WEDG which they used for machining micro-slots on brass with the same setup (Figure 2.9). The use of WEDG for production of milling tools has several advantages. The geometry can be changed quite easily and the potential of scaling down the size of the milling tools is

very high. Even though their results were promising there was clear indication, as mentioned in their article, towards the need for dedicated compound micromachining equipment for performing TCMMPs. They used a commercial micro-EDM machine (Panasonic MG-ED72W) which has a record of performing excellently for micro-EDM process but lacked rigidity and accuracy required of a micro-milling machine, as the equipment was not designed to perform micro-milling.

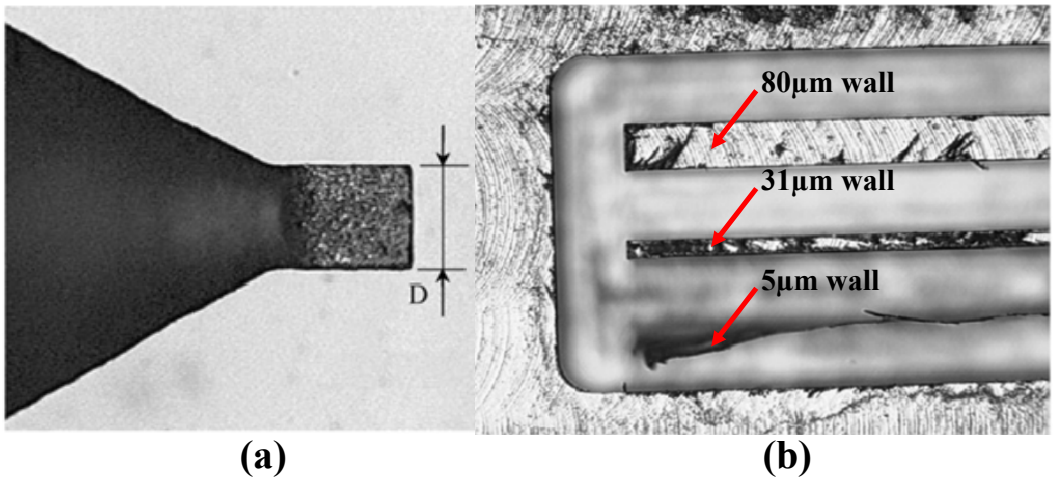

Figure 2.8 (a) Tungsten carbide micro-tool D=100µm, (b) machined micro thin-walled structure (Chern, G. L., et al., 2007).

WEDG process has been applied for machining of customized micro-drilling tools by Egashira, K., et al. (2002). He fabricated a 17µm diameter micro-drill with a D-shaped cross-section and cutting edge radius of 0.5µm in 5 minutes and machined 90µm deep hole of 22µm diameter on britlle material like monocrystalline silicon. They achieved comparatively accurate tool alignment and eliminated run-out since the process of tool machining by WEDG as well as the micro-drilling was carried out in-situ using a single setup. This study clearly indicated the potential that TCMMPs have in fabrication of micro-parts and MEMS components.

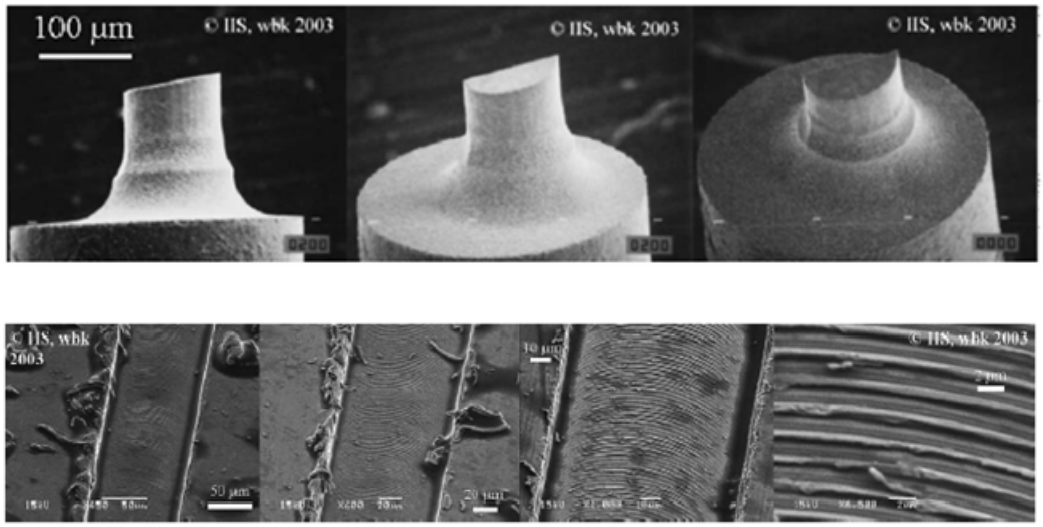

Figure 2.9 Top row shows micro-EDM machined milling tools in tungsten carbide, diameter 100µm and the bottom row shows machined slots on brass workpiece (Fleischer, J., et al., 2004).

Cheng, X., et al. (2008) developed a unique ultraprecision machine tool for tool machining using WEDM and ductile mode micro-milling using the fabricated tool. In their research work, in addition to process development, they have clearly highlighted the need to develop a dedicated machine tool for performing TCMMP. In their developed machine, they employed advanced control system to reduce vibration due to high acceleration and deceleration. They also developed a CAM system for the custom tool machining on the 6-axis machine tool where tool geometry could be defined to generate NC programs automatically and using this system they developed custom-designed micro-PCD cutters of 1 mm and 200µm in diameter. Using the fabricated tools, sophisticated miniature 3D geometric features were produced, which included a long 3µm wide curved rib of tungsten carbide with an aspect ratio of 10 was successfully machined in ductile mode, achieving the machined surface roughness R_a of less than 10nm and peak-to-valley R_y of less than 30nm.

2.3.3 TCMMP for micro-grinding

Micro-tools made of PCD offer new promise for micromachining hard and brittle materials. PCD consists of micrometer-sized diamond grains sintered under high temperature and pressure with metallic cobalt (Morgan, JC., et al., 2004). The cobalt fills the interstices between the diamond particles and forms an electrically conductive network. This conductivity makes PCD suitable for micro-EDM process and this provides an opportunity to fabricate micro-size micro-grinding tool. After shaping, the surface of a PCD tool contains protruding diamond grains that are randomly distributed, which can act as hard and tough cutting edges for micro-grinding. The feasibility of micromachining glass and ceramic materials with PCD micro-tools that are prepared in a variety of shapes using the non-contact micro-EDM process has been proposed by Morgan et el. (2004). The PCD tool contains randomly distributed protrusions of diamond with dimensions in the range of few microns that serve as the cutting edges for micromachining on glass. They found that in cases where the depth of cut was too large, brittle fractures around the edges of the grooves or pockets were observed and where the depth of cut was below brittle-to-ductile transition, brittle fractures were not apparent and ductile cutting marks were clearly evident on the machined surfaces, and PCD tools showed very little wear. During their experiment the tool was fabricated on a commercial micro-EDM machine (Panasonic MG-ED82W) but in order to meet the demand of nanometer level adjustments in the depth of cut, they installed an additional nanopositioning stage (Polytee PI Nanocube) on the micro-EDM machine.

Masaki, T., et al. (2007), presented further results in using PCD to accomplish the micro-shape grinding of micro-freeform surfaces. They fabricated a spherical PCD

tool by EDG with a pin gauge tool electrode made of tungsten carbide that was manufactured precisely by controlling its diameter and straightness. Using this spherical PCD tool fabricated on-machine they performed a series of micromachining of various shapes from flat, concave, convex to freeform machining and achieved mirror surface finish on tungsten carbide with surface roughness of 5nm R_a. On conventional machining center – ball endmills are used for milling of a variety of complex shapes. A ball endmill has a normal hemisphere and therefore four or five axis control is necessary to realize the high degree of freeform shaping and convex and concave shapes machining. They demonstrated that the micro-EDMed spherical PCD tool, which has innumerable cutting edges uniformly located along its entire surface, can be used for machining orthogonal micro-freeform shapes on XY and YZ plane using a 3 axis machining platform (Figure 2.10(a)). Figure 2.10(b)Figure 2.10 shows the concept of freeform machining using the on-machine fabricated spherical PCD tool (Figure 2.10(c)) and image of a shaped convex spherical surface on tungsten carbide is shown in Figure 2.10(d). In 2009, Chen, ST., et al., proposed another compound study for machining of diamond micro-grinding tool by using TCMMP. They presented a machining technique of micro-diamond tool which is 100μm in diameter and performed precise micro-grinding of miniature dies. They used a compound process technology involving WEDG and precision composite electroforming to fabricate micro-diamond tools for the micro-grinding of the micro-dies.

2.3.4 Surface improvement using TCMMP

The surface generated by micro-EDM is relatively rough compared to micro-ECM. On the other hand micro-ECM does not provide excellent shape control like micro-EDM. There exist few research efforts to improve surface roughness of micro-EDMed hole

using micro-ECM. T Kurita et al. (2001, 2005, 2006) proposed a machine tool where they performed three steps - electrode machining by milling, hole shaping by micro-EDM, and hole finishing by micro-ECM to improve surface roughness and these steps were performed in sequence on the same machine tool. He also proposed micro-EDM and micro-ECM-lapping complex process to further enhance the surface roughness from 1µm after micro-EDM to 0.06µm R_a after applying micro-ECM lapping.

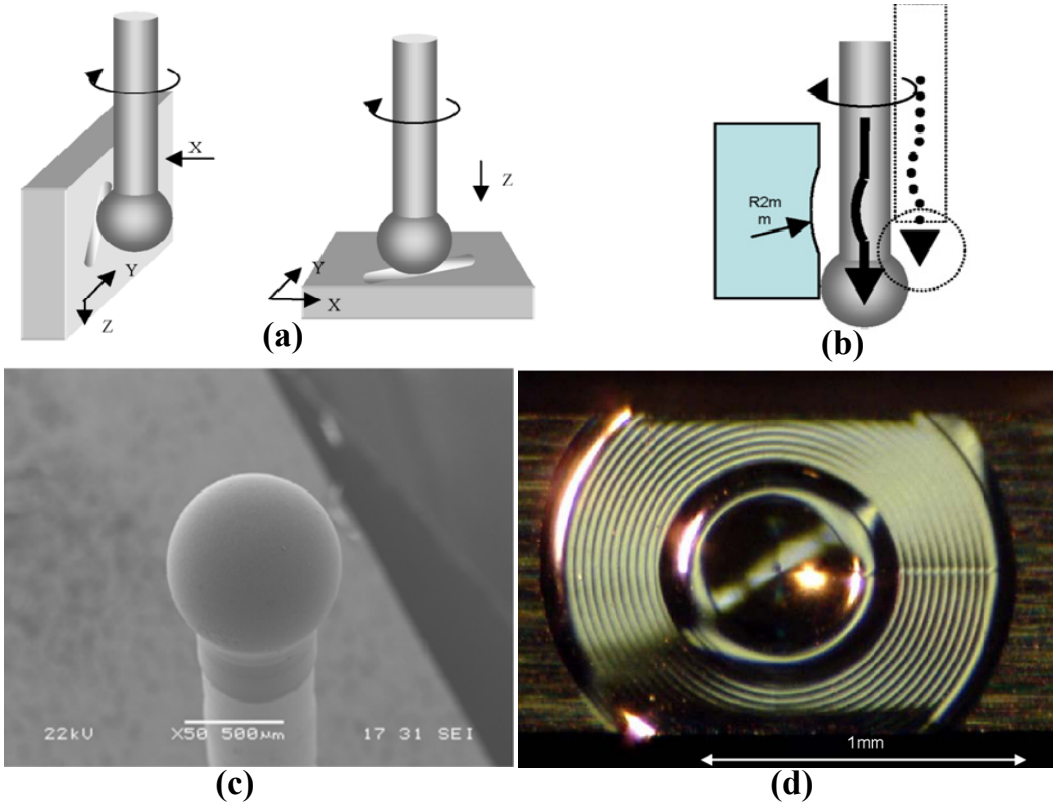

Figure 2.10 (a) The concept of machining on XY and YZ plane using a spherical PCD tool on a 3-axis machine, (b) concept of freeform surface generation, (c)on-machine fabricated spherical PCD tool and (d) machined sample of a shaped convex spherical surface on tungsten carbide (Masaki, T., et al., 2007).

Hung, JC., et al. (2006) published their study on combining micro-EDM and electro polishing to improve surface roughness of micro-holes. During the machining process, a tool was fabricated by WEDG directly and using it for micro-EDM of the micro-

hole, followed by electro polishing with the same tool but using a different location of the tool that was not used during the micro-EDM process. By the electro polishing method, high surface quality hole wall was obtained by applying a suitable electrolytic voltage and an appropriate concentration of electrolyte in about 5 minutes of machining time. The taper and burrs of the inlet of holes were reduced and the surface roughness reduced from 2.11μm R_{max} to 0.69μm R_{max} after electro polishing.

Masuzawa et al. (1994) proposed a compound process of micro-EDM, micro-ECM and electroforming for complex high-aspect-ratio micro-nozzle production (Figure 2.11) and demonstrated that this compound process can be used to fabricate a wider choice of complex shapes, instead of just straight rods, such as tapered and stepped shapes at various sections. In their study, they also proposed another TCMMP process, wire electrochemical grinding, which does not use any abrasive, as in the normal chemical grinding process, but is an electrochemical process with a setup similar to WEDG, by simply replacing electric discharge with electrochemical dissolution to provide better surface quality.

2.3.5 On-machine micro-assembly after micromachining

Kuo, CL., et al. (2003) proposed another exciting compound process in which they used micro-EDM to fabricate micro-parts followed by laser welding to micro-assemble 3D metal microstructures in the same setup. To illustrate the micro-assembly strategies and procedures, a diverse pin-plate metal microstructure was used and discussed in the study. They also demonstrated further machining on top of the 3D metal microstructures even after assembly. Using these procedures, diverse patterns, and

high-aspect-ratio and high joint strength microstructures can be created precisely, and these serve as examples of complex micromachining applications.

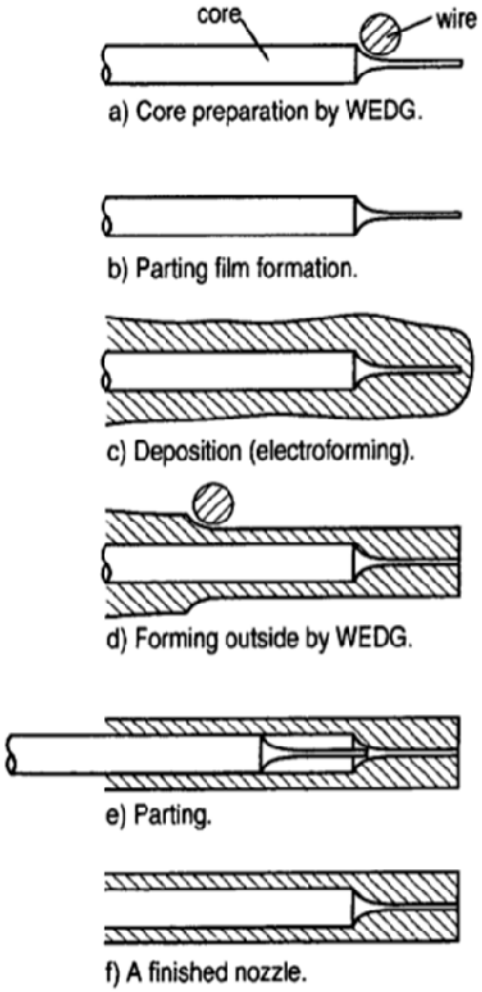

Figure 2.11 Processes involved in the fabrication of micro-nozzle (Masuzawa et al,. 1994)

Langen, HH., et al. (1995) introduced a method for machining and assembly of high-aspect-ratio microparts. Pins with a diameter of 100μm were produced by WEDG and connected into a thin plate using ultrasonic vibration for smooth insertion and finally ultrasonic bonding. They defined such a pin/plate assembly as a workstation which could work as tool workstation or subassembly workstation in a more compound assembly process. They used the tool workstation to machine the inside shape of a

workpiece by reverse micro-EDM to enable it for further assembly purposes and they considered the machining of a micro-ion beam emitter as an example.

2.4 Concluding Remarks

Even though tool-based conventional micromachining processes have several advantages over the present day semiconductor machining technologies for micromachining, they presently face significant challenges at such miniaturized dimensions. One of the main challenges has been posed by the cutting forces involved and therefore the full potential of having the theoretical unit removal capability of as small as 1 nm found from molecular dynamics simulation (Masuzawa, 2000) could not be practically realized.

The micro-EDM process has the advantage of machining with minimal cutting force but the main disadvantage is in the UR capability in addition to electrode wear and low material removal rate. Even though micro-EDM has always been considered as a potential candidate for micromachining applications, available machine tools and process characteristics are still not sufficiently effective and efficient to facilitate and control unit removal. In particular, the process characteristics are heavily stochastic in nature and the interaction between power supply and the spark characteristics has not been studied enough to elucidate the process parameter selection process.

A compound process involves a combination of processes of complementary strengths. There exist excellent research demonstrations that highlight the potential of compound micromachining, but most of them tend to be discrete exploratory work in nature, requiring customized machining setup and targeting for one particular application, and

hence is probably not suitably developed to serve industry-scale manufacturing needs. Therefore, the major difficulty in realizing TCMMP is the lack of machine tools capable of such multiple processes. Attempts have been made to perform TCMMPs by modifying a machine tool that is suitable for one process but has to be adapted for the complementary process which it consequently performs at a mediocre level (e.g. modification of a micro-EDM machine for micro-milling or micro-milling machine for micro-EDM). While the capability has been demonstrated but its full potential is neither realized nor received much industrial acceptance due to the setup being weak in providing equitable support to all of the involved processes (Cheng, X., et al., 2008; Chern, G. L., et al., 2007; Egashira, K., 2002; Fleischer, J., et al., 2004; Lim, HS., et al., 2002; Morgan, JC., et al., 2006). Most of the demonstrations in compound micromachining are also not from the lower dimensional scale (between 5µm~50µm feature size range) of the micromachining domain.

The above concluding remarks following the literature study point to the need for a dedicated platform for performing TCMMPs where compound micromachining could be fully realized. The following research plan aims to enable the bridging of the gap between discrete exploration of TCMMPs and industrially scalable applications in compound micromachining technology:

- An earlier developed UMMT (Rahman, M., et al., 2003) will be the targeted machine tool for this research as it has been specially designed for performing compound micromachining. It will be evaluated for conventional microcutting and for non-conventional micromachining like micro-EDM. Initial focus of this research is to provide a platform for tool-based conventional micromachining (like

micro-milling, micro-turning, micro-drilling and micro-grinding) and electric micromachining using micro-EDM for performing micromachining in the lower dimensional range of micromachining domain (between 5μm~50μm feature size range). These processes have been selected as it is evident from the literature that these processes are of highest potential for compound micromachining.

- The evaluation methods will be developed with the aim to assess the capability of machine tools for compound micromachining in the lower dimensional range of micromachining domain. The equipment will be further developed for performing at the state-of-the-art benchmark based on the above review.
- While precision, rigidity and repeatability of machine tool structure are the critical factors from the machine tool point of view for conventional micromachining processes; non-conventional micromachining processes like micro-EDM require advanced process control capability. Therefore, the focus will be given in researching on the process physics for understanding the interaction between power supply and plasma characteristic which will enable more fundamental understanding and assessment of the throughput, quality and minimum achievable feature size from micro-EDM process.
- TCMMPs will be demonstrated on the dedicated UMMT by generating and exploring new and novel process ideas and readily executing them. This will have the potential to bring a ready platform for exploration of compound micromachining ideas compared to the discrete exploration observed in the review of literature.

3 Performance Evaluation of UMMT

This chapter evaluates the performance of an UMMT developed by Rahman et al. (2003), for performing compound micromachining. The objective of the evaluation is to ensure that the UMMT is capable of performing in the feature size range of between 5µm~50µmin the micromachining domain. The first section of this chapter provides a brief description of the concept of UMMT. The second section evaluates the machine using ISO – 230/1 and 230/2 standards (ISO 230–1, 1996; ISO 230–2, 2006) and compares the result with the requirements asserted by the target of performing micromachining. The third section evaluates the dynamic performance of the UMMT by machining tests. The fourth section evaluates the response time and dynamic positioning of the Z-axis which is extremely important for the evaluation of gap control performance of the machine tool. The fifth section theoretically analyses the requirements of the micro-EDM power supply and evaluates the power supply of the UMMT against the requirements. The final section draws a conclusion on the capability and potential development areas of the evaluated UMMT to meet the requirements of performing micromachining between 5µm~50µm feature size range.

3.1 Design Concept of UMMT

There is much hardware duplication or commonality between different machine tools designed to be used for different processes. Die-sinking EDM and Wire Electric Discharge Machining (WEDM) machines can be considered as an example. They have a major part of the hardware in common e.g., X and Y axes of the machine, machine

bed, EDM power supply unit etc. The few main differences include the absence of a Z axis and a spindle unit, and the presence of a wire-running and wire-tension control unit in WEDM machine, compared to EDM machine. The UMMT developed at National University of Singapore (Rahman et al., 2003) has such units like spindle and wire guiding unit as a standard attachment which can be attached to configure the machine for a particular process and has the capability to perform non-conventional micromachining processes like micro-EDM, WEDM, WEDG in addition to tool-based conventional micromachining processes like micro-milling, micro-drilling and micro-turning on the same machine tool. Figure 3.1 showcases the machine tool with some of the processes that it can perform, Figure 3.2(a) shows the close up while configured with spindle unit for EDM and Figure 3.2(b) shows the machine tool configured with WEDM unit. For conventional machines a spindle unit or a wire guiding unit weighs more than few hundred kilograms. For the case of the UMMT that has been developed, such units weigh only a few kilograms, thus making universality of machine tool a practical and feasible solution for such machines.

Multiple processes on one machine enable significant reduction in investment which otherwise requires purchase of different machine tools and also correspondingly much more space required for the installation of the machines. Experiments suggest that the replacement of attachment requires less than half an hour to configure the machine for a different process. Several micromachining techniques, such as micro-EDM, WEDG, micro-WEDM, micro-milling, micro-turning and their combination, can be carried out using different spindle unit and different attachment on the same machine.

Figure 3.1 Showcase of Universal Miniature Machine Tool

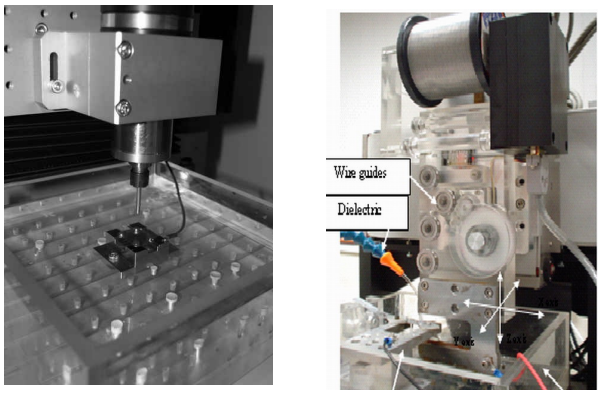

(a) Machine configured with spindle for EDM process.

(b) Machine configured with wire guide for WEDM process.

Figure 3.2 Machine configured for EDM and WEDM process

3.2 Evaluation of the UMMT

Evaluation experiments to determine the geometric accuracy, positioning accuracy and the repeatability of the UMMT have been conducted after upgrading the machine tool system with more rigid structure, better drive system and better servo feedback system. The evaluation has been conducted in accordance with ISO – 230/1 and 230/2 standard which includes the test code for machine tools. A list of the equipment used for the evaluation tests is given in Appendix A. Appendix B contains the details of the inspection item, inspection method and measurement results. The results indicate that with 3D dynamic compensation of positional accuracy of UMMT could be contained to less than 1μm over the full travel for all 3 axes. For the machining on small workpieces of ~20mm having feature size between 5μm~50μm, the positioning accuracy of the UMMT meets the requirements.

3.3 Dynamic Performance Evaluation from Machining Tests

The positioning accuracy measurement of the machine tool mentioned in section 3.2 does not test the machine during machining conditions while under dynamic loading (as per the ISO – 230/1 guideline). Fleischer, J., and Masuzawa, T., et al., (2004) performed TCMMP using a combination of WEDG and micro-milling. From their experimental results they identified that the Panasonic (MG-ED72W) micro-EDM lacked the required rigidity for micro-milling operation, even though the equipment is reputed to be one of the best-in-class for micro-EDM operation. Hence, Fleischer, J. et al., (2004) planned to perform the micro-milling operation on Kugler micro-milling machine (a machine well known for excellent performance for micromachining operation). Therefore, the UMMT was evaluated by performing cutting tests. For

cutting performance tests of the UMMT, machining has been performed using comparatively large sized tools (1mm diameter). This allowed evaluating the machine under much higher cutting force than the expected cutting force for micromachining operation to provide sufficient safety factor. A set of micro-milling and micro-drilling tests have been conducted. 3×10 array of holes positioned at 1mm apart were drilled on Cu plated epoxy using a 0.5mm drill bit to observe the positioning accuracy of the holes. Holes were drilled at a feedrate of 5 mm/min and 2800 rpm spindle rotation speed. The workpiece is shown in Figure 3.3 (a) and (b). The UMMT machined the holes with an average hole positioning error of less than 0.5µm. Micro-milling test was performed using a 0.5mm endmill cutter and 3 circles with an island of 0.5 mm, 1.0 mm and 1.5 mm were machined on the same workpiece at a feedrate of 10 mm/min, 20mm/min, 40mm/min, 80mm/min and 160 mm/min to observe the machine tool's performance during reversal of motion. The UMMT machined circles with less than 1.0µm error during reversal of quadrant without any motion reversal compensation being employed for up to 40mm/min as could be seen in Figure 3.3(c). Quadrant reversal error and tool deflection was observed at 160mm/min as could be seen in Figure 3.3(d). It was also observed at 80mm/min feedrate but to a lesser extent compared to 160mm/min. Many micro-milling and micro-turning operations are generally performed in the range of 1mm/min~60mm/min feedrate (Adams DP., et al., 2001; Fang F. Z., et al., 2003; Fang, F. Z., et al., 2006; Picard, YN, et al., 2003; Rahman, A., et al., 2005; Schaller, T., et al., 1999). Therefore, 160mm/min can be considered comparatively higher end of feedrate for micro-milling operations.

Comparing these results with other high end reputed micromachining machine tool (e.g., Kugler MICROGANTRY – Micro with positioning error ≤1.5µm), the observed

positioning error of ≤0.5µm and error at quadrant reversal of ≤1.0µm can be considered satisfactory. Additionally, as one objective of this research work is to perform micromachining between 5µm~50µm range and accuracy of present micro-EDM process technology is 1~2µm (Kawakami, T., et al., 2005; Kunieda, M. et al., 2005), the performance of this machine tool can be considered suitable for TCMMP need.

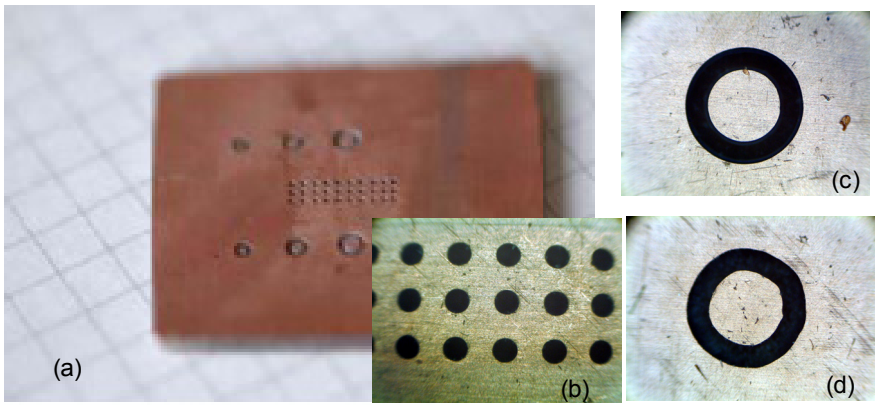

Figure 3.3 (a) Cu Plated PCB workpiece with machined holes (b) close-up of holes, (c) circle with island at 40 mm/min and (d) circle with island at 160 mm/min. While (c) does not show any significant error during quadrant reversal, (d) shows quadrant reversal error.

3.4 Evaluation of the Motion Controller for Gap Control

Along with the development of a precision mechanical structure, a specialized precision motion control system is another major requirement for a UMMT which needs to be evaluated. For micromachining, for example for having micro-EDM and micro-turning on the same system, the CNC system is expected to provide the function of synchronized servo feed control based on real-time monitoring of process control

parameters which are sometimes difficult to integrate into the conventional machine tool. For example, the accuracy and speed of micro-EDM process depends a great deal on the gap control performance of the motion controller (Lim, HS., et al., 2002; Lim, HS., et al., 2003). This might be sometimes very difficult to implement with a commercially available motion controllers.

Motion required for micro-EDM milling can be another example of special trajectory requirement. Due to tool wear, there exist serious issues in micro-EDM milling related to tool wear compensation, maintaining the tool shape from side wear while machining by only bottom wear, and control of the layer thickness to be machined. Therefore, quite a number of motion control strategies as well as wear compensation methods have evolved to handle such issues each with its unique advantages in specific situations (Bleys, P., et al., 2004; Bleys, P., et al., 2002; Hang, G., et al, 2006; Lim. H.S., et al., 2003; Yu, Z. Y., et al., 1998). To cater to all such different algorithms with the concern that a little delay in the sampling of the gap voltage can result in breakage of the fine electrode used (Kunieda, M. et al, 2005) an open architecture motion controller has been adopted which can be programmed at the embedded level to provide necessary trajectory control of the machine tool. The controller has a multi-processor-based design, where programs and scheduling can be developed for real-time process control accordingly so as to meet the synchronized servo motion required for some of the micromachining processes. At the same time, since the motion controller was developed jointly by NUS and an NUS venture company (Mikrotools Pte Ltd) for the multi-process machine tool, programs and scheduling can be accessed and developed to meet the time critical requirements, which is a key development area

for micromachining processes. For example, process parameter sampling can be done as fast as a 20 KHz rate, while still managing other job schedules.

Practically, the mechanical system performs slower in the order of magnitude compared to the maximum speed that the commands could be issued when the requirement is reversal of motion or sudden change in speed with high acceleration. Fast reversal movement is required for the gap control during micro-EDM process and the servo system has been tested to have a rise time of less than 30ms, which is found to be sufficient for gap control during micro-EDM process without using a fast linear actuator (Imai, Y., et al., 2004; Kunieda, M., et al., 2004; Lim, HS., et al., 2003). Figure 3.4(a) shows a plot of reference position and servo response position and following error against time. The data was captured at a 2ms sampling rate and motion command is issued at 100ms interval to move the Z axis upward by 50µm in every step at 80mm/min. The machine responds to the command within 10ms and settled within less than 1µm position error within 20ms and eventually reached the target within 80ms. Given that, even at lower range of micro-EDM power settings the electrode gap is around 1.20µm (Table 4.1) and a common setting of micro-EDM feedrate is 2µm/s (Masaki et al., 2010(b)) this response can be considered satisfactory for micro-EDM gap control operation.

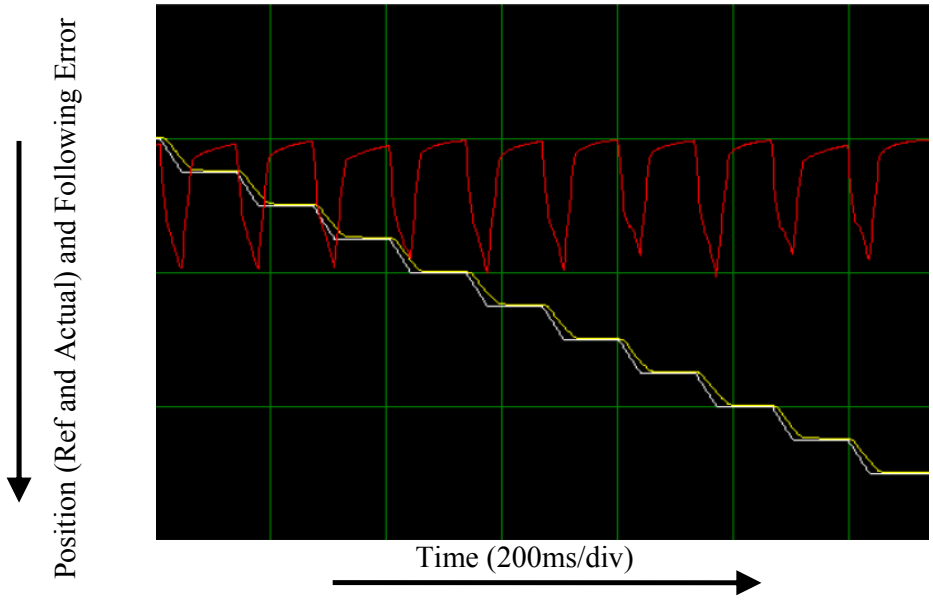

Figure 3.4 Commanded position (white line), actual position (yellow line) and following error (red line) vs time to obtain the response and settling time. The scale along base axis is 200ms/div, along secondary axis is 200µm/div for reference and actual position; and 10µm/div for following error.

3.5 Theoretical Evaluation of Micro-EDM Power Supply

While precision, rigidity and repeatability of machine tool structure are important factors from machine tools point of view for conventional micromachining processes, non-conventional micromachining processes, like micro-EDM, requires advanced process control capability in addition to the required performance of machine tool structure. For example, to realize precision micromachining one important factor is that the UR should be minimal which the volume or the size of the part removed from the workpiece by one unit of the removal phenomenon. For example, in mechanical operations, the UR consists of the feed pitch and cut depth and length corresponding to one chip of material removed (El-Hofy, H., et al., 2002) and in micro-EDM, the UR is a crater produced by one pulse of discharge (Masuzawa et al., 2000; Masuzawa et al. 1997). To minimize the UR in micro-EDM the pulse shape needs to be controlled such that less energy is discharged in every pulse as opposed to the mechanical cutting

processes where the UR consists of depth of cut, feed pitch and the cut length corresponding to the chip. Since UR controls the surface roughness, the smallest machinable feature size, accuracy of feature control and machining quality, the amount of energy released in every spark, determines such output parameters in micro-EDM. The UR of micro-EDM is quite big but cutting force is very small. Therefore, for micromachining by micro-EDM, it is essential to minimize the spark energy released from each spark to achieve smaller UR, which will result in smaller machinable feature size and finer surface roughness. But in addition to that, it is also important to maintain high machining throughput by increasing the material removal frequency, and in micro-EDM the number of sparks over a period of time needs to be increased that can vary significantly because of the spark condition.

Given the target of this research project is on micromachining in the range of 5µm~50µm feature it is important to critically analyze the requirement of the power supply by highlighting the relationship of pulse energy and achievable feature size. The minimum feature size attainable by a micro-EDM setup coupled to the spark energy delivered in every quantum can be estimated by simple knowledge of the every crater at the spark energy being employed. It is postulated that feature size is unachievable when there is no material left in some places of a machined feature because of overlapping of valleys from one surface with the valleys of the adjacent surface and therefore, minimum attainable feature size can be estimated from the accuracy of the motion control system over the feature size length and a delta amount added to two times R_z – average distance between the highest peak and lowest valley formed from the spark energy provided by the power supply settings (Moylan, SP., 2005). This has been illustrated in Figure 3.5, taking the case of machining a vertical

wall as a feature and therefore, milling micro-EDM is required to be performed on both sides of the wall. In the schematic, a top view of a wall is shown, which experienced micro-EDM on both sides of the wall. When the two rough surfaces overlap, as in the second case Figure 3.5(b), the machined structure becomes discontinuous because of overlapping of valleys causing formation of holes in the wall, resulting in an unsuccessful machining of the feature. From this illustration it can be observed that the target crater depth R_z needs to be as small as possible and preferably below 2μm to obtain small feature size which requires the micro-EDM power supply of the UMMT to be capable to provide this range of fine spark size.

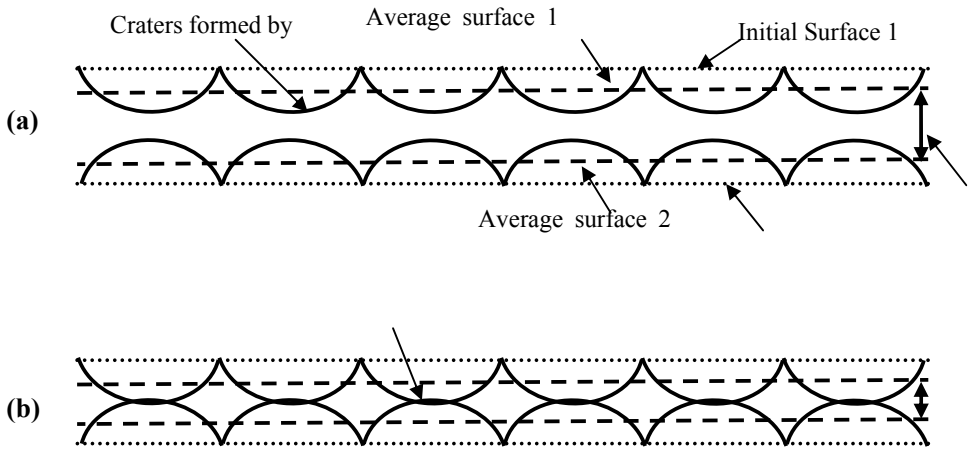

Figure 3.5 Schematic showing the simplified estimation of minimum achievable feature size from crater size of micro-EDM, (a) shows the top view of a case of forming a thin wall by micro-EDM milling on both sides of the wall and, (b) shows failure in machining due to the expected wall thickness being smaller than 2 times of average crater size (Moylan, SP., 2006).

3.5.1 Types of micro-EDM power supply

There are two major types of micro-EDM power supply, namely Resistance-Capacitance (RC) or Relaxation type and Transistor type power supply (Figure 3.6), The RC based power supply has found widespread applications in micro-EDM, and is

somewhat a rebirth after being replaced by transistor type power supply for conventional EDM power supply (Han, F., et al., 2004; Hara, S., 2001; Kunieda et al., 2005; Kunieda et al., 2004; Masahiro et al., 1995; Masaki et al., 1990(a and b); Masaki et al. 1989). In transistor type power supply the discharge energy in every spark is controlled by the resistance across the circuit and the voltage (V and R in Figure 3.6(a)) and UR in transistor type power supply is minimized by increasing the resistance as at very low voltage settings (less than 60 V) results in unstable discharges (Masaki et al, 1990 (a)). Spark energy obtained from a single spark in transistor type power supply is given by equation 3.1 (Son et al., 2007).

$$E_d = V\, i T_{on} \tag{3.1}$$

where, E_d is the discharge energy, V is the applied voltage, i is the discharge current and T_{on} is the pulse on time of the transistor.

In an RC or relaxation-type circuit, discharge pulse duration is dominated by the capacitance of the capacitor and the inductance of the wire connecting the capacitor to the workpiece and the workpiece to the tool, (Rajurkar et al., 2006; Rajurkar et al., 2000); and the discharge energy is determined by the used capacitance and applied voltage. In the case of typical RC type power supply shown in Figure 3.6(a), the repetition of the charging discharging occurs in which capacitor C is charged through resistor R and discharged between the electrode and workpiece produces an extremely short width pulse discharge. The pulse energy E_d induced in the gap is calculated by using the formula of equation 3.2 (Masuzawa, T., et al., 1997; Masaki et al., 1990 (b)), assuming that the gap voltage V_g is constant during the discharge.

$$E_d = 2CV_g(V - V_g) \tag{3.2}$$

where, C is the discharge capacitance and V is the supplied DC voltage. When $V=2V_g$, the discharge energy is the maximum $1/2CV^2$, which is equal to the energy stored in the capacitor. For a more realistic case, the RC type pulse supply will also have stray capacitance contributed by the electric feeder, the tool electrode holder and work table, and between the tool electrode and workpiece. The stray capacitance contributes in parallel to the installed capacitor and equation 3.2 gets modified to the following equation:

$$E_d = 2(C_1 + C_2)V_g(V - V_g) \tag{3.3}$$

where, C_1 is the stray capacitance and C_2 is the installed capacitance. This means the minimum achievable discharge energy per pulse is determined by the stray capacitance when C_1 is set to 0, and thus in order to reduce the pulse energy, it is important to reduce the stray capacitance between the wire and the workpiece. Stray capacitance can be estimated by integrating the area under the voltage and current waveform or by extrapolating the capacitance value for discharge current pulse width at stray capacitance (Masaki, 2010(a)).

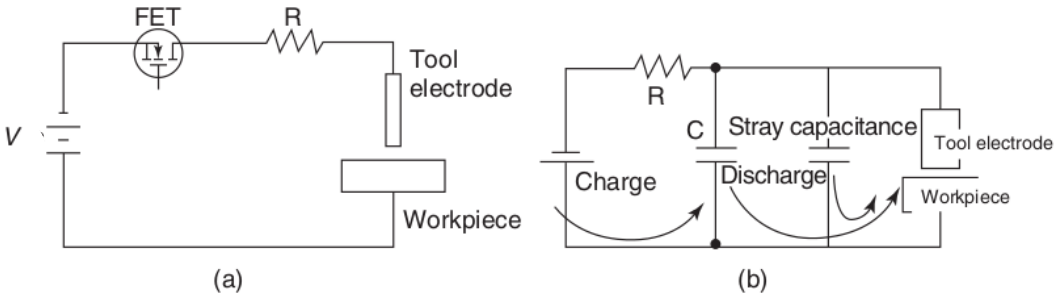

Figure 3.6 Schematic representation of basic circuit diagram of (a) transistor-type and (b) RC -type power supply.

3.5.2 Theoretical evaluation of smallest discharge energy

- Let us consider our smallest UR is craters with diameter 2µm for micro-EDM, which means the smallest volume removal is equal to the volume of a hemisphere having diameter 2µm which is the size of the crater formed. Thus UR is given by equation 3.4 below:

$$V_{UR} = \frac{1}{2} \times \frac{1}{6} \times \pi d^3 = 2.094 \times 10^{-18} m^3 \tag{3.4}$$

- Let us consider SUS-304 as the workpiece material with the following thermo physical properties (Wong, YS., 2003):
  - density, ρ = 8000 kg/m^3;
  - specific heat capacity, c_p = 500 J/kg ◦C;
  - ambient temperature, T_0 = 20 ◦C;
  - melting point temperature, T_m = 1450 ◦C;
  - boiling or vaporization temperature, T_b = 3000 ◦C;
  - latent heat of fusion or melting, L_m = 300 kJ/kg;
  - latent heat of vaporization, L_v = 6500 kJ/kg;

- Wong et al., 2003 derived the following equation (3.5) and equation (3.6) for micro-EDM using the theory of calorimetry

$$\begin{aligned} H_v &= \int_{T_0}^{T_m} c_p dT + L_m + \int_{T_m}^{T_b} c_p dT + L_v \\ &= c_p[(T_m - T_0) + (T_b - T_m)] + L_m + L_v \end{aligned} \tag{3.5}$$

$$H_m = \int_{T_0}^{T_m} c_p dT + L_m = c_p(T_m - T_0) + L_m \tag{3.6}$$

Equation (3.5) provides the estimation of minimum energy required to vaporize the cathode material per unit volume and equation (3.6) estimates the minimum energy required to melt the cathode material per unit volume.

- Using the above equations 3.5 and 3.6 energy for smallest UR can be estimated. If all the material removal is by melting of the material then the required energy is 16.965nJ considering that the shape of the crater is hemisphere. Similarly, if the removal action is solely vaporization of material then the required energy is around 138.86nJ.

- Wong et al. (2003) explained that only a maximum of 20% of material is removed by vaporizing the molten metal at low energy settings. At the same time considering that in lower energy discharge even though the erosion efficiency is much higher than the higher energy erosion efficiency, practically achievable maximum erosion efficiency, η, is only around 0.4 (considering a spark gap between 1 to 3.5μm) and therefore, the discharge energy per spark needs to be below 100nJ. Additionally, multiple continuous spark contributes to the creation of a single crater at low energy settings with very fine discharge pulse (Masaki et al., 2010a) – a simple estimation is that the power supply should have the smallest energy settings around 30nJ~50nJ.

3.5.3 Evaluation of micro-EDM power supply of UMMT

The UMMT is installed with a transistor type power supply with the range of settings shown in Table 3.1. With the given parameter ranges of the micro-EDM power supply the smallest discharge energy could be obtained at 75V with 100Ω resistor with

transistor-on-time set to 1μs. Using equation 3.1 the smallest discharge energy provided by the power supply can be estimated to be around 56.25μJ. This energy is about 2000 times larger than the energy requirement established in section 3.5.2. Figure 3.7 shows the entrance view of a feature machined using a square electrode at the smallest energy settings of the transistor-based power supply of the UMMT. It shows that the discharge energy is very large and there is a significant amount of re-solidification of the molten material which is common in long discharge pulse. From this it is evident that the micro-EDM power supply of the UMMT requires significant modification or replacing the power supply with a RC-based power supply setup with a DC source is another choice for performing at the desired range of machining at the lower boundary of micromachining domain.

Table 3.1 Parameter settings of the transistor type micro-EDM power supply

Parameter	**Settings Range**
Voltage (V)	2 settings – 75V and 150V
Resistance (Ω)	6.8, 15,33, 100
Pulse ON time (μs)	1μs ~ 100μs with 1μs increment
Pulse OFF time (μs)	1μs ~ 100μs with 1μs increment

While RC type power supply has the potential to provide extremely high frequency of pulse rate with discharge energy as small as provided by the stray capacitance alone, it has quite a number of disadvantages compared to transistor type power supply (Kunieda, M., et al., 2004; Han, F., et al., 2004). While extremely low discharge energy is expected from the power supply during finishing condition, high discharge energy and faster machining rate for rough cut is expected. On RC circuit, discharge energy by increase in capacitance value and discharge frequency has inversely

proportional relationship. This is mainly due to the reason that when capacitance is increased to increase discharge energy the charging up time of capacitor becomes higher thus minimizing discharge frequency (as more time is needed for the circuit before the next spark can occur). However, for most micro-EDM application the material to be removed is generally much smaller compared to the requirement of large material removal amount for conventional EDM. Another problem is - uniform surface finish is difficult to obtain because the dielectric breakdown can occur at any stage and during the capacitor charging up phase if a suitable condition is produced a half charged capacitor can discharge as well. This causes variable discharge energy and results in different crater size and variable surface roughness (Kunieda, M. et al., 2005). Thermal damage occurs easily on the workpiece if the dielectric strength is not recovered after the previous discharge and the current continues to flow through the same plasma channel in the gap without charging the capacitor (Han, F., et al., 2006).

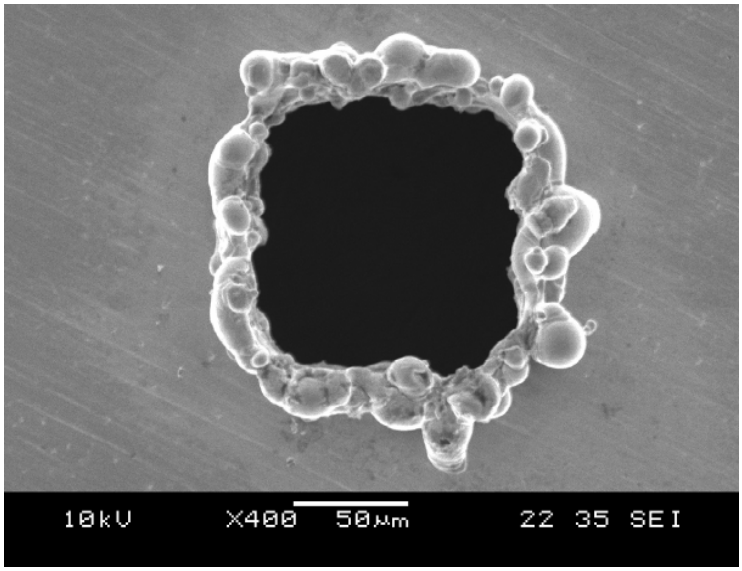

Figure 3.7 Machined hole using square electrode at the lowest energy setting of the transistor based micro-EDM power supply of the UMMT.

On the other hand, the transistor type power supply is widely used in conventional EDM where UR can be much higher and provides much higher MRR as there is no need to charge any capacitor. The pulse duration and discharge current can arbitrarily be changed depending on the machining characteristics required and can provide for very uniform pulse shape resulting in much better control of surface roughness. One option for modification of the transistor based power supply for lower energy settings can be done by employing high speed transistor to reduce pulse ON time which will also pave for higher discharge bandwidth by minimizing the OFF time and at the same time ensure discharges with equal discharge duration. By using a transistor capable of providing 10ns ON/OFF time the lower energy can be reduced by 100 times to 560nJ discharge pulse energy. But, this is probably the best achievable improvement as increasing the resistor significantly more than 100Ω will reduce the peak current. For instance, using a 2kΩ resistor will allow for reduction of pulse discharge energy by another 20 fold reducing the discharge energy to the expected range around 28nJ but practically this will also reduce the peak current to 37.5mA which may not be even sufficient current for breakdown of dielectric and holding the plasma. On the other hand with the same amount of discharge energy one with higher peak current and short time width will have higher proportion of material removed by vaporization compared to a pulse with smaller peak current but larger pulse width which can be explained by considering a disk heat source based electro-thermal model (Yeo et al., 2008; Dibitonto et al., 1989). Over longer spark duration but with the same amount of energy delivered – there is sufficient time for the heat to get conducted and proportion of material removal by melting action is higher compared to vaporization. On the other hand with very short pulse there is rather less time for heat conduction through

workpiece. Due to higher energy density (as the width is smaller, but the energy is equal) there is more energy to raise temperature as well as to provide for the extra energy needed for latent heat of vaporization, thus increasing the proportion of removal by vaporization. Higher proportion of material removal by vaporization is preferred r as that will have less solid debris, less re-solidification and smaller crust layer. Therefore, the choice remains to use RC-based power supply for extremely small discharge with present state of design options using transistor-based micro-EDM power supply.

3.6 Conclusion

From the evaluations of the UMMT performed in this chapter it can be concluded that the performance of cutting test, accuracy and rigidity can be considered sufficient for performing micromachining at the lower boundary of the micromachining domain. This can be concluded by comparing the results with micromachining machine tool that are well known for performing micromachining (e.g., Kugler MICROGANTRY - Micro) and other micro-EDM machine tool (e.g., Panasonic, Sarix, Agie, Pacific Controls) (Moylan, SP., 2006). Additionally, as one objective of this research work is to perform micromachining between 5µm~50µm range and accuracy of present micro-EDM process technology is 1~2µm (Kawakami, T., et al., 2005; Kunieda, M. et al., 2005), the performance of this machine tool can be considered satisfactory. Definitely, there are significant scopes of further improvement by utilizing advanced control mechanisms, such as using a piezoelectric translator with short stroke but with quick response for improved gap control; and use of hydrostatic/aerostatic linear guideway for even better precision and accuracy in motion. But, the primary research work required to achieve the objective of this project is in micro-EDM. There is a need for

significant improvement on the micro-EDM power supply of the UMMT as the smallest discharge energy is too large for performing micromachining and therefore, also not suitable for compound micromachining as has been explained earlier. As RC power supply is capable of providing small discharge energy, small pulse width and sharp peak current in a very simple manner it is preferred over the transistor-based power supply. The following chapter will provide a theoretical analysis on the electric characteristic of RC-based micro-EDM power supply employing plasma property which is necessary for designing RC power supply capable of performing micromachining at the lower boundary of micromachining range.

4 Analysis of Micro-EDM Electric Characteristics Employing Plasma Property

Plasma in EDM process is generated by an electric breakdown in the gap space filled with dielectric under a condition when the electric field strength exceeds the dielectric strength of the dielectric; and finally this ignition process leads to a subsequent current flow that generates an electric discharge. Usually in EDM process a direct current (DC) voltage is applied to the electrode system, namely electrode and workpiece, consisting of parallel plates of area defined by the common area on both the electrodes facing each other across a couple of microns gap. The objective of this theoretical analysis is to model the electric properties of micro-EDM plasma for an RC power supply circuit with a DC source since it was observed in Chapter 3 that the UMMT requires improvement in micro-EDM power supply. The analysis and understanding developed through the model proposed in this chapter will considerably leverage the design of a power supply fitting the appropriate role of all of the three components Resistance (R), Inductance (L) and Capacitance (C).

4.1 Electrical Equivalent Network of micro-EDM Plasma

The two parallel electrode plates across which the EDM plasma forms is shown in Figure 4.1(a) (Lieberman, 2005) where due to a very high electric field strength initially a weakly-ionized channel forms which then rapidly grows from one electrode to the other and results in primary electron avalanche starting from the cathode. Subsequently this forms a streamer as the initiation of a discharge process as could be

seen in Figure 4.2 (Descoeudres, 2008, Descoeudres, A., 2006). During the discharge process the electrons will have thermal energy of a few eV to bring atoms into excited states and from the collision process dielectric molecules gets dissociated which finally forms plasma to conduct current with very high current density. Even though the usual RC based micro-EDM circuit is powered by a constant DC power supply, the presence of the large series resistor limits the current flowing into the channel. Most of the power dissipated in the plasma is supplied by the capacitor placed in parallel to the plasma and therefore micro-EDM discharge can be compared to the commonly used capacitive discharges in plasma engineering (Piel, 2010) as opposed to other type of discharge known as inductively coupled plasma discharge where the electric field is generated by a time-varying magnetic field of transformer action.

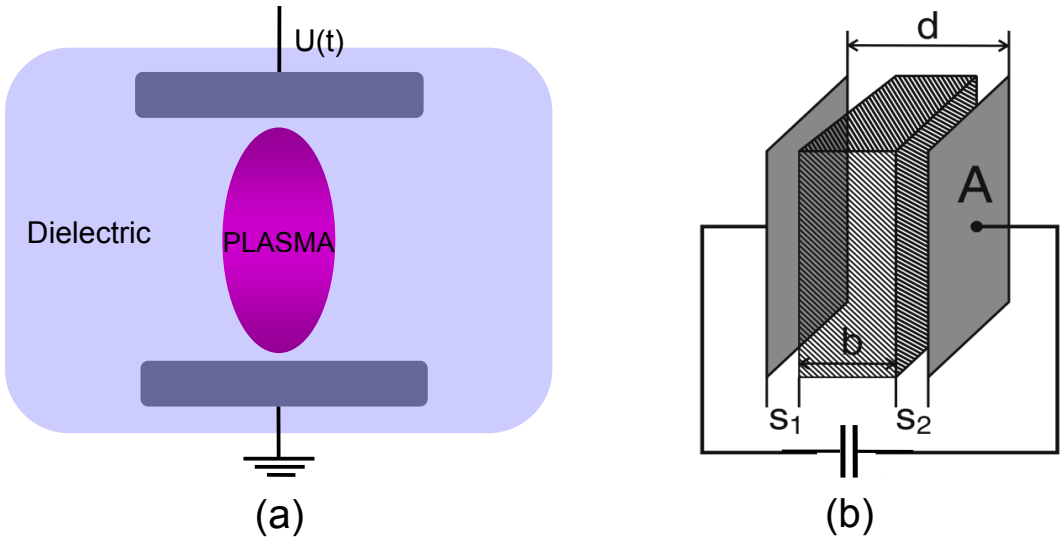

Figure 4.1 Parallel Plate Model of micro-EDM Plasma.

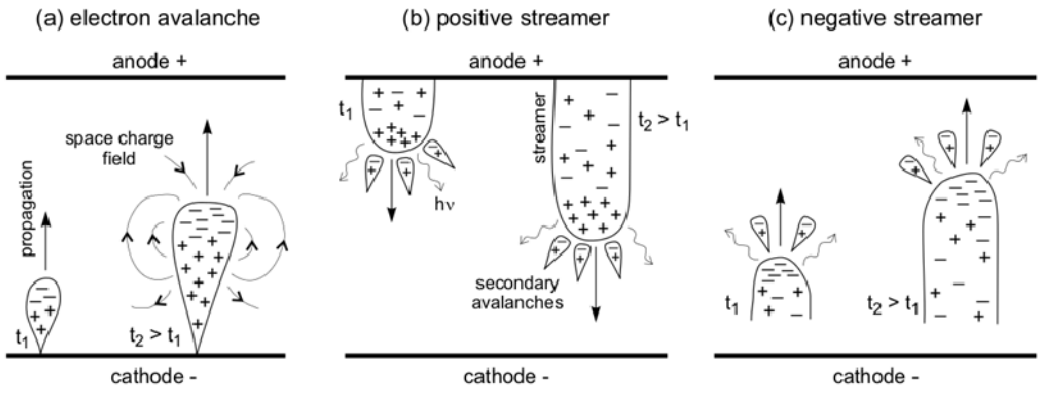

Figure 4.2 Breakdown mechanisms leading to a spark discharge. Propagation of: (a) the primary electron avalanche; (b) a positive streamer; (c) a negative streamer (Descoeudres, A., 2006; Raizer, YP., et al., 1991).

In capacitive discharge, obviously, the electric field results from surface charges on electrodes and charges in dielectric filling up the gap space. Figure 4.1(b) shows the homogeneous model of plasma (Lieberman, 2005; Piel, 2010), where the plasma is divided into a central quasineutral bulk of thickness b and space charge sheaths of width s_1 and s_2. A current i flows across the discharge plates and the plates are separated by a distance $d = b + s_1 + s_2$ and having cross sectional area A. In response to the current flow, a discharge plasma forms between the plates, accompanied by a voltage v across the plates and a power discharge P into the plasma. Assuming that the plasma is in a quasineutral state, it can be considered that almost everywhere the electron density and ion density are equal, *i.e.* $n_e \approx n$. In this given model it is also considered that the sheath regions are much smaller compared to the width of the bulk plasma; $b >> (s_1 + s_2)$. According to this model the plasma impedance is defined as the ratio of voltage and current for current flow in a capacitor given by equation 4.1 (Piel, 2010; Rizzoni, 2005).

$$Z_b = \frac{U_b}{I_b} = \frac{1}{i\omega C_b} \tag{4.1}$$

where, U_b is the voltage across plasma, I_b is the current through the plasma, C_b is the capacitance of the plasma, $C_b = \varepsilon_b C_0$; and C_0 is the vacuum capacitance of a capacitor given by $C_0 = \varepsilon_0 A/d$. ε_0 is the dielectric constant of vacuum, ε_b is the plasma dielectric constant which is given by equation 4.2 (Lieberman, 2005).

$$\varepsilon_b = 1 - \frac{\omega_{pe}^2}{\omega(\omega - j\nu_m)} \tag{4.2}$$

In equation 4.2 ω is the angular frequency of the oscillation of plasma, ω_{pe} electron plasma frequency and ν_m is the effective electron-ion collision frequency for momentum transfer. Using the value of C_b and ε_b, finally the bulk plasma containing two parallel electrodes can be represented by a combination of an inductor (representing electron inertia) in series with a resistor (representing electron-neutral collisions), and a parallel capacitor (representing the electric field in the bulk plasma) and could be expressed by equation 4.3 (Piel, 2010).

$$\frac{1}{Z_b} = j\omega C_0 + \frac{1}{R_b + j\omega L_b} \tag{4.3}$$

where, C_0 is the vacuum capacitance, L_b is the inductance of the bulk plasma given by equation 4.4 and R_b is the resistance of the bulk plasma given by equation 4.5.

$$L_b = \frac{1}{\omega_{pe}^2 C_0} \tag{4.4}$$

$$R_b = \nu_m L_b \tag{4.5}$$

In equation 4.4, electron plasma frequency is denoted as $\omega_{pe,}$ which can be evaluated using equation 4.6; and ν_m is the effective electron-ion collision frequency for momentum transfer.

$$\omega_{pe} = \sqrt{\frac{n_e e^2}{\varepsilon_0 m_e}} \tag{4.6}$$

where, m_e = mass of electron, n_e = electron density in plasma, ε_0 = vacuum permittivity, and e = charge of electron. Now from the above discussion, the network shown in Figure 4.3(a) can be considered as the electric circuit equivalent of plasma and can be replaced as the plasma in the electric network of power supply circuit shown in Figure 4.3(b). In Figure 4.3(b), R_d is the Resistance of the discharge line including the resistance of the cable, L is the inductance of the discharge path, C is the capacitance of the installed capacitor including the stray capacitance and R is the resistance of the resistor installed after the DC source.

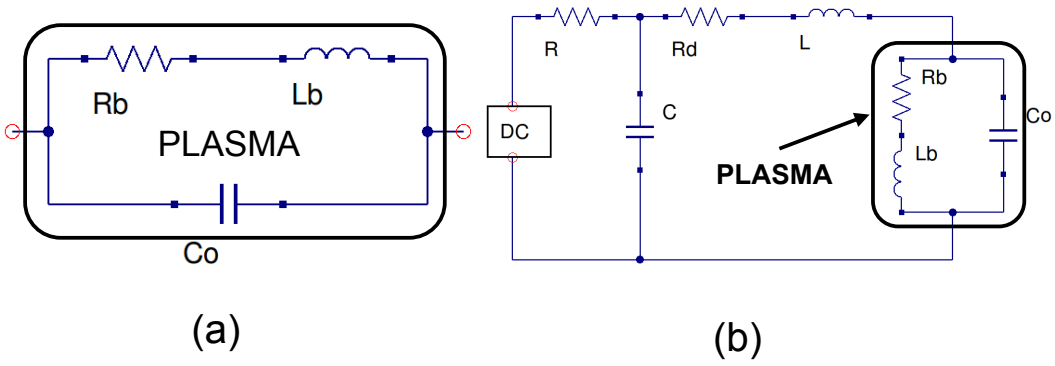

Figure 4.3 (a) Electrical equivalent circuit of plasma, (b) electrical network of RC power supply with a DC source having micro-EDM plasma replaced by the equivalent circuit.

4.2 Evaluation of Electric Components in Plasma

4.2.1 Evaluation of C_0

C_0 is the vacuum capacitance of a parallel plate capacitor with an Area of cross section A and a distance between the capacitor d, as shown in equation 4.7.

$$C_0 = \varepsilon_0 \frac{A}{d} \tag{4.7}$$

Table 4.1 below shows values of experimentally obtained electrode gap at spark for Tungsten electrode and SUS-304 workpiece in Total EDM 3 dielectric oil with a simple implementation of RC setup without any gap control and was performed on the UMMT proposed by Rahman et al. (Rahman, 2003). Since, the theoretical analysis and the experimental works of this thesis is focused on the context of micromachining in the lower dimensional range of micromachining domain, practically the maximum applied voltage can be 100V~110V and capacitance is 470pF and the electrodes will be between 20µm~40µm diameter. From Table 4.1 and above argument a fair assumption can be made that the value of d will be between 1.2µm~6µm and the range of cross section area A will be a theoretically bounded by the surface area of 20µm~200µm diameter plate for the range of voltage and capacitance settings.

Figure 4.4(a) shows plot of C_0 at different gap distance d and ranging between surface area of 20µm~200µm electrode diameter. The maximum obtained value of plasma capacitance is only 0.2782pF in the simulation range which is even 20~30 times smaller compared to stray capacitance of the system and electrode holder (Masaki, 2010a). Practically, the value of C_0 is even smaller as during the discharge the plasma only forms over a small portion of the electrode and not the common cross section on

the electrodes facing each other. Descoeudres et al. (2008) reported that the contact surface between the plasma and the electrodes can be estimated to be equal from measurements of crater diameter, which was ~10μm. Their experiments were conducted at a much higher power settings compared to the usual power settings for micro-EDM (Masaki, 2010a) where the crater sizes ranges from 2.2μm to 5μm. Practically, since the plasma temperature in micro-EDM is extremely high and much higher than the boiling temperature of SUS-304, electrode plasma interface diameter can never be larger than the crater size as at the interface of plasma and electrode definitely erosion of metal will occur rendering the electrode plasma interface diameter to be slightly smaller or equal to the crater diameter, r (Descoeudres, 2008). Therefore, it can be assumed that the interface diameter is 0.1μm~0.2μm smaller than the crater diameter. Figure 4.4(b) shows the plot of C_0 at different gap distance d and ranging between surface area equaling to the electrode plasma interface diameter of 2μm~5μm and this resulted in a capacitance value of 1.7385×10^{-04} pF making at approximately 35,000 times smaller than the stray capacitance. Therefore, it can be concluded that C_0 in micro-EDM plasma with the electrode dimension and electrode gap at spark mentioned above can be really small and in analyzing the electric interaction with the capacitance C_0 can be ignored.

Table 4.1 Gap width at different voltage and capacitance

Voltage (V)	**Capacitance (pF)**	**Electrode Gap (μm)**
60	Stray (11pF)	1.20
60	470	3.30
100	Stray (11pF)	3.30
100	470	5.90

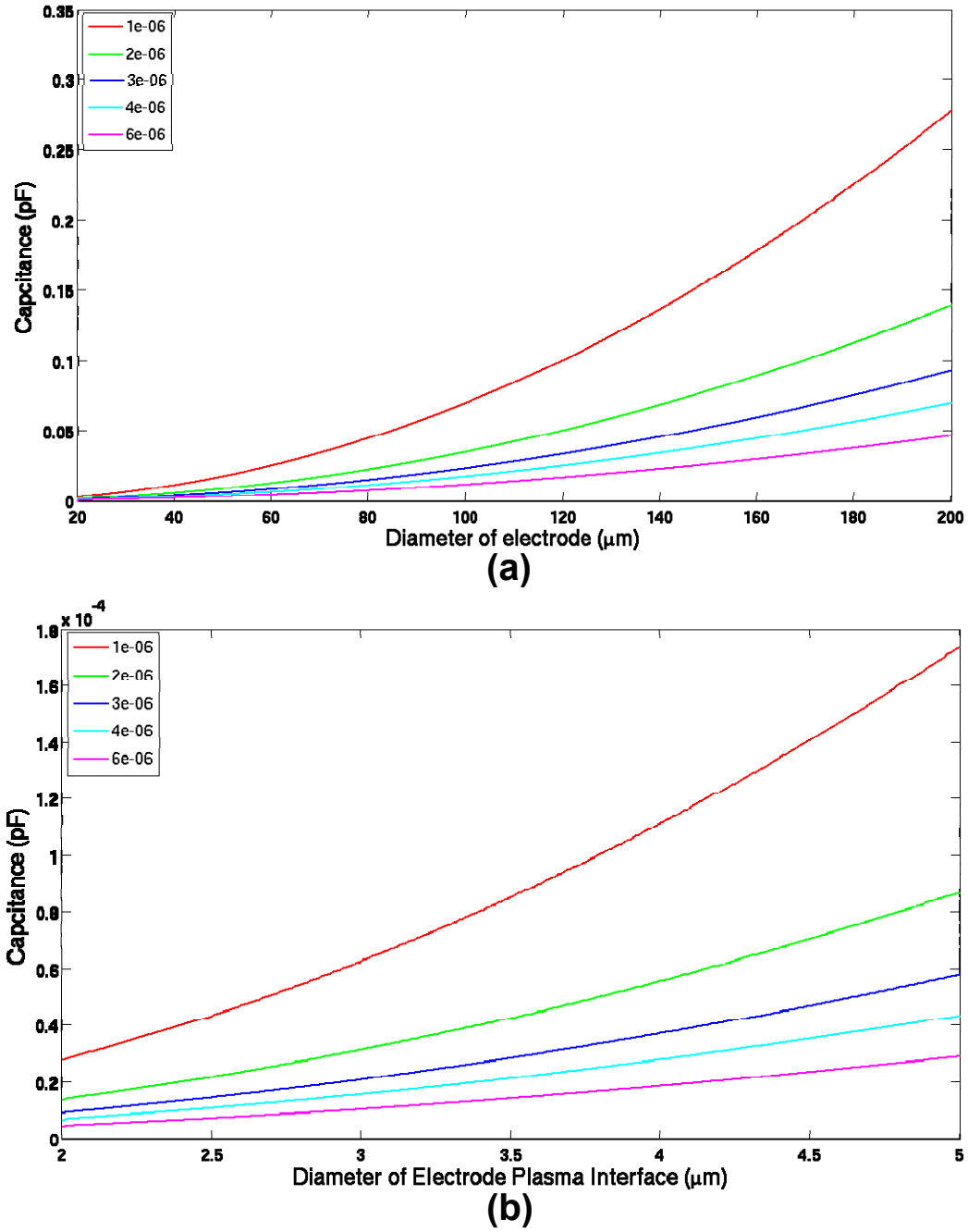

Figure 4.4 (a) Plot of plasma capacitance vs electrode area at different electrode gap; (b) the effective area contributing to the capacitance is taken as the electrode plasma interface diameter of 2µm~5µm.

4.2.2 Evaluation of L_b

From the definition of inductor it is known that an inductor will try to resist any change in the flow of current. Under an electric field the electrons in plasma gains directional kinetic energy and any changes in the flow of current will be resisted by the inertia of the particles; therefore, it can be said that the inductance of plasma is the ensemble of the inertia of particles and is related to the characteristic frequency at which the electrons oscillate among the heavier immobile ions. This electron plasma frequency is related to electron density n_e and given by equation 4.6. From equation 4.4, 4.6 and 4.7 we can obtain equation 4.8.

$$L_b = \frac{1}{\omega_{pe}^2 C_0} = \frac{dm_e}{Ae^2 n_e} \tag{4.8}$$

Descoeudres et al. (2004, 2008) reported that electron density at the beginning of the discharge is 2×10^{18} cm^{-3} and electron density reported by Nagahanumaiaha et al. (2009) is 3.5×10^{18} cm^{-3}. For the simulation of inductance value the electron density value can be considered to be bounded in a range of 1×10^{18} cm^{-3} to 3.5×10^{18} cm^{-3}. Concerning the surface area contributing to the inductance of the plasma is also given by the electrode plasma interface diameter and can be estimated to be in between 2μm~5μm for this analysis, which was mentioned earlier. Figure 4.5(a) shows the plot of plasma inductance at varying electrode diameter and electron density of plasma at 1.2μm electrode gap and Figure 4.5(b) shows the same at 6μm electrode gap. The result shows that the plasma inductance value ranges from 0.65pH~67.8pH. Even with a power supply circuit configuration with the minimum wire length of 10cm, the inductance contributed by the wire is 0.1090μH for tin plated copper stranded AWG20

wire (Grover, 2004; Rosa, 1908); which is about 1600 times larger than the inductance of this micro-sized plasma and therefore, the inductance of the plasma can also be neglected.

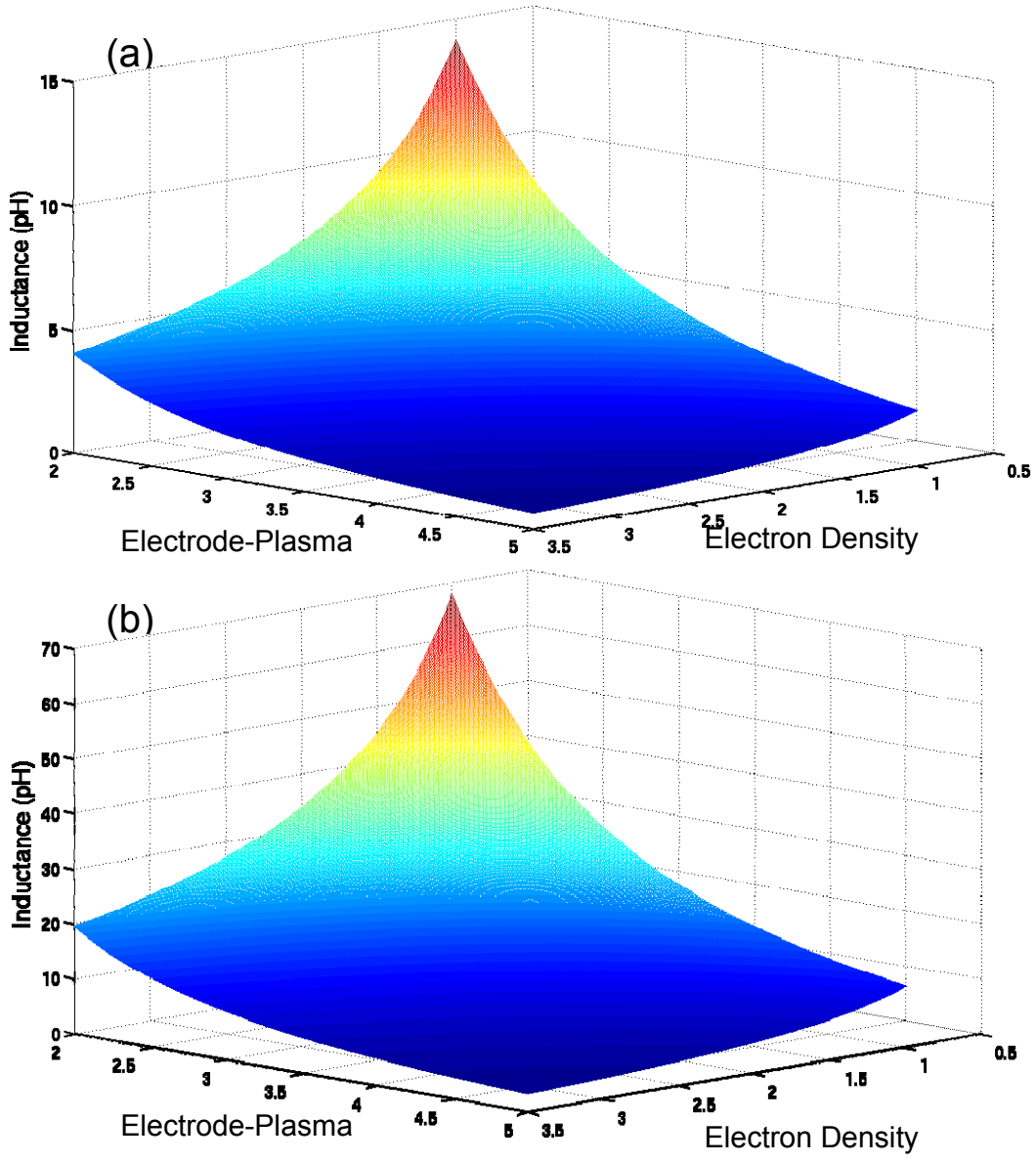

Figure 4.5 (a) Plot of plasma inductance at various electron density and electrode plasma interface diameter at 1.2µm electrode gap; (b) and at 6µm electrode gap.

4.2.3 Evaluation of R_b

Equation 4.5 states the value of plasma resistance R_b and combining equation 4.4, 4.5 and 4.6 we obtain equation 4.9 as the following:

$$R_b = v_m L_b = \frac{v_m}{\omega_{pe}^2 C_0} = \frac{m_e v_m d}{n_e e^2 A} \tag{4.9}$$

Now, we know from the definition of resistivity,

$$R_b = \rho_b \frac{d}{A} = \frac{m_e v_m d}{n_e e^2 A} \tag{4.10}$$

Therefore, the plasma resistivity can be stated as the following in equation 4.11

$$\rho_b = \frac{m_e v_m}{n_e e^2} \tag{4.11}$$

Where, v_m is the effective electron-ion collision frequency in quasineutral plasma. The electron-ion collision, v_m can be computed from Coulomb force and is given by equation 4.12 (Piel, 2010).

$$v_m = \frac{n_e e^4}{16\pi\varepsilon_0^2 m_e^2 V^3} \tag{4.12}$$

where, V is the characteristic velocity of a Maxwell-Botzmann distribution and can be considered as equal to the mean thermal velocity given by equation 4.13 (Roth, 1995)

$$V = \bar{v}_{th} = \left(\frac{8k_B T}{\pi m_e}\right)^{1/2} \tag{4.13}$$

where, T is the temperature of plasma in Kelvin and Botzmann's constant is denoted by k_B. Now, replacing equation 4.13 in equation 4.12 we obtain

$$v_m = \frac{n_e e^4 \pi^{1/2}}{(4\varepsilon_0)^2 m_e^{1/2} (8k_B T)^{3/2}} \tag{4.14}$$

Now, replacing v_m in equation 4.11 we obtain the following for plasma resistivity:

$$\rho_b = \frac{m_e v_m}{n_e e^2} = \frac{m_e^{1/2} e^2 \pi^{1/2}}{(4\varepsilon_0)^2 (8k_B T)^{3/2}} \tag{4.15}$$

This estimation of Coulombic collision was based on the assumption that the deflection angle after collision is large; but a more detailed treatment leads to Spitzer resistivity given by equation 4.16 (Piel, 2010)

$$\rho_b = \frac{m_e v_m}{n_e e^2} = \frac{m_e^{1/2} e^2 \pi^{1/2}}{(4\varepsilon_0)^2 (8k_B T)^{3/2}} \ln \Lambda \tag{4.16}$$

where, the correction factor $ln(\Lambda) \approx \ln(\lambda_D/b\pi/2) = \ln(4\pi N_D)$, called the Coulomb logarithm that is related to the number of particles N_D in a Debye sphere and from our assumption $N_D=1$, resulting in $\ln(\Lambda) \approx 2.531$, which also shows good agreement to the value of $\ln(\Lambda) \approx 2.2$ obtained by Descoeudres et al. (2008).

Descoeudres et al. (2008) reported from their observation that the plasma temperature reaches 8110K and remains constant throughout the discharge; and Nagahanumaiaha (2009), reported that plasma temperature ranges from 5167 K to 7889 K with an average plasma temperature of 6170 K. Therefore, we can estimate that the plasma temperature remains in a range of 5167K~8110K to compute a possible range of plasma resistivity which is shown in Figure 4.6.

Now, again consider that the electrode plasma interface diameter is 2µm~5µm for this analysis, as has been mentioned earlier. Figure 4.7(a) shows the computed resistance at different plasma temperature at 1.2µm electrode gap and at 6µm electrode gap shown in Figure 4.7(b). It can also be assumed that crater diameter ranging around 2.2µm can only be obtained at very small energy settings and at those settings the required electrode gap is in the range of 1.2~1.5µm. Therefore, in Figure 4.7(a) we can ignore

the resistance value shown in higher electrode plasma interface diameter and can only focus between 2µm~2.5µm interface diameter based on the earlier assumption that the interface diameter is 0.1µm~0.2µm smaller than the observed crater diameter. In this range of electrode plasma interface diameter the plasma resistance R_b varies between 25Ω~80Ω (with mean around 50Ω). Similar arguments can be placed for the case of a 5µm crater size which can only be obtained at larger capacitance and voltage settings; and that will yield a larger electrode gap, like 6µm for spark. At 5µm electrode plasma interface diameter and 6µm electrode gap it can be seen from the Figure 4.7(b) that the plasma resistance R_b also varies in the range between 30Ω~76Ω (mean ~50Ω). Therefore, it can be assumed that micro-EDM plasma resistance remains between 25Ω~80Ω, with a mean around 50Ω for electrode gap within 1.2µm~6µm and for obtained crater diameter between 2.2µm~5µm.

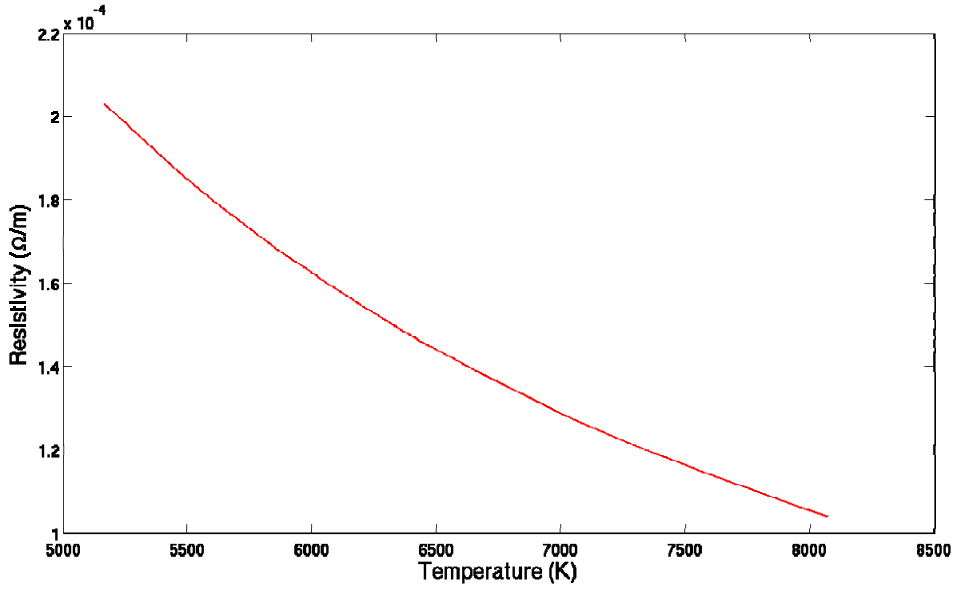

Figure 4.6 Plasma resistivity at different temperature.

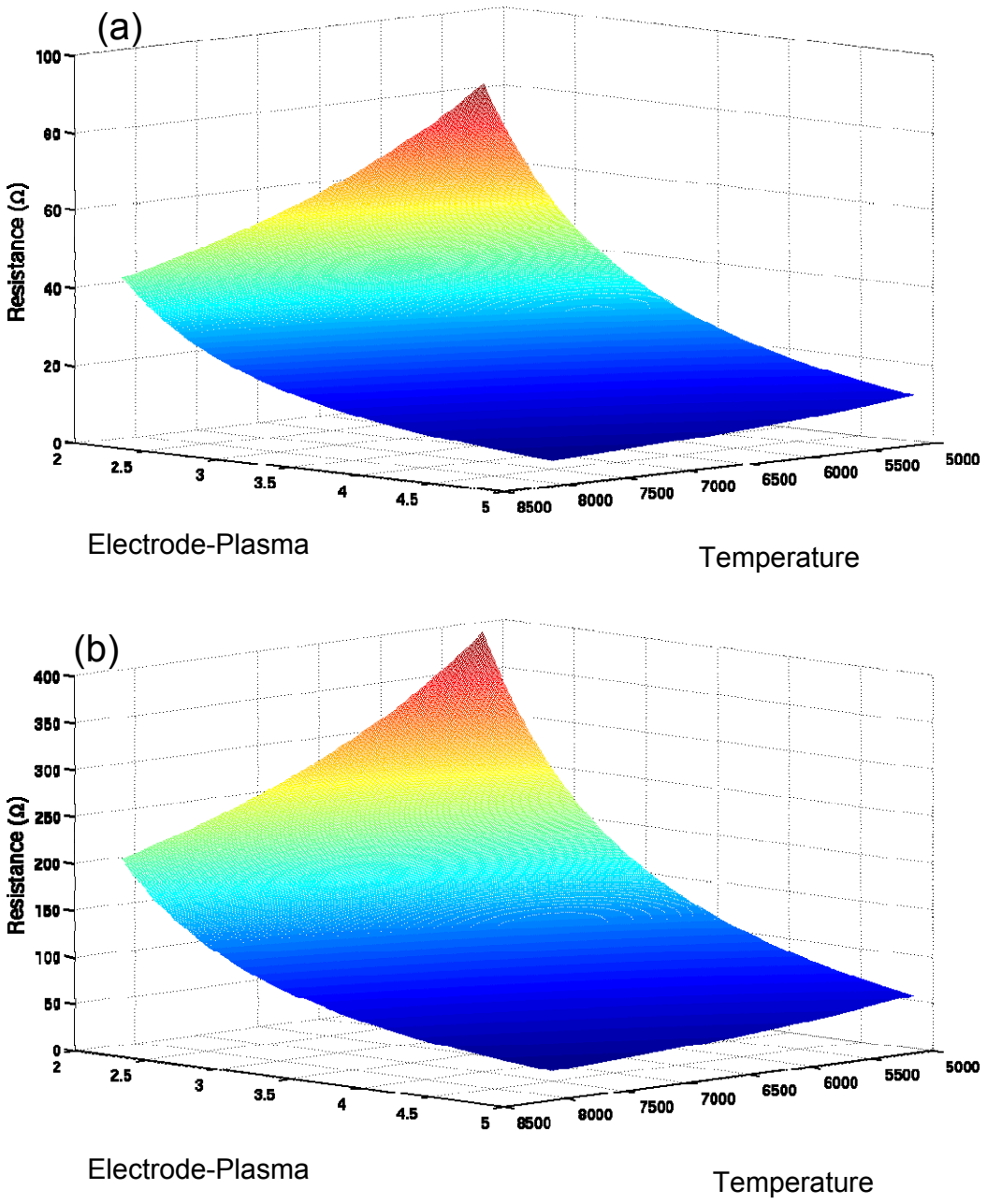

Figure 4.7 (a) Plot of plasma resistance at different temperature and electrode plasma interface diameter at 1.2µm electrode gap; (b) and the same at 6µm electrode gap.

4.3 Analysis of the RC Power Supply Electric Network Involving Micro-EDM Plasma

From the evaluation of the equivalent electric network of plasma, the inductive and capacitive load of micro-EDM plasma can be essentially ignored and consider only the resistive network. From the evaluation of plasma resistivity, $\rho_{b,}$ it can be observed that the plasma resistivity is only dependent on plasma temperature and not on electron/ion density of the plasma. Observation from Descoeudres et al. (2008) and detailed theoretical analysis of micro-EDM plasma by Dhanik et al. (2005) indicated that the plasma temperature can be considered to remain constant throughout the discharge process – and therefore, the resistivity can be considered to remain constant. The electrode plasma interface diameter was reported to grow slightly during the discharge by Descoeudres et al. (2008) but for very fine short pulse ranging between 20ns~100ns – it can be considered that the electrode plasma interface diameter remains constant; and from this assumption the plasma can be simplified to a resistive network with constant resistance during the discharge. This will allow simplifying the electric network shown in Figure 4.3(b) to the network shown in Figure 4.8.

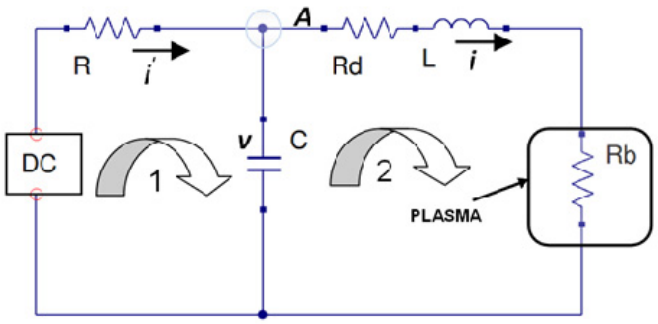

Figure 4.8 Simplified Electrical Network of Plasma with the Power Supply Network (RC circuit with a DC source)

Let us, consider that the voltage across the capacitor is *v*, and the current flowing to node marked *A* is $i^{'}$ and the current flowing out from node *A* to the plasma is *i*. Now, applying Kirchhoff's voltage law (KVL) in loop 2 we obtain equation 4.17, applying KVL in loop 1 we obtain equation 4.18 and applying Kirchhoff's current law (KCL) in node *A* we obtain equation 4.19.

$$v = R_d i + L\frac{di}{dt} + R_b i \tag{4.17}$$

$$E - v - Ri^{'} = 0 \tag{4.18}$$

$$i = i^{'} - C\frac{dv}{dt} \tag{4.19}$$

Now, combining equation 4.18 and 4.19 to replace i' we obtain equation 4.20

$$i = \frac{E - v}{R} - C\frac{dv}{dt} \tag{4.20}$$

Differentiating equation 20 we arrived to equation 4.21

$$\frac{di}{dt} = -C\frac{d^2v}{dt^2} - \frac{1}{R}\frac{dv}{dt} \tag{4.21}$$

Now, replacing *i* and *di/dt* in equation 4.17

$$v = R_d(\frac{E-v}{R} - C\frac{dv}{dt}) + L(-C\frac{d^2v}{dt^2} - \frac{1}{R}\frac{dv}{dt}) + R_b(\frac{E-v}{R} - C\frac{dv}{dt}) \tag{4.22}$$

Rearranging equation 4.22 and dividing both the sides of the equation by *LC* we obtain the following:

$$\frac{d^2v}{dt^2} + (\frac{R_d + R_b}{L} + \frac{1}{RC})\frac{dv}{dt} + (\frac{1}{LC} + \frac{R_d + R_b}{RLC})v = \frac{R_d + R_b}{RLC}E \tag{4.23}$$

Now, in equation 4.23 it can be observed that both R_d and R_b come as a summed term. The resistance of AWG20 tin plated copper stranded wire is about 34mΩ/m and the resistance contributed by tungsten electrode system is around another 20mΩ. Therefore, even for a 1 meter long wire with a 32μm electrode in the discharge path

will make R_d = 54mΩ; and thus we can consider the $R_d + R_b \approx R_b$ to obtain the following:

$$\frac{d^2v}{dt^2}+(\frac{R_b}{L}+\frac{1}{RC})\frac{dv}{dt}+(\frac{1}{LC}+\frac{R_b}{RLC})v=\frac{R_b}{RLC}E \tag{4.24}$$

The characteristic equation of the 2nd order differential equation given by equation 4.24 is given by the equation in 4.25 and the solutions are given by equation 4.26.

$$s^2+(\frac{R_b}{L}+\frac{1}{RC})s+(\frac{1}{LC}+\frac{R_b}{RLC})=0 \tag{4.25}$$

$$s_{1,2}=-\frac{(\frac{R_b}{L}+\frac{1}{RC})}{2}\pm\frac{1}{2}\sqrt{(\frac{R_b}{L}+\frac{1}{RC})^2-4(\frac{1}{LC}+\frac{R_b}{RLC})} \tag{4.26}$$

Now, we have the 3 cases of the solution, namely overdamped for real distinct roots, critically damped for real repeated roots and underdamped for complex conjugate roots. Investigating the discriminant will allow to analyze the type of solution that is required to be computed for some practical values of the circuit element. Let, R=1kΩ, L=0.1090μH; and C=53pF for this investigation which are some of the values reported by Masaki et al. (2010a).

By taking the 1st and 2nd derivative of the discriminant with respect to R_b given by equation 4.26, equation 4.27 and 4.28 could be obtained

$$\frac{dD}{dR_b}=\frac{2}{L^2}R_b-\frac{2}{RLC} \tag{4.27}$$

$$\frac{d^2D}{dR_b^{\,2}}=\frac{2}{L^2} \tag{4.28}$$

By setting equation 4.27 equal to 0 and since equation 4.28 is always positive, we can obtain that the minima of the discriminant of equation 4.26 is when R_b = 2Ω and at that

value equation 4.26 results in complex conjugate solution $1.8608\times10^{07}\pm j4.1605\times10^{08}$ and demonstrates to be an underdamped case. Similarly, for values of R_b computed in section 4.2.3 to be between 25Ω~80Ω the solution yields a complex conjugate root. On the other hand, when the value of R_b changes to 93Ω the solution turns to and overdamped having real distinct root. Moreover, for sweeping the equation between wide range of R and L values it is required to obtain all of the 3 solutions of the differential equation given by equation 4.24.Solving the underdamped, overdamped and critically damped cases of the differential equation given by equation 4.26 the following equation for voltage v and current i could be obtained (where, P and Q are given by equation 4.29 and 4.30).

$$P = \frac{1}{2}\left(\frac{R_b}{L} + \frac{1}{RC}\right) \tag{4.29}$$

$$Q = \sqrt{\left(\frac{1}{LC} + \frac{R_b}{RLC}\right) - P^2} \tag{4.30}$$

- **Solution of underdamped case**

$$v = E\left(1 - \frac{R_b}{R+R_b}\right)e^{-Pt}\left(\cos Qt + \frac{P}{Q}\sin Qt\right) + \frac{R_b}{R+R_b}E \tag{4.31}$$

$$i = CE\left(1 - \frac{R_b}{R+R_b}\right)e^{-Pt}\left(\frac{P^2}{Q} + Q\right)\sin Qt + \frac{E-v}{R} \tag{4.32}$$

- **Solution of overdamped case**

$$v = \frac{R_b E}{R+R_b}\left[-\left\{\frac{1}{2Q}(P-Q)+1\right\}e^{(-P+Q)t} + \frac{1}{2Q}(P-Q)e^{(-P-Q)t} + 1\right] \tag{4.33}$$

$$i = -C\frac{R_b E}{R+R_b}\left[\left\{\frac{1}{2Q}(P-Q)+1\right\}(P-Q)e^{(-P+Q)t} - \frac{(P^2-Q^2)}{2Q}e^{(-P-Q)t}\right] + \frac{E-v}{R} \tag{4.34}$$

- **Solution of critically damped case**

$$v = \frac{R_b}{R+R_b} E(1 - e^{-Pt} - Pe^{-Pt}) \tag{4.35}$$

$$i = -C\frac{R_b E}{R+R_b} Pe^{-Pt}(1+P) + \frac{E-v}{R} \tag{4.36}$$

4.4 Model Validation

4.4.1 Validation of the model by varying *L*

Masaki et al. (2010a) added varying length of wire in the discharge loop to experimentally evaluate the effect of varying wire length (and essentially the effect of inductance, *L*) on discharge current waveform. In their experiment, the authors varied the wire length from 0.1m (which is the minimum length required to connect the spindle head (tool electrode) to the capacitor) to 15m and experiments were conducted at two different capacitance values: stray capacitance and 53pF. In this section, the proposed model of micro-EDM electric network defined by the equations 4.31 to 4.36 (which are the solutions of the differential equation 4.24) involving the plasma impedance will be validated using experimental results reported by Masaki et al. (2010a). Table 4.2 shows the condition used for easy referral. Masaki et al. (2010a) only reported the length of the wire used in the experiment and the experimentally obtained current waveform. For the computation of the model defined by equation 4.31 to 4.36, the inductance value of the wire length is required to be computed using equation 4.37(Grover, 2004; Rosa, 1908). The computed inductance value is also shown in Table 4.2.

$$L = 0.002l\left[\ln\frac{2l}{d_w} - \frac{3}{4}\right] \text{(Grover, 2004; Rosa, 1908)} \tag{4.37}$$

where, d_w is radius of the wire in cm and l is the length of the wire in cm and the obtained value of L is in μH.

Table 4.2 Conditions and setting values for obtaining current waveform of varying L (adapted from Masaki et al., 2010a, except the equivalent inductance value which was not computed in the original report).

Item	**Conditions and Value**
Voltage [V]	60
Capacitor Capacitance [pF]	6,47+6
Resistance [kΩ]	1
Cable length [m]	0.1, 0.5, 1.1, 2, 3.9, 7.6, 15
Equivalent Inductance [μH]	**0.1090, 0.7059, 1.7265, 3.3782, 7.1084, 14.8663, 31.3811**
Machined depth [μm]	10
Dielectric	EDM oil (CASTY-LUBE EDS)
Tool Electrode	Tungsten 32μm diameter
Workpiece Material	Stainless steel SUS304

In addition to the minimum wire length of 10cm to configure the discharge circuit, as reported by Masaki, 2010a, there is also dead length of wire which has to be added in the return path of the current after discharge which contributes to additional inductance. Considering the structure of the equipment used by Masaki et al. (2010a) ((the distance between the connections on the mandrel and XY table is approximately 20cm) and travel length of both X and Y axes are 5cm it can be considered that a minimum of additional 25cm of wire is required to configure the return path of the current (this required minimum length was also confirmed from personal communication with Masaki et al. (2010a)). Inductance is also contributed by the electrode, feeding system and workpiece. Considering a 3cm long 0.300mm diameter tool electrode – the contributed inductance should be around 0.0314μH (this is about 35% of the contribution by 10cm wire). Therefore, it can be assumed that the system had additional inductance equivalent to a total of 30cm wire length (0.3929μH) in the

return path of the discharge current contributed by the wire in the return path , the tool electrode and other component of the feeding system.

In order to validate the proposed model, computer simulation was performed using Matlab using the equations 4.31 to 4.36. The program was written to compute the determinant equation based on the input R, L and C value to identify the appropriate solution case (underdamped, overdamped and critically damped). Simulation was performed at 3 different plasma resistance values – taking R_b = 40Ω, 50Ω and 60Ω, keeping 50Ω as the mean. The current waveform obtained from the simulation and the experimental waveforms of Masaki et al. (2010a) are compared in Figure 4.9. Two important parameters of current waveform are the pulse width and peak current, which are compared between experimental and simulation results (Figure 4.9). Pulse width is defined by the time between the beginning of a discharge to the first zero crossing of the current waveform and peak current is defined by the peak value of the current over the discharge duration. The experimental current waveform for 0.1m shows smaller peak current (300mA) compared to the value obtained from the model (415mA), but considering micro-EDM as a stochastic process and the presence of a debris particle in gap space might change the conductivity of plasma which may result in quite a significant difference in peak current as well as in waveform. Comparing Figure 6(a) and Figure 10(a) of Masaki, 2010a, the same can be concluded as at the same setting one profile shows a peak at 300mA and the second one shows a peak at 400mA. Moreover, usually the peak of the current profile shows a well formed peak as could be seen in Figure 10(a) of Masaki et al. (2010a) as opposed to the valley shaped peak that could be seen in Figure 6(a) which indicates that the peak value of profile in Figure 10(a) is more appropriate.

Another factor that might have contributed to the little difference is due to the fact that the current probe used for performing these experiments was band limited between 1.2 kHz to 200 MHz (Tektronix Current Probe – Model CT2) which signifies that a very sharp movement happening in less than 5ns will display an averaged response in the oscilloscope. Therefore, some variation with experimental data is expected but the congruency between the overall waveform and the changes observed due to varying L demonstrates excellent fit of the theoretical value to the experimental data.

Masaki et al. (2010a) reported that the current waveform generated at 15m wire length was not showing clear waveform to measure pulse width and peak current. This phenomenon could be explained well using this model if it is assumed that given the experimental settings and inter-electrode gap if the steady state current drops below 30~40mA the discharge stops and R_b becomes an extremely large resistor until the next breakdown, whereas if the steady state current remains above 50mA then continuous arc discharge takes place – then. This makes a fair assumption based on the fact that in plasmas energy is dissipated in inelastic collisions, including the ionization events which maintain the plasma, and excitation collisions which lead to photon emission that makes the plasma visible; and electron energy is also dissipated in elastic collisions with the background neutral dielectric which causes the heat to get transferred to the ambience formed by dielectric and electrodes, thus continuous power to the plasma is needed to maintain it. Figure 4.11 shows the simulated waveform at 15m wire length and it can be observed that the slowly varying waveform did not cross below 30~40mA at steady state and this caused a continuous power flow to the plasma to keep it at arcing condition thus the peak and the pulse width were not identifiable.

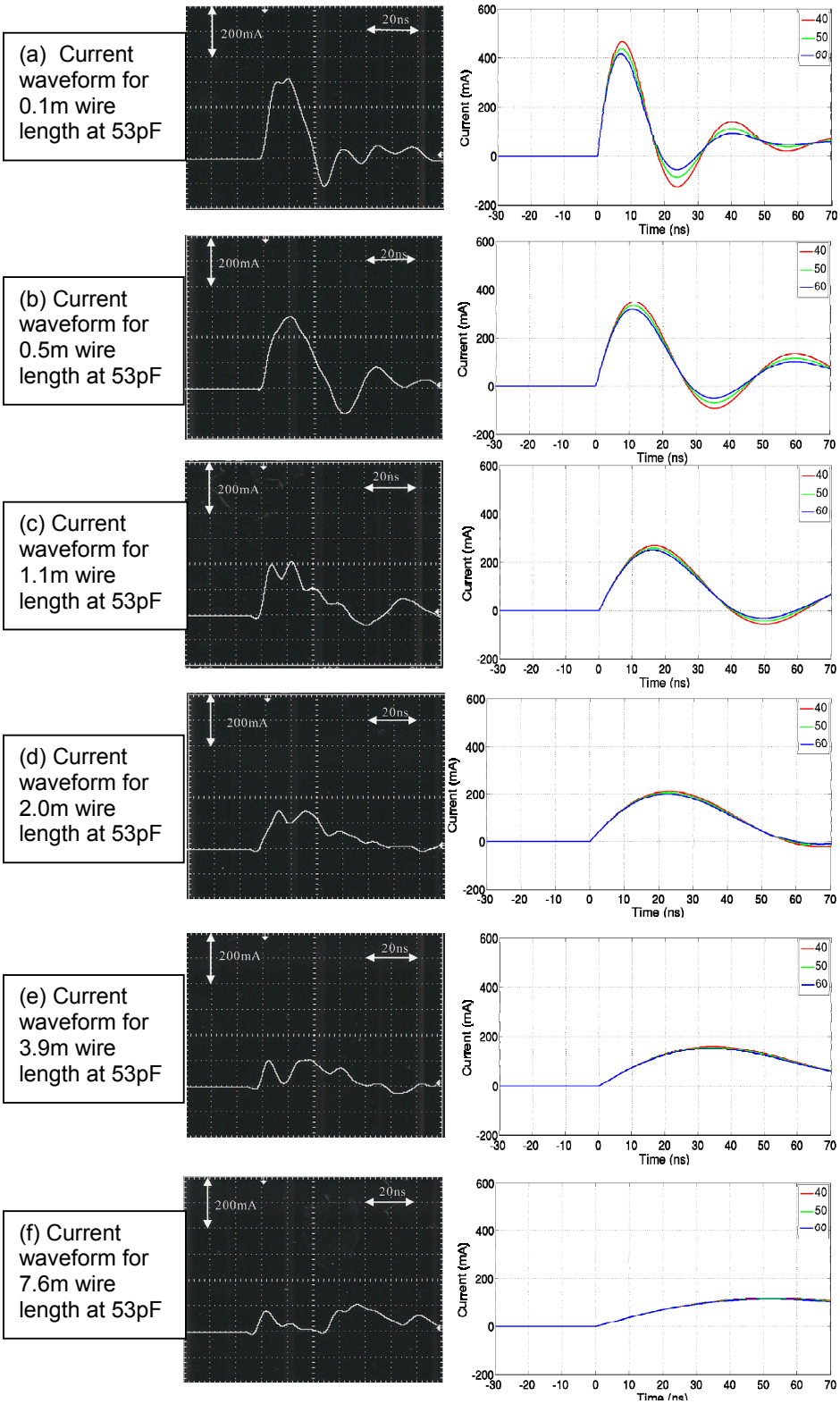

Figure 4.9 Showing experimentally obtained (left column) (Masaki, 2010a) and simulated current waveform at 3 different R_b values (40Ω, 50Ω, 60Ω). Observed peak current and pulse width values are plotted in Figure 4.10.

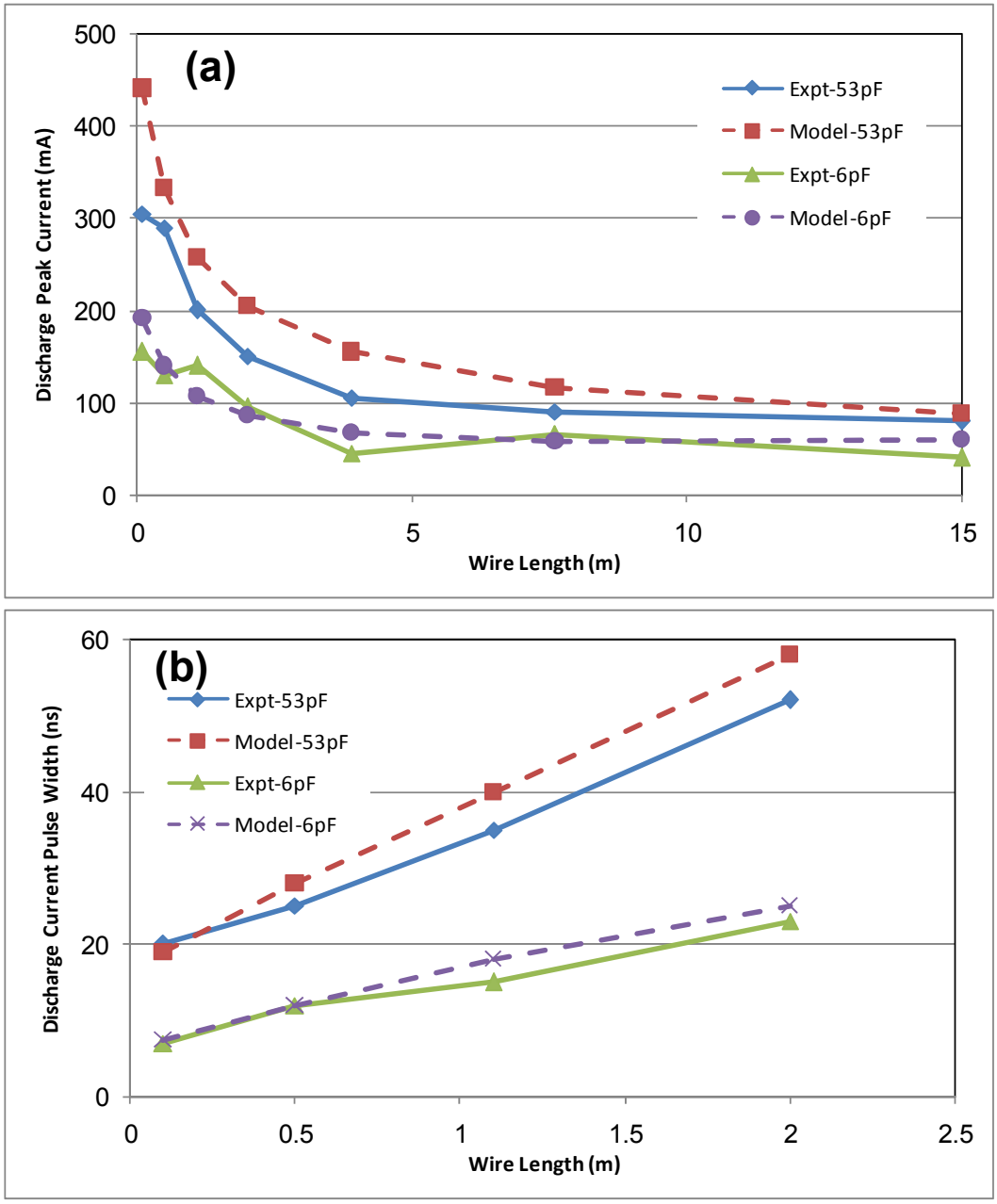

Figure 4.10 Comparison between experimental and theoretical values for 53pF and 6pF capacitance of (a) discharge peak current at varying wire length and (b) discharge current pulse width at varying wire length.

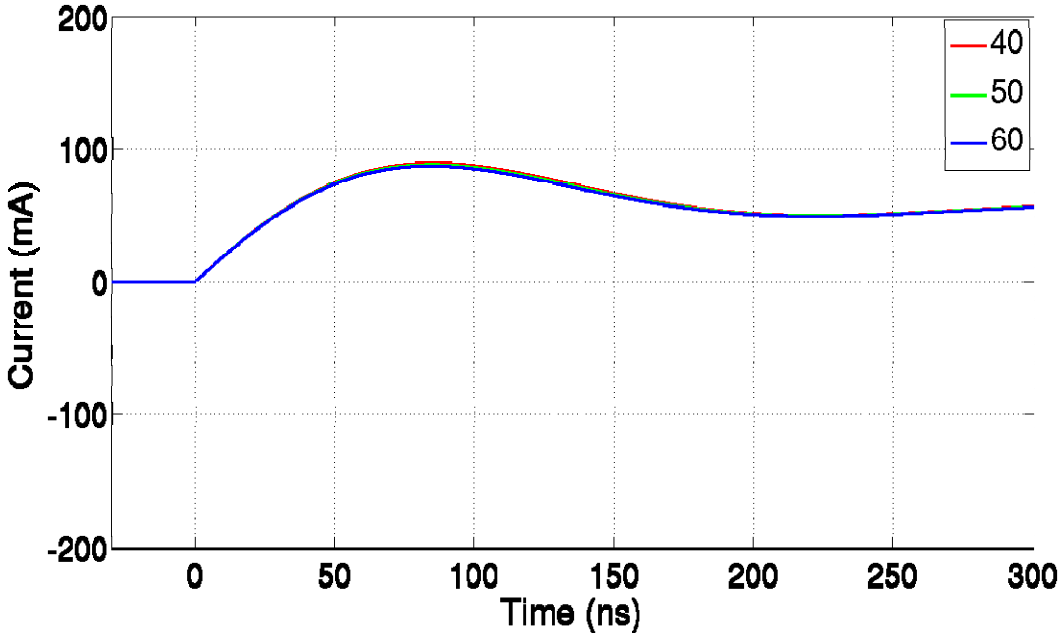

Figure 4.11 Shows that the theoretical pulse waveform remains above 50mA which may cause a continuous arc discharge.

4.4.2 Validation of the model from discharge energy

In the case of RC type power supply shown in Figure 4.8, the repetition of the charging and discharging occurs in which capacitor *C* is charged through resistor *R* and discharged between the electrode and workpiece and therefore, the energy deposited in the gap from the spark is commonly computed by the energy that can be stored in the capacitor which is given by $\frac{1}{2}CV^2$ (Masuzawa, 2000; Wong, 2003). But, this assumption may not hold true always as the discharge can be from a partially charged capacitor and as well as for a small power would be supplied by the main DC source through the charging resistor R to the plasma during the discharge. Masaki et al (2010a) proposed that discharge energy can be also measured by obtaining both the voltage waveform and current waveform and then multiplying the area under both the curves (since, power $P(t) = V(t) \times I(t)$).

The proposed model given by equations 4.31~4.36 has been used to compute the discharge energy in a single discharge from the theoretically computed voltage and current waveforms. Figure 4.12 compares between the discharge energy obtained from the theoretical computation, experimental data of Masaki, 2010a and the discharge energy obtained by computing $\frac{1}{2}CV^2$. The model shows excellent agreement to both the data validating the model. The theoretical model deviates between 4%~7% from the $\frac{1}{2}CV^2$ method of computation, which is due to the fact that the model accounts for the power imparted to the plasma directly from the DC source during the discharge.

Comparing to the experimental values, both the values obtained from $\frac{1}{2}CV^2$ method and values obtained using this proposed model fit nicely at smaller discharge energy; but at higher energy both the values are overestimated from the experimentally obtained result. This could potentially indicate that the particular discharge captured was not from a fully charged capacitor, or it could even deviate from the assumption that the electrode plasma interface diameter remains same throughout the discharge – which may not be the case for larger pulse width; meaning that the plasma resistance was reducing gradually due to the slow expansion of interface diameter and thus less heat was deposited in the gap. But, this argument requires further investigation.

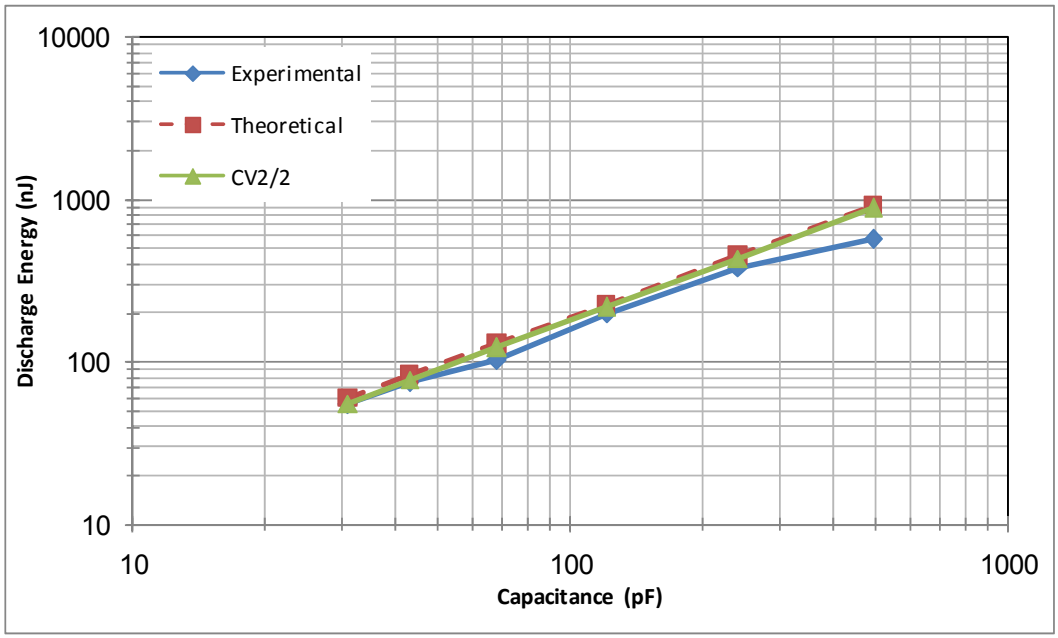

Figure 4.12 Comparison between discharge energy computation methods.

4.4.3 Validation of the model at lower DC supply voltage and at higher discharge energy

Masaki et al., (2010a) performed experiments to observe the effect of supply voltages at 40V and below on peak discharge current. The theoretically computed value by using this proposed model at 60V or below did not show good fit to the experimental results for values of voltage below 60V as could be seen Figure 4.13 (red line). This evaluation was done using R_b=50Ω which has been computed with the assumption that the value of electrode plasma interface diameter is 2µm~2.5µm (section 4.2.3). But, practically for voltages lower than 60V the assumptions on diameter of electrode plasma interface needs to be corrected as the crater size changes significantly at such low voltage settings. Masaki, 2010a observed that the crater size became 1.22µm for 30V input voltage. Therefore, the electrode plasma interface diameter can be

considered as 1.0μm (as it has been assumed that the electrode plasma interface diameter is slightly smaller than the crater size). Using plasma electrode interface diameter as 1.0μm, plasma resistance was recomputed to be 165Ω~325Ω (with mean around 250Ω) for the model (Figure 4.14). With this corrected assumption, the model yielded good agreement with experimental findings at lower voltages (Figure 4.13). Using plasma resistance value 250Ω shows better agreement than the computation at 50Ω which is shown in Figure 4.13 as well.

At the same time, this also needs to be observed that the model predicts a linear relationship at different voltages and peak current while the experiment indicates a sort of exponential relationship (shown by gray color exponential trendline in Figure 4.13). Furthermore, while the calculation based on corrected assumption obtained better fit with the experimental observation for lower voltages it deviated from the peak current that was observed at 60V. This actually further establishes and validates the theoretical analysis that the model is based on the plasma resistance. In the mode value of plasma electrode interface diameter is required as an input to the model and is estimated from the crater size. Therefore, the value of inter-electrode gap and plasma electrode interface diameter (given by the crater diameter) plays a very important role in the understanding of micro-EDM energy discharge characteristics and interaction with plasma.

The capability of the proposed model was further explored by comparing the theoretical result to experimental results published by Mahardiaka et al. (2008) which was done at higher voltage and larger capacitance settings. Their experimental conditions were: Supply voltage V=110V, C=3300pF, R=1000Ω and during their

experiments they used another additional voltage probe (Tektronix P6109B) for taking voltage reading which added additional inductance of approximately 0.288μH (L=25cm, d_w=0.075cm). From the experimental results of Han, F., et al., (2006) it can be observed that the crater size obtained from this voltage and capacitor settings is about 12μm on tungsten and tungsten carbide workpiece. Using this assumption the plasma resistance was recomputed to be between 5Ω~10Ω. Figure 4.15(a) shows the experimentally obtained pulse profile and the simulated pulse profile is shown in Figure 4.15(b) where good agreement between the pulse width (175ns experimental value; simulated 165ns~171ns, mean 168ns) and the pulse peak (experimental value 4.9A; simulated 4.7A~5.6A, mean 5.1A) can be observed.

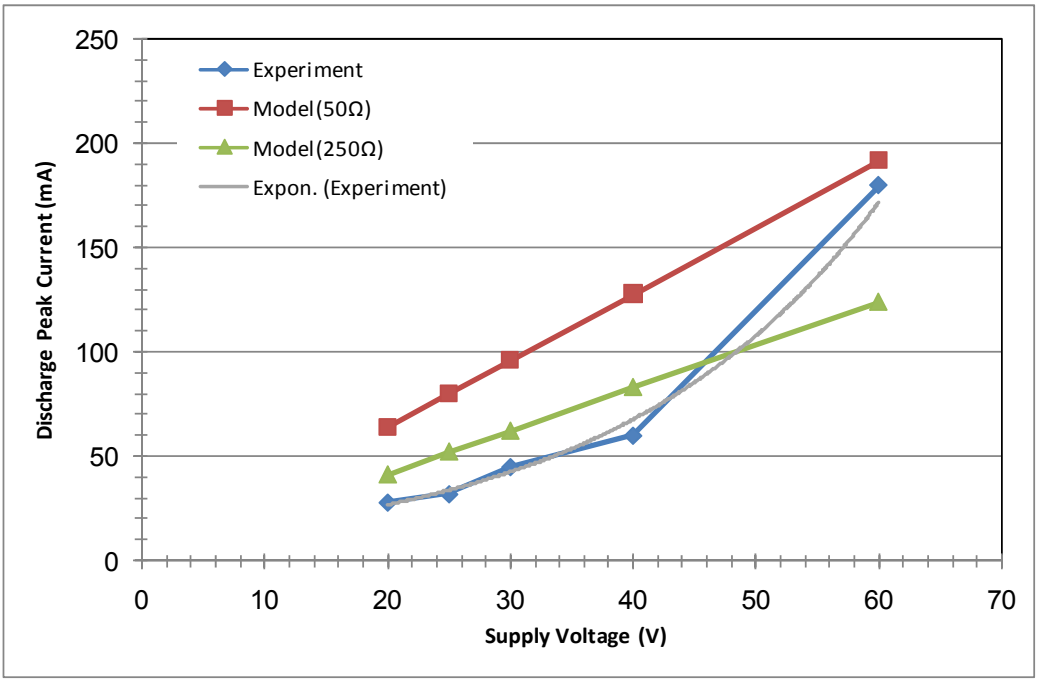

Figure 4.13 Comparison between experimental and theoretical value of peak current at different voltage settings. The gray line shows exponential trendline fitted on the experimental data.

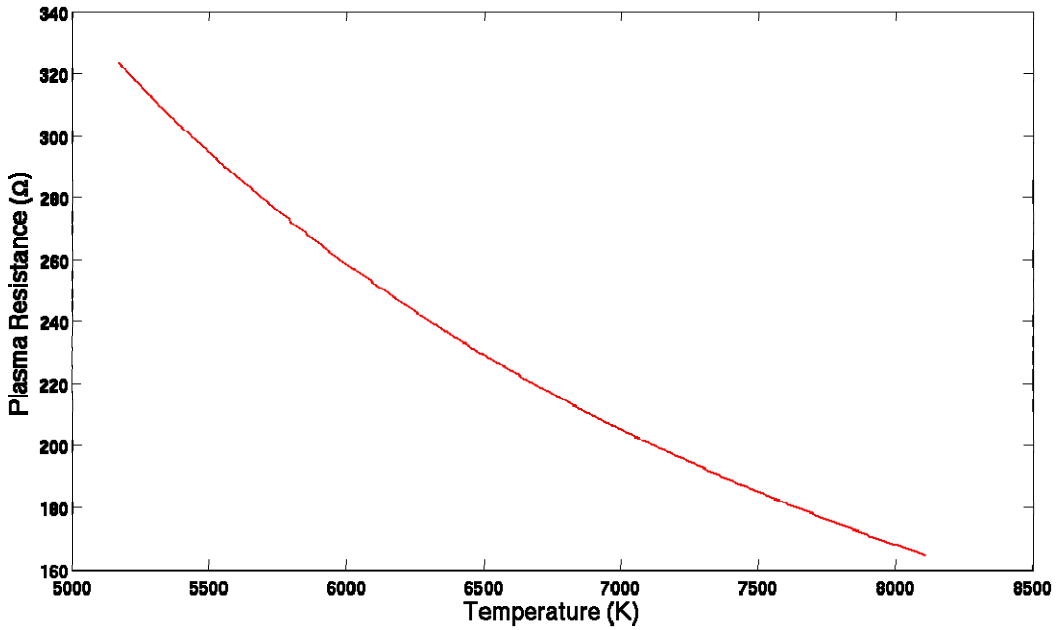

Figure 4.14 Plasma Resistance for electrode plasma interface diameter 1μm.

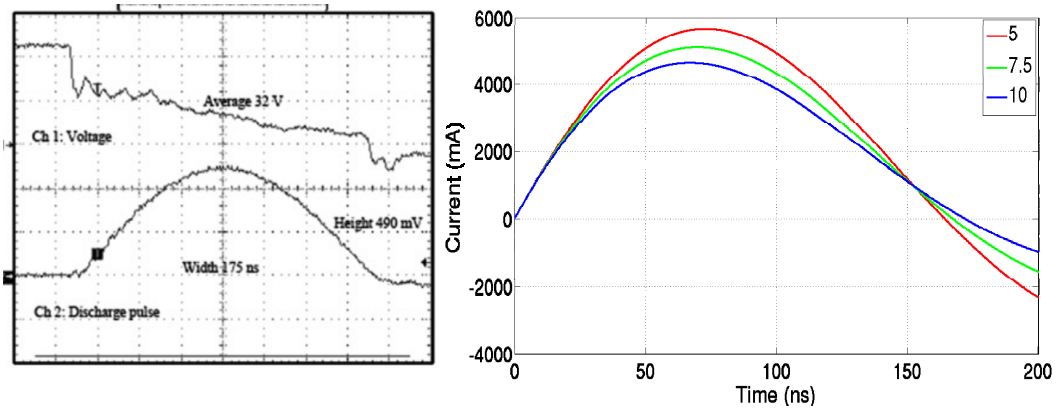

Figure 4.15 Current Waveform (Mahardika, et al., 2008) and simulated value at C=3300pF, V=110V. Excellent match of pulse width (175ns experimental value; simulated 165ns~171ns, mean 168ns) and the pulse peak (experimental value 4.9A; simulated 4.7A~5.6A, mean 5.1A) can be observed.

4.5 Observation on the Current Waveform Generated by the Proposed Model

As the proposed model investigates into the interaction between the micro-EDM power supply and micro-EDM plasma it can be used for elucidating the theoretical relationship of different circuit parameters and how that may change the energy discharged on the workpiece by a spark. In this section the effect of varying R on the pulse waveform will be analyzed which will lead to the selection of an appropriate value of *R* for micro-EDM power supply circuit to be developed. Effect of varying voltage *V*, inductance *L* and capacitance *C* on current waveform will also be observed from the model which will provide sufficient background understanding for selection of these parameters during an experiment for desired output. This model can also be used for obtaining stray capacitance and inductance of the power supply circuit contributed by obtaining a current waveform and then using non-linear curve fitting of the current waveform to the mathematical model.

4.5.1 Effect of varying resistor *R* and selection of *R* for micro-EDM power supply

Resistor *R*, shown in Figure 4.8, plays a very critical role in designing the micro-EDM RC power supply. The main role of *R* is to limit the supply of current to the capacitor as well as to the plasma contained in the gap immediately after a discharge such that after the spark the discharge stops due to the lack of necessary flow of current required to maintain the plasma. This energy is needed to maintain the plasma as there is loss from inelastic collisions, ionization events which maintain the plasma, energy dissipated in the form electromagnetic radiation loss ranging from visible light to other

frequencies of electromagnetic waves including X-rays, and heat transferred to the background. Therefore, a large *R* is preferred from this concern to minimize arcing current. On the other hand after one discharge, as soon as the plasma is switched off, the best condition is to have the capacitor fully charged for the next discharge. But the charging time of the capacitor will be based on the time constant formed by the capacitor and the resistor. For a practical settings of micro-EDM experiment, *C*=100pF capacitor, *V*=60V and *R*=400Ω, 1kΩ, 2kΩ will have time constant τ = 10ns, 100ns and 200ns respectively. Essentially this will result in charging 63% of the capacitor and in most part of this period the capacitor is not charged enough to make the spark happen. From this perspective smaller settings of R will allow the capacitor to get quickly charged. Therefore, due to this contradictory relationship the value of R needs to be optimized such that it provides a balance between minimizing charging time and reducing the chance of arc.

This is usually done by performing experiments as the fastest machining time resembles the optimal setting. In arcing condition the machine requires to perform back and forth motion repeatedly to stop the short condition which extends the machining time whereas, in slow charging case the machine takes longer time simply because of the reduction in spark per second. Experiments were conducted on the UMMT using the machining conditions shown in Table 4.3 and the machining time is shown in Figure 4.16. The machining time indicates 1kΩ gave the best machining time whereas 400Ω took significantly longer machining time and at 2kΩ the machining time was slightly longer than 1kΩ, even though statistically the difference was not significant (the same experiment was performed 3 times to obtain experimental test-retest repeatability).

The above experimental results could be similarly observed for optimizing R for micro-EDM RC circuit by computing the waveform profile at R=400Ω ~ 2kΩ using this proposed model, as could be seen in Figure 4.17. The current waveform up to R=600Ω had no zero crossing and remained above 100mA at 60V supply voltage beyond the first 90ns which can be considered as large enough current to maintain the plasma. From R=700Ω to R=2kΩ it had zero crossing within the first 60ns which may indicate that the power from the plasma was cutoff within this time and thus arcing was minimized. Therefore, practically the power supply circuit for micro-EDM should be designed with resistance R> 700Ω. At resistance values above 900Ω it can also be observed that the negative dip was below 50mA compared to those at 700Ω and 800Ω. Given that micro-EDM is a stochastic process with significant amount of process noise and presence of debris in the gap space changes the waveform – it can be concluded that a value of above 900Ω will provide sufficient safety margin in avoiding continuous arcing in the circuit.

Table 4.3 Machining Conditions for WEDM Experiments Varying R.

Item	**Conditions and Value**
Setup used	WEDM
Feedrate	2.0μm/s
Voltage [V]	60
Capacitor Installed [pF]	100pF
Resistance [Ω]	400, 1000, 2000
Estimated Inductance L [μH]	1.9043
Machined slot size [mm]	1.0
Dielectric	Total EDM 3 oil
Tool Electrode	Tungsten wire (Agie Charmilles) 70μm diameter
Workpiece Material	Stainless steel SUS304

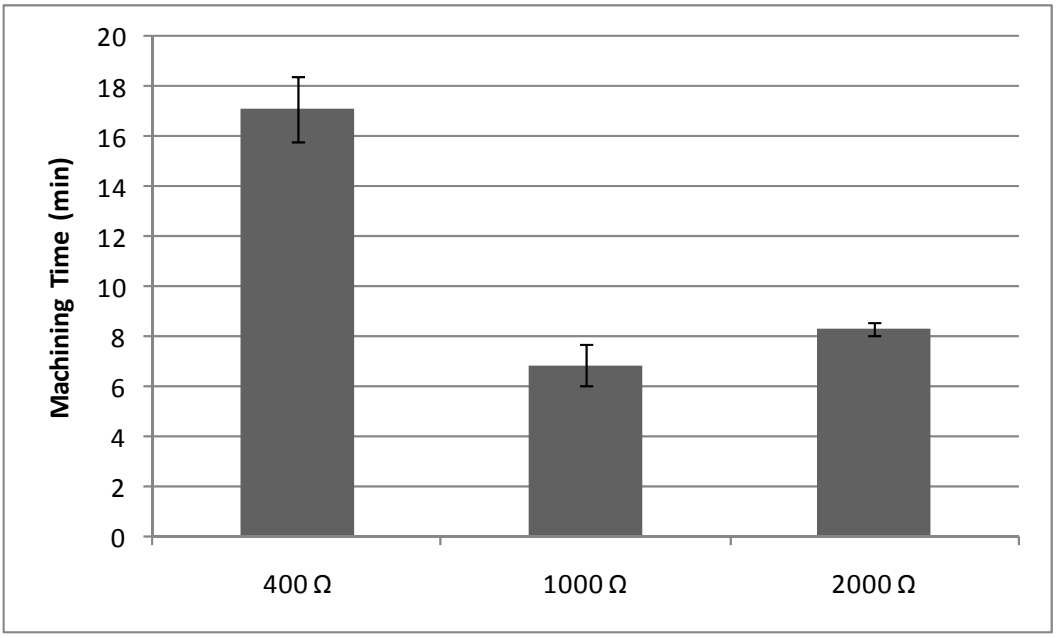

Figure 4.16 Machining time of 1mm slot by WEDM using R=400Ω, 1kΩ and 2kΩ. The error bars are one SD (n=3).

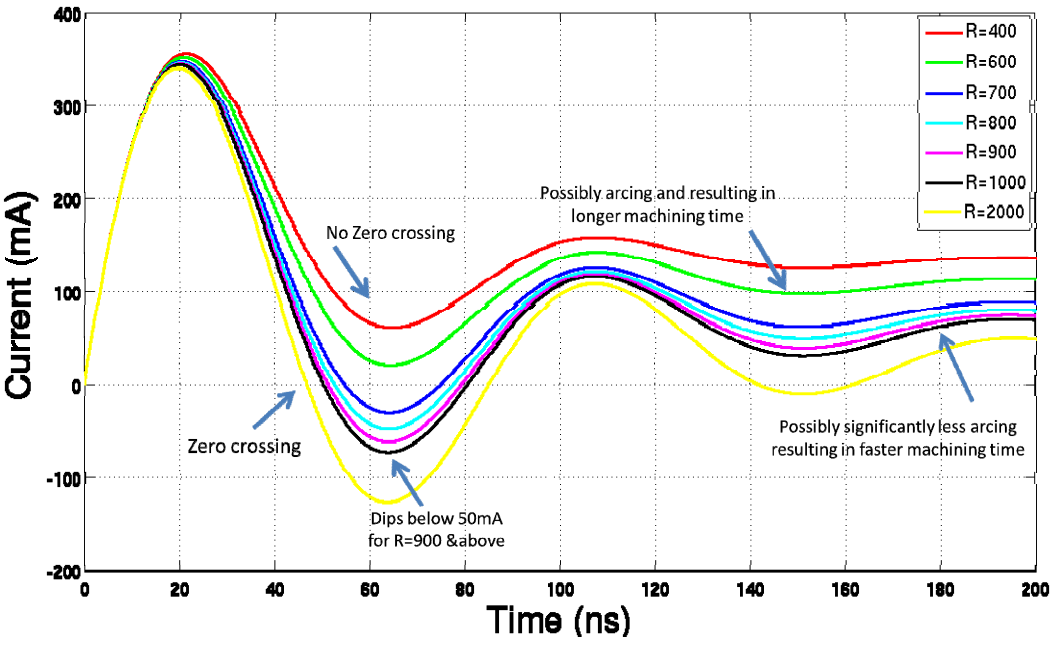

Figure 4.17 Current waveform computed theoretically at R=400Ω ~ 2kΩ (C=100pF, L=1.9043μH, V=60V, Plasma resistance R_b=50Ω).

4.5.2 Effect of inductance on the current waveform

In section 4.4.1 as part of the validation of the model, current waveforms at different wire length in order to vary the inductance were generated using this model and was compared with the experimental data shown in Figure 4.9. In this section, changes in current waveform with varying inductance will be further discussed. It can be observed in Figure 4.18 that the peak current changes significantly from 660mA to 530mA and the pulse becomes broader from 20ns to 30ns (first zero crossing of current after the beginning of a discharge) for a change of inductance from 0.2457μH (l = 0.20m; AWG20 wire) to 0.5469μH ((l = 0.40m; AWG20 wire). At L=1.9043μH (l = 1.20m; AWG20 wire) the pulse becomes much broader having a width of around 50ns and the pulse peak changes to 360mA. But the computed energy under all these three waveforms remains the same at around 190nJ. The similar effects of varying inductance by varying the length of the wire can also be observed in Figure 4.9. Masaki, 2010a, observed that by increasing the wire length, the craters on the surface became larger, shallower and flat; and therefore, this can be applied to improve the properties of the machined surface. One possible explanation to this can be provided assuming that the disk heat source based electro-thermal model is more appropriate at very small energy spark compared to the point source head model (Yeo et al., 2008; Dibitonto et al., 1989); and therefore, over longer spark duration but with the same amount of energy delivered – there is sufficient time for the heat to get conducted and material removal by melting action is higher. On the other hand with very short pulse – there is rather less time for conduction and due to higher energy density removal by evaporation is increased where the heat is lost to the dielectric rather quickly. However, this argument requires further investigation. But, this can be stressed from the experimental observation that variation in L can be instrumental in changing

surface properties of machined workpiece. Larger L increases machining time as the pulse gets larger but switching L can be an option where the initial machining is done with smaller L value and the finishing can be obtained by larger L value.

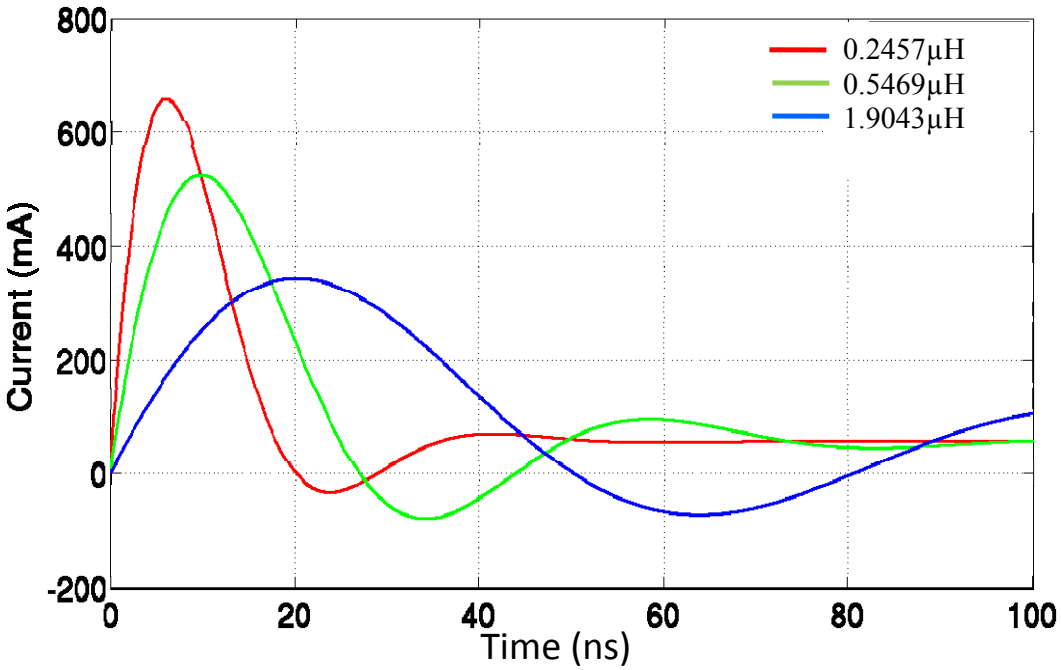

Figure 4.18 Current waveform at varying inductance value at 0.2457µH, 0.5469µH and 1.9043µH (C=100pF, R=1kΩ, V=60V, Plasma Resistance R_b=50Ω) for equal energy discharged in all 3 profiles around 190nJ.

4.5.3 Effect of capacitance *C* and supply voltage *V* on the waveform

Varying capacitance C and V increases the amount of energy stored in the power supply (as E_d=½CV^2). The effect of C can be observed from the simulation of pulse waveform shown in Figure 4.19 with 3 capacitance values of C=50pF, C=100pF and C=200pF. Pulse peaks were at 265mA, 345mA and 440mA; and pulse width was found to be 37ns, 50ns and 70ns respectively (which are given by the first zero crossing of current after the beginning of a discharge). It can be observed from the current waveform that both the peak and pulse width changed due to the change in capacitance which is similar to the change in inductance L. This is due to the fact the C

actually changes the impedance and thus modulates the frequency of the waveform and at the same time there is higher energy stored which forces the pulse peak to be higher. Experimentally this was also observed in the pulse waveform shown in Figure 4.15 obtained at 110V but a much higher capacitance value which significantly changed the pulse width to 165ns~171ns and the pulse peak to 4.7A~5.6A indicating a change in both pulse width and peak.

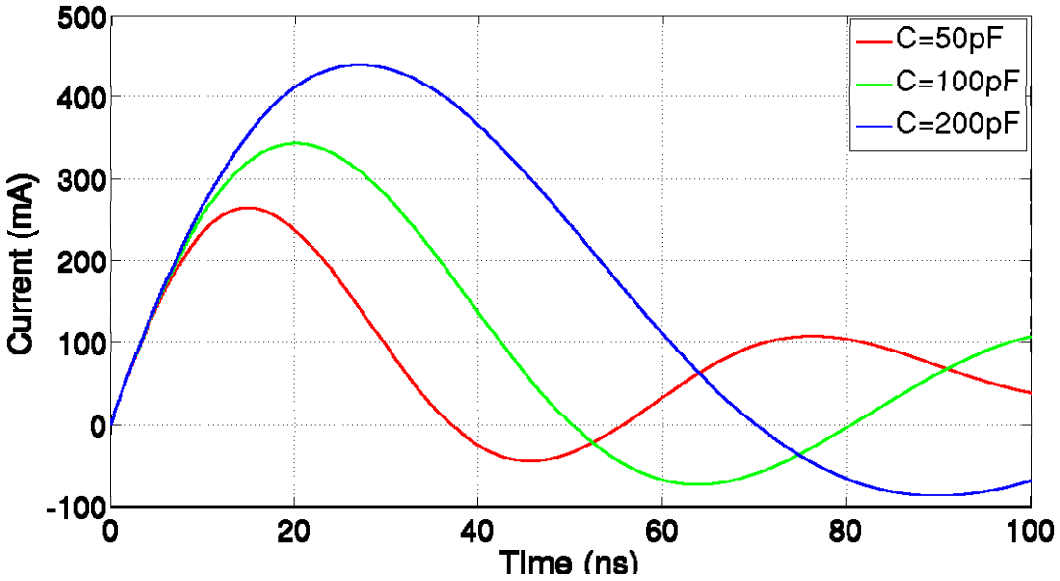

Figure 4.19 Current waveform at varying capacitance (C=50pF, 100pF, 200pF) (V=60V, R=1kΩ, L=1.9043μH, Plasma Resistance R_b=50Ω).

On the contrary, changing the supply voltage V (60V, 80V and 100V) did not change the value of pulse width (remained at 50ns) but significant change in the pulse peak was observed (345mA, 460mA, 575mA respectively) as could be seen in Figure 4.20. This is also to be noted that the energy to be discharged in a pulse changes proportionally to the square of the input voltage. Therefore, it can be inferred from the earlier discussions in this chapter that higher input voltage will create a deep crater and will have increased proportion of removal by vaporization. Therefore, for rough

machining higher supply voltage value around 110V~120V is preferred and for final finishing cut the voltage needs to be reduced to 60V.

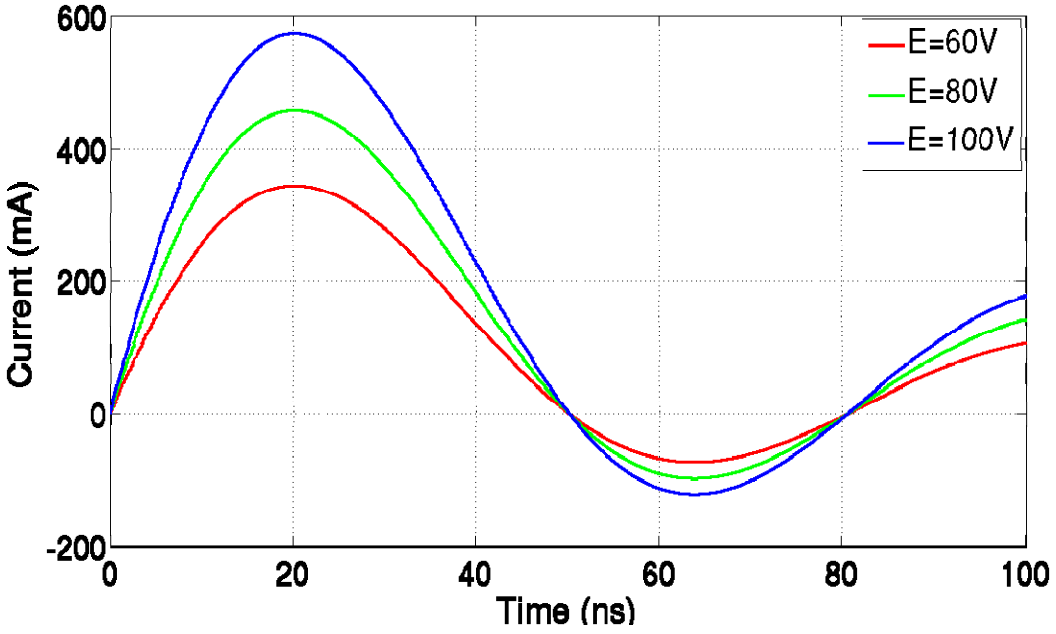

Figure 4.20 Current waveform at varying supply voltage (V=60V, 80V, 100V) (C=100pF, R=1kΩ, L=1.9043μH, Plasma Resistance R_b=50Ω).

4.5.4 Non-linear curve fitting for estimation of stray capacitance and inductance

Stray capacitance determines the amount of minimum energy spark size that a circuit is able to provide and therefore it is desired to have the equipment and power supply to be designed with minimum stray capacitance. Existing methods for estimation of stray capacitance depend on the fact that the discharge current pulse width depends on the capacitance which is a rather indirect and inaccurate inference for measurement of stray capacitance. Masaki and colleagues (2010a) proposed that the measurement of stray capacitance can be performed from actual discharge energy by observing the

current and voltage waveform and computing their product. This requires a voltage probe to be connected to the circuit for simultaneous acquisition of a voltage and a current waveform which introduces additional stray capacitance and therefore, incurring inaccuracy in its measurement. During the computation of stray capacitance, Masaki et al, 2010a, computed the total discharge energy to be 31pF and the system was installed with a 10pF capacitor. During the measurement they used a voltage probe with 13~17pF capacitance and from this they concluded that the system had a stray capacitance between 4~8pF with a mean value of 6pF. This clearly indicates the inaccuracy in the measurement of stray capacitance. Another alternative solution for stray capacitance measurement is to obtain the current waveform alone (without installing a voltage probe) from inductively coupled current probe (inductively couple probe does not have any loading or minimal loading effect on the power supply network) and then performing non-linear curve fitting of the waveform with this model (given by equation 4.31 and 4.32). The green profile in Figure 4.21 shows one such plot obtained from the system using only a current probe. As there is sinusoidal oscillation in the current waveform, the underdamped case was taken as the solution for fitting. Non-linear curve fitting was done to obtain the value of C in the equation and the input values were R = 1000Ω; L = 0.5019μH (total 10cm wire for the capacitor to tool electrode and 30 cm for workpiece to capacitor in the return path; explained in section 4.4.1); R_b = 50Ω, V=60V. The experimentally obtained current waveform provided input value for the current at stray capacitance.

The fitting was performed using custom written Matlab program and the non-linear fitting was done using Matlab routine lsqcurvefit (lsqcurvefit, R2012a). This routine performs non-linear fitting to obtain least square error and finds coefficients x that best

fit the equation of the model (equation 4.32) and the optimization is done by computing the following equation:

$$\min_x \frac{1}{2}\left\|F(x, xdata) - ydata\right\|_2^2 = \frac{1}{2}\sum_{i=1}^{m}(F(x, xdata_i) - ydata_i)^2 \qquad (4.38)$$

where, input data is xdata, and the observed output is *ydata*; and *xdata* and *ydata* are vectors of length *m* and *F (x, xdata)* is a vector-valued function (equation 4.31 in this case). Large scale optimization was used as the fitting option with an initial guess of C=50pF. The fitting program returned the value of stray capacitance based on the best fitted curve.

The red profile in Figure 4.21 has been obtained from the model of equation 4.32 computed using the value of stray capacitance, *C,* obtained from curve fitting. After 18 iterations of computation the model estimated the stray capacitance to be 6.58pF which matches well with the experimentally reported value of 6pF by Masaki et al. (2010a). Similar fitting can also be performed for obtaining any other parameters of the proposed model. Non-linear curve fitting was performed with another current waveform (Figure 4.22) for computing the value of inductance. With an initial guess of L=5μH and input values of R = 1000Ω, C=39pF, R_b = 50Ω and V=60Vthe model computed the value of L = 0.58936μH (actual L = 0.5776μH).

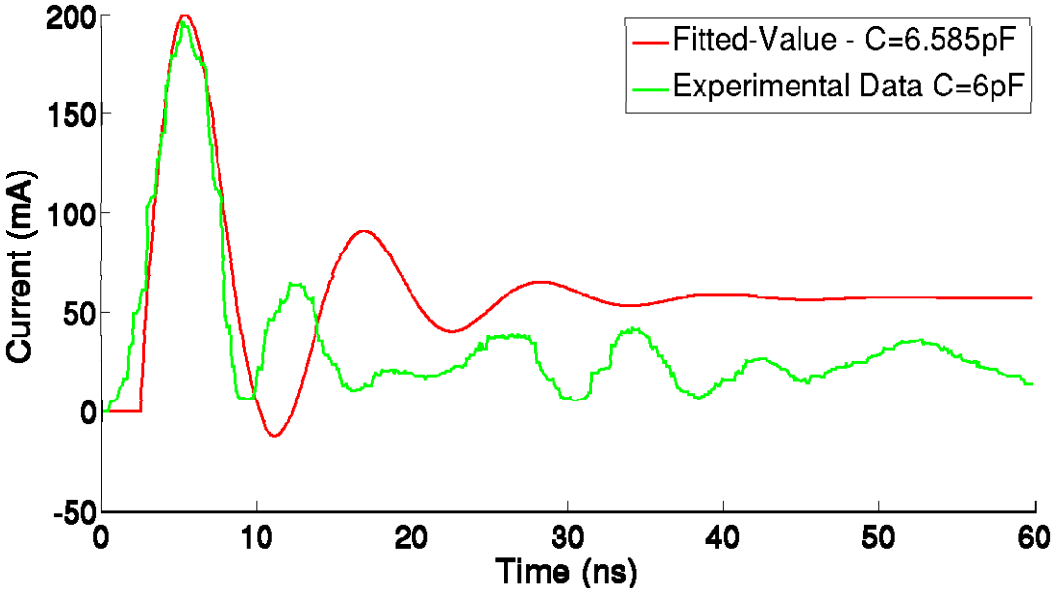

Figure 4.21 Non-linear curve fitting of the current waveform for computing stray capacitance. For fitting input to the model was R = 1000Ω; L = 0.5019μH; R_b = 50Ω, V=60V and initial guess of C=50pF.

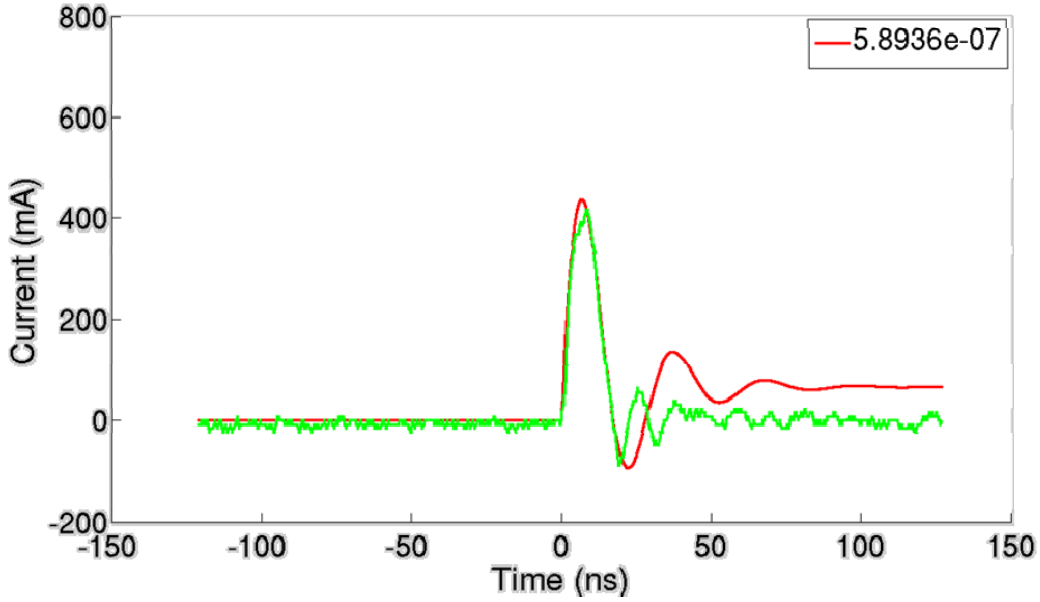

Figure 4.22 Non-linear curve fitting of the current waveform for computing the value of inductance. R = 1000Ω, C=39pF, R_b = 50Ω, V=60V actual L = 0.5776μH. With an initial guess of L=5μH the model computed the value of L = 0.58936μH.

4.6 Conclusion

In this chapter a model of the *RLC* network of micro-EDM plasma and power supply was proposed. For capacitive plasma discharge the plasma can be resolved into capacitive, resistive and inductive components. For micro-EDM capacitive and inductive component of the plasma can be ignored and the model was proposed using the resistive component of the plasma. Circuit equations can then be obtained based the equivalent resistive component and the proposed model current waveform and discharge energy. The proposed model, when suitably configured and used, has shown good agreement with experimental data. Robustness of the model was demonstrated by validating it on multiple experimental results reported in the literature. Using the proposed model the changes in the waveform due to changes in parameters like input voltage, capacitance and inductance were observed which provided significant insight to the process physics of micro-EDM process which can be utilized for process parameter optimization. Optimization on the resistance R in the charging loop of the capacitor was also performed and was compared with experimental results for selection of optimum resistance to minimize arcing during machining which is utilized for the design of RC relaxation type power supply. This model has also demonstrated the capability of calculating inductance and capacitance using non-linear least square fitting to the model. It was observed that significant changes in the supply voltage and use of large capacitance require the plasma resistance to be recomputed as these change the electrode plasma interface diameter significantly. In the following chapter the design of a power supply will be presented based on the fundamental of process physics elucidated from this model.

5 Micro-EDM Setup for Complex Micromachining

This chapter focuses on the development of power supply, improvement of machining performance by improving gap control, and implementation of 3D-synchronous milling EDM for machining true 3D features. The first section of this chapter presents the design of a micro-EDM power supply based on the fundamental insights developed and observation from the theoretical analysis in chapter 4. The second section discusses a new algorithm based on variable feedrate for gap control for the improvement of machining time. The third section focuses on the implementation of 3D micro-EDM milling for machining complex shapes and structures. The fourth section presents a new and improved electrode machining technique for machining of straight electrodes, which is a combination of existing block EDG process and 3D micro-EDM milling process. The fifth section of this chapter presents the experimental results of studying electrode wear ratio (EWR), machining time, MRR and spark gap. The experiments will be conducted to understand the machining characteristics of the developed setup which is essential for performing complex 3D micromachining experiment. The sixth section demonstrates the capability of the micro-EDM setup by presenting a wide range of micromachining examples of holes and 3D features between 5μm~50μm around the lower boundary of micromachining domain which prepares the UMMT for exploration of compound micromachining.

5.1 Design of Micro-EDM Power Supply

Stray capacitance determines the amount of minimum energy spark size that a circuit is able to provide and therefore it is desired to have the equipment and power supply to be designed with minimal stray capacitance. A careful design of the equipment and control circuits is needed to shorten the electric feeders, minimize usage of parallel metal plates around the discharging circuit that can function as electrodes, and increase the distance between unavoidable parallel electrodes in the discharge line and power supply unit. The use of a granite base for the machine tool minimizes stray capacitance in addition to its other role of vibration damping. UMMT presented in chapter 3 (Rahman et al., 2003) of this thesis was initially designed with the concern of minimizing stray capacitance and therefore, this design effort was solely focused on the development of power supply and signal generation for short circuit detection to be employed for gap control with the motion controller.

The schematic of the developed circuit is shown in Figure 5.1 and the picture of the circuit is shown in Figure 5.2. The value of the resistance *R* in the charging loop of the circuit was selected based on the discussion and experimental results presented in section 4.5.1 of this thesis. From the discussion it was concluded that using 1kΩ resistor for micro-EDM is an optimized value between minimization of arcing and quick capacitor charging time. Based on the discussions in sections 4.4.1 and 4.5.2 it was concluded that the circuit will be designed to have minimum *L* for most general purpose application and therefore, the circuit was connected to the Z axis head and Y table of the UMMT with the minimum cable length possible. Due to the limitation of structure in the setup – the minimum length of the cable required for connecting both

the workpiece and electrode to the capacitor is 1.2m and AWG20 diameter copper wire was used for the connection. The diameter of the wire cannot be increased significantly as at larger diameter the inductance is reduced but this also leads to the increase in stray capacitance as the stray capacitance of a wire is proportional to the core diameter and thickness of the insulation of the wire. This wire contributed to 1.9043µH inductance to the designed circuit.

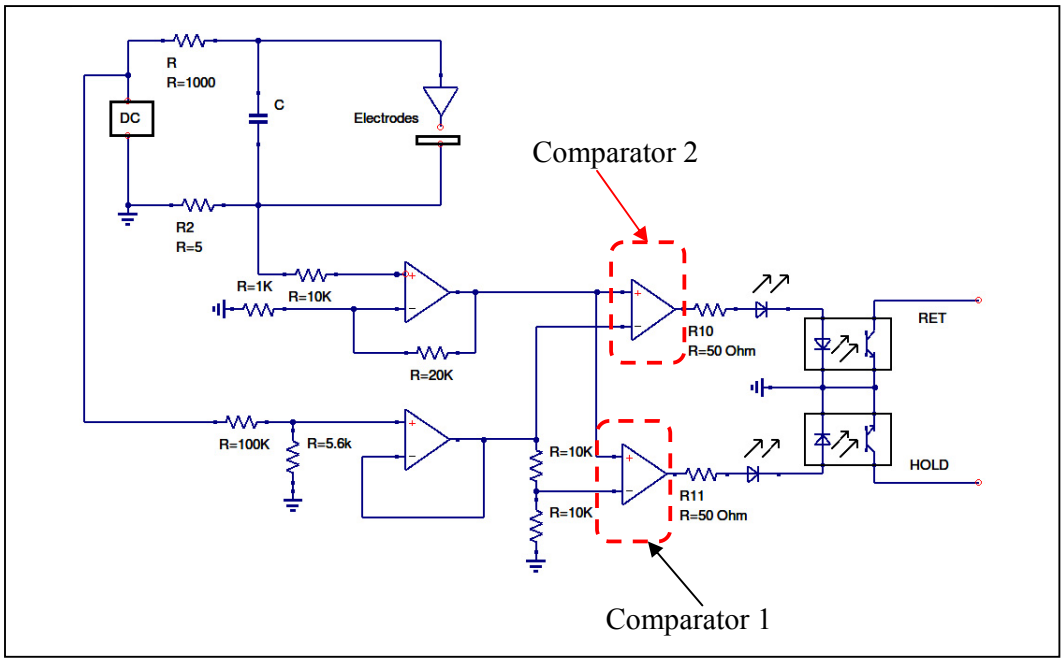

Figure 5.1 Schematic of the designed micro-EDM power supply circuit.

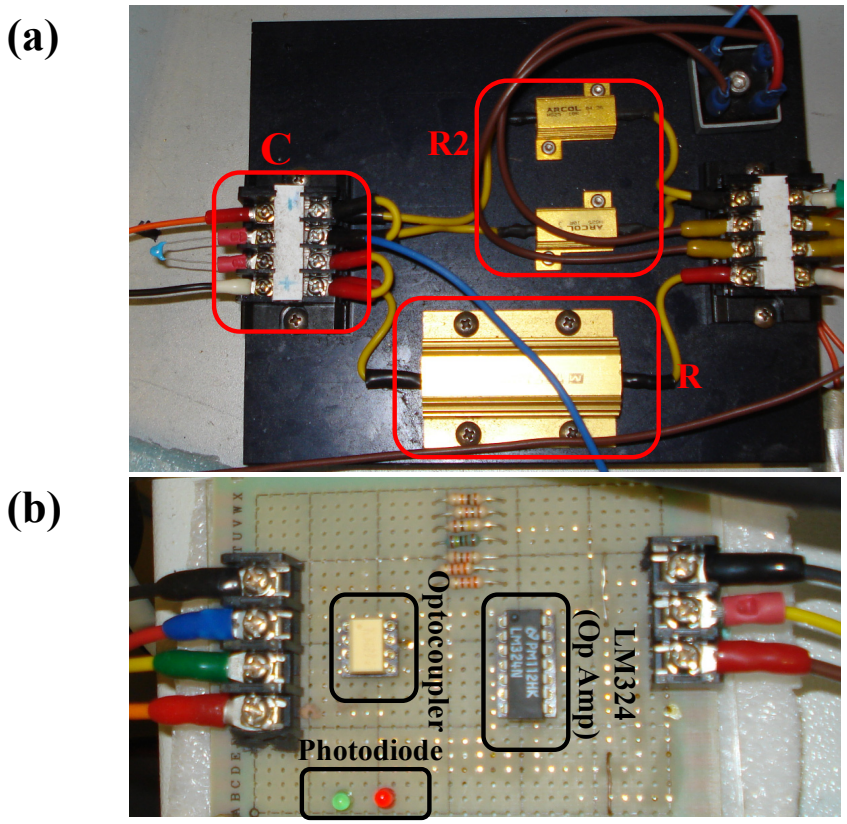

Figure 5.2 (a) Shows the main RC power supply unit; (b) shows the logic unit for feed, return and hold signalling to the motion controller.

5.1.1 Comparator logic for feeding, holding and retracting in gap control

The original gap condition monitoring CPU interfaced to the UMMT employed a mixed signal microprocessor for EDM condition monitoring. Earlier implementation of the circuit was done to continuously sample an averaged form of discharge current at a very high frequency using a fast analog-to-digital converter. As practically there is no physical switching off in the power supply in RC-based power supply contrary to the transistor-based power supply, the pulse frequency is extremely fast in terms of tens of nano-seconds in RC-based unit. Additionally the direct measurement using ADC may cause quite a bit of loading on the inductance and capacitance on the circuit

due to the long wire needed to feed the signal to the signal processor board. Hence, a new design was made which considers three scenarios of gap conditions to be discriminated through the use of 2 comparators connected to detect voltage drop across a very small resistor *R2* (Figure 5.3) placed in the charging loop. The comparators (implemented using LM324 operational amplifier) take the scaled down supply voltage as a reference input and compares with the voltage drop across the resistor *R2* for logic output. The three conditions and the corresponding outputs of the comparators are listed in Table 5.1. The advantage of the comparator circuit is that the power supply remains isolated from the rest of the circuit and signal cables primarily by means of operational amplifiers with high impedance, and since the comparator logic is binary in nature the signal feeding lines were further isolated using optocouplers.

Table 5.1 Comparator logic table for feeding, holding and retracting condition

EDM Condition	Comparator 1 (25% threshold)	Comparator 2 (50% threshold)
No spark or minimal spark observed and therefore the Z axis should continue feeding down	Low	Low
Spark observed and discharge current crossed the primary threshold value and therefore, Z axis should hold on to feeding, but retracting is not required	High	Low
Spark observed and discharge current crossed the secondary threshold value and therefore, Z axis should retract to clear the short circuit condition.	High	High

It is not expected that a continuous current flows through the resistor R2 unless there is a short circuit or a continuous discharge occurring resulting in a current flowing from the DC source via *R* to through the shorted electrodes and returning to ground via *R2*.

This is not acceptable favorable scenario in micro-EDM and therefore, in both of those cases the tool electrode needs to retract. The secondary threshold value defines the voltage drop across the resistor *R2* at which tool electrode requires to be retracted. The primary threshold on the other hand indicates the *hold* condition to signal temporary stop of feeding Z axis until the voltage across resistor *R2* has dropped below the threshold. The detection thresholds selected for primary threshold is approximately 25% and secondary threshold is approximately 50% of the maximum voltage drop across *R2* when the circuit is continuously ON over a sampling period (or the primary and secondary threshold values are approximately 0.125% and 0.25% of the supply voltage respectively). The 25% threshold value for *hold* condition and 50% threshold value for r*eturn* condition can be approximated from simple calculations using an estimate of charging and discharging time of the RC circuit. Let us, consider a case where DC supply source is set to 100V. Therefore, through the charging loop, if the electrodes are shorted together, voltage drop across *R* would be 99.5V and across *R2* would be 0.5V which is the case of shorting and this is the maximum voltage drop across the resistor *R2*. If over a period the averaged value across the resistor *R2* is above 0.125V (25% of 0.5V) then the primary threshold will be set to *High* to indicate that the hold condition has occurred; and similarly, if the voltage across resistor *R2* is above 0.25V (50% of 0.5V), then the secondary threshold will also get set to *High* to signal retraction of the tool electrode.

The smallest obtainable pulse width for the discharge pulse is around 30ns with only stray capacitance (20 pF; the value of the stray capacitance is discussed in section 5.1.2) and after a discharge the capacitor requires to be charged. During the charging cycle, with 1KΩ resistance for the resistor *R* and 20pF stray capacitance would give a

time constant τ = 20ns (given by R×C) and 5 times τ would be 100ns (with varying current flow rate over time). The voltage profile across *R2* during the charging could be seen in Figure 5.3. Now one of the probable fastest discharge scenarios can be considered where a discharge occurs followed by only 63% charging of capacitor which takes only one τ (20ns) and immediately after that there is another discharge and continues in the same manner. This can be considered as the fastest discharge as during a charging cycle over the first τ the fastest voltage recovery occurs. While, during the first τ – the gap voltage recovers to 63%, over the second τ this only recovers another additional 23% of the voltage. Thus for a hypothetical case – this can be considered a fastest discharge. In such a scenario the total cycle time is only 50ns, 30ns for during the discharge when there is no current flowing through *R2* and 20ns charging when current is flowing through *R2* following the profile of Figure 5.3. During the second and subsequent discharges, if the discharge follows immediately after one τ of charging (63%) then a small amount of current that will still flow through *R2* even during the discharge in the discharge loop. But, as the objective of this calculation is to provide for a rough estimation of the voltage which can be used as threshold and given that micro-EDM is a stochastic process and the fastest case may or may not happen, the flow of current during the discharging phase can be ignored. . Now the mean voltage over one such cycle is computed to be 0.125V (computed by integrating the area under the curve of Figure 5.3 up to one τ to obtain the voltage and then divided by 50ns to compute the mean) which is about 25% of the maximum voltage drop value (0.5V) and this is set as the primary threshold for the comparator signaling *hold* signal. If a true discharge caused the threshold to reach this value then during the hold period the discharge frequency will be reduced as the electrode stops approaching towards the workpiece and thus the *hold* signal will get cleared.

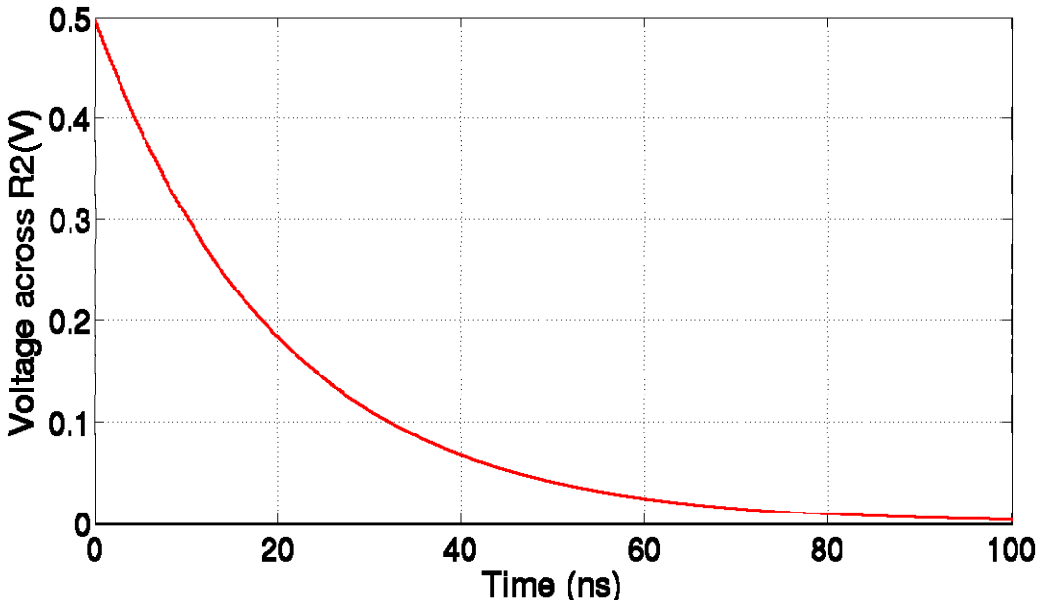

Figure 5.3 Voltage profile across resistor *R2* during the charging of capacitor *C* following a discharge.

On the contrary, if a short circuit or arcing has caused this situation then during the hold the arcing may still continue and the voltage drop across the resistor *R2* will be even higher. Therefore, the secondary threshold needs to be above 25% of the maximum voltage drop value in order to determine the return condition and over the value above primary threshold (25%) but below secondary threshold will be considered as the *hold* condition. It is desirable to minimize the false positive detection to minimize time spent in gap control and also to minimize false negative as arcing causes damage to the workpiece. Therefore, a threshold value in the middle of 25% to 100% (62.5%) can be considered to balance the false positive and false negative. But, practically as arcing is less desirable compared to cost of increase in machining time by gap control – a 50% threshold was set to fulfill the *return* condition. This indicates that if the voltage drop across *R2* is 0.25V or above (50% of the maximum possible

voltage drop across *R2*) then this will assert a short circuit condition in the logic output and the machine would require retracting the tool electrode.

5.1.2 Discharge current waveform at stray capacitance

It has been mentioned earlier in this chapter that the presence of stray capacitance in the circuit is one factor that determines the limit of minimization of the discharge energy. Energy minimization is required for machining very fine features and in section 3.5.2 of this thesis it has been established that for micromachining in the lower dimensional range of micromachining domain the micro-EDM power supply should be able to provide pulses with discharge energies around 15nJ~30nJ. In section 3.5.3 of this thesis it has also been discussed that the present transistor type micro-EDM power supply provides discharge energy around 56.25μJ in its finest setting which lead to this development work with a target of obtaining discharge energies around 30nJ~50nJ. Figure 5.4 shows a fine spontaneous spark of 30 ns pulse width using stray capacitance at 60V supply voltage. The peak current is 200mA as could be seen in the trace. Using the micro-EDM power supply model presented in chapter 4 of this thesis and applying non-linear curve fitting to the pulse waveform (explained in section 4.5.4) the stray capacitance is estimated to be around 20pF~21pF having discharge energy of around ~37nJ. This can be compared to the requirement of smallest discharge energy established in section 3.5.2 which was estimated to be in between 30nJ~50nJ.

The fitting to the waveform is shown in Figure 5.5 which shows good agreement between the data fitted to the model and experimental waveform profile (specially, the first lobe of the discharge waveform). However, the subsequent ringing after the first

lobe shows a comparatively less damped response with higher amplitude of oscillation (specially, observable in the second lobe) in the experimentally obtained waveform. Even though, the amplitude deviates, the overall pattern and the frequency of oscillation match well for the second lobe. This indicates that the capacitive and inductive reactance of the model matches well with the experimental setup (as the ringing oscillation of underdamped circuit is contributed by the presence of capacitive and inductive element in a circuit). The deviation in amplitude can be explained by considering the presence of debris in the discharge gap generated after the first lobe of discharge which caused the overall resistance of the plasma to be reduced and thus allowing larger current to flow through the gap.

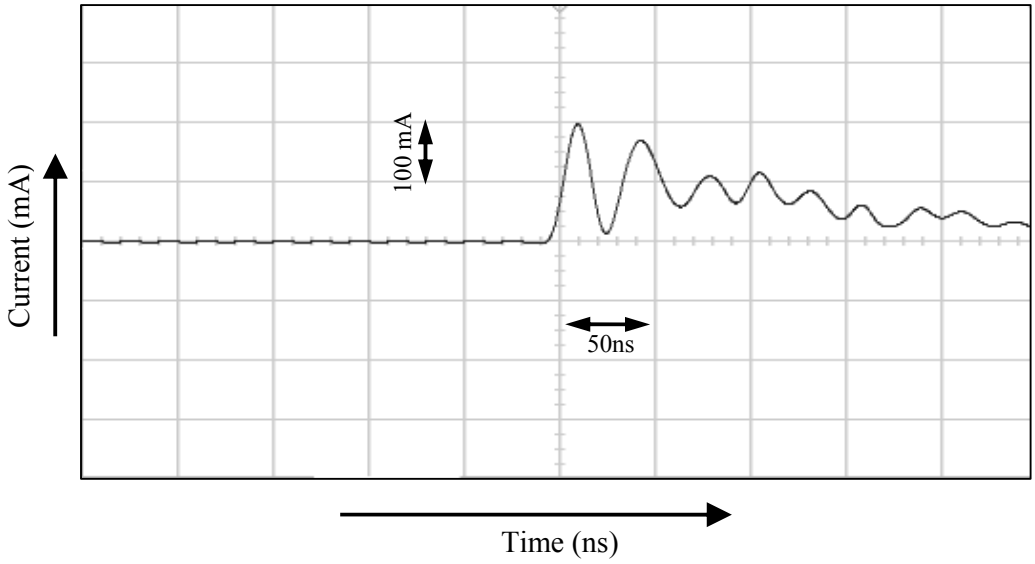

Figure 5.4 Discharge pulse waveform obtained at supply voltage of 60V with stray capacitance obtained from the new power supply developed for UMMT. The observed pulse width is around 30ns and pulse peak is 200mA.

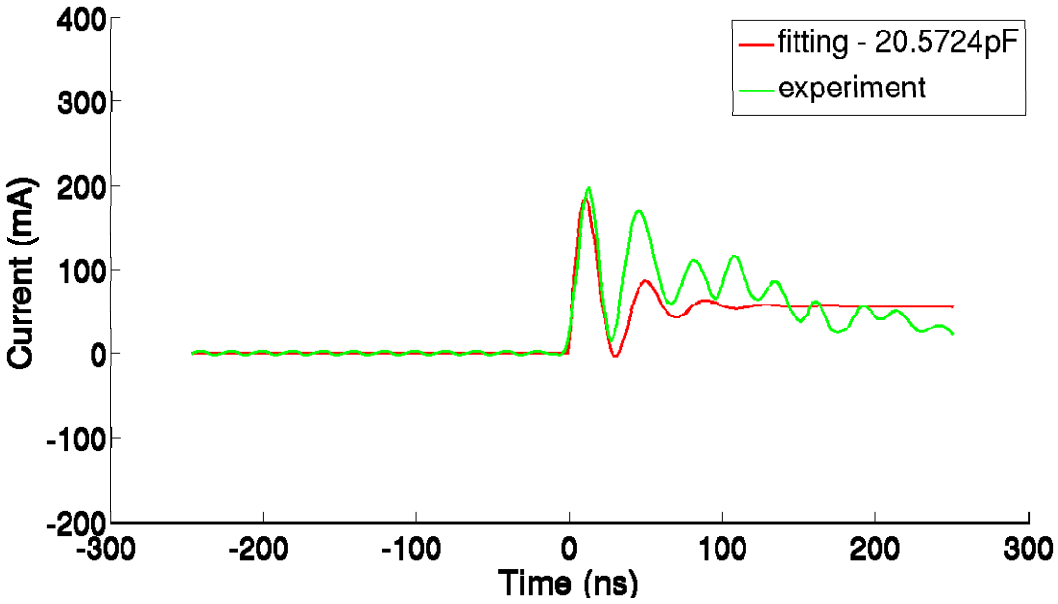

Figure 5.5 Non-linear least square curve fitting of the current waveform for computing stray capacitance. For fitting input to the model was R=1005Ω; L=1.9043µH; plasma resistance R_b=50Ω, supply voltage V=60V. The initial guess for the stray capacitance was set to 50pF.

Experiments were performed to study the crater size on the machined surface and machinable feature size using the power supply developed. Figure 5.6(a) shows the SEM image of a surface machined using stray capacitance at 60V supply voltage and crater sizes around ~2µm can be observed. Figure 5.6(b) shows two 10µm thru slots on 50µm thick SUS-304 plate with 2.5µm wall separating the slots was machined using stray capacitance at 60V. The slots were machined using 3D micro-EDM milling which will be explained in details in the following section. Figure 5.6(c) shows machined hole using square electrode (120µm length) and also shows fine edges with very thin crust layer indicating reduced re-solidification and increase in removal by vaporization. This can be compared to Figure 3.7 which shows a similar hole machined by a square electrode using the finest energy settings of the transistor-based power supply. The improvement in machining performance using micro-EDM is

evident from the edge of the machined hole. The importance of minimum energy settings in obtaining fine features and shapes can be observed in Figure 5.6(d) which shows a failed attempt to machine walls and steps of 1µm size. It can be seen that overall a pyramid looking structure could be seen but the steps and walls are not formed.

As accuracy of present micro-EDM process technology is around 1~2µm (Kawakami, T., et al., 2005; Kunieda, M. et al., 2005), thus the above experimental results can be considered state-of-the-art for micro-EDM and suitable for fine micromachining (this will be further established by performing complex micromachining of high-aspect-ratio features in section 5.6). Furthermore, with the designed circuit the minimum discharge energy requirement of 30nJ~50nJ is achieved (discharge energy of the developed setup at stray capacitance ~37nJ). Extensive research in comparing the RC power supply designed in this section and the existing transistor power supply on the UMMT has been reported by Jahan et al. elsewhere (Jahan, MP., et al., 2009(a); Jahan, MP., et al., 2008). Their experimental results clearly substantiated the claim that the RC power supply performed significantly better for micro-EDM compared to transistor-based power supply as well as this is suitable for performing fine quality machining.

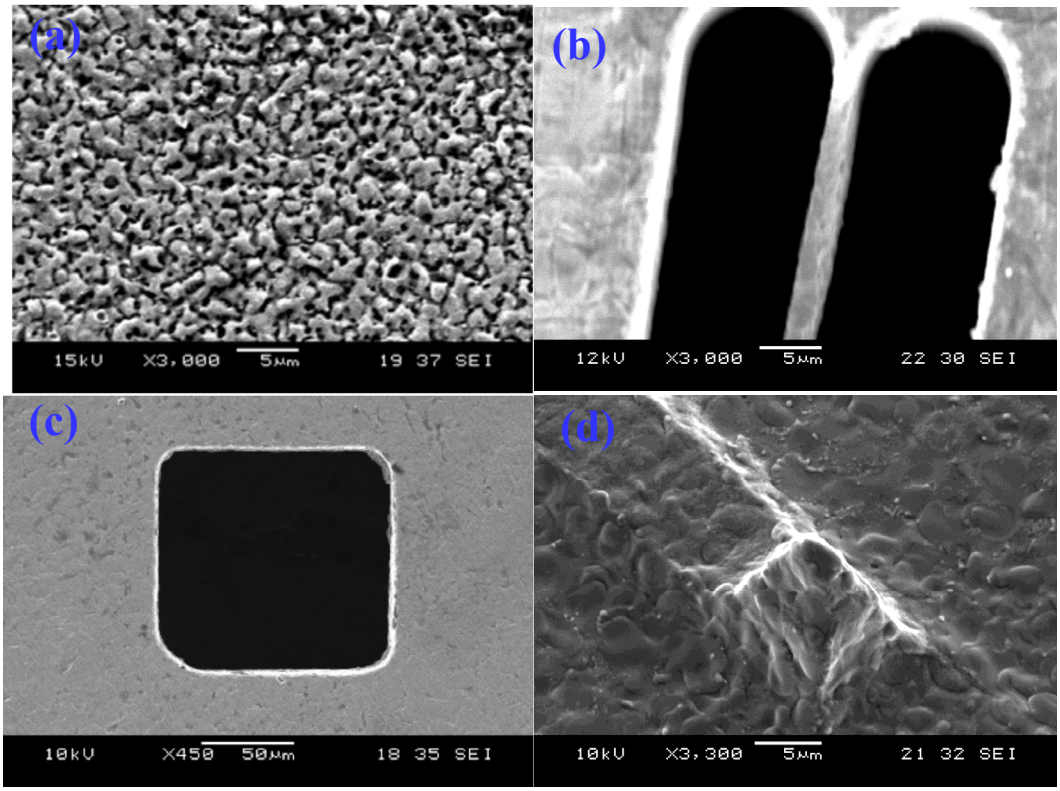

Figure 5.6 (a) ~ 2µm crater size obtained by machining only with stray capacitance at 60V which resulted ~37nJ discharge energy. (b) Two 10µm thru slots on 50µm thick SUS-304 plate with 2.5µm wall separating the slots was machined using stray capacitance at 60V. (c) Machined hole using square electrode shows fine edges with very thin crust layer indicating reduced re-solidification and increase in removal by vaporization. (d) A failed attempt to machine walls and steps of 1µm size to indicate the low energy settings and machinable feature size in micro-EDM.

5.2 Implementation of Jump Distance Based Gap Control

In micro-EDM electrode gap condition monitoring is critical to successful machining and the objective is to maximize the time spent during the process in discharge spark and to minimize the time spent during the process in getting the electrodes shorted and arcing. One requirement is to identify the condition by observing the discharge current which has been implemented in the new power supply hardware proposed and discussed in details in section 5.1. The second requirement is to retract the tool

electrode opposite to the feed direction when the hardware detects a retract condition and sends the signal to the motion controller. In large die-sinking EDM servo control of the gap is usually performed using hydraulic servo system. The UMMT in discussion is designed using an advanced numerical control motion controller where all 4 axes can be positioned in coordinated manner simultaneously.

In the original implementation of the gap control on the UMMT, the tool electrode was retracted opposite to the feed direction using the same feedrate used for feeding the electrode for machining. Figure 5.7 shows a simplified form of the decision making flowchart for the gap control. Usually micro-EDM is not a fast process having maximum feed at few microns per second which is comparatively slow in changing the flushing condition. Figure 5.8(a) shows the oscilloscope trace across the electrode gap to show machining condition during gap control where the retraction occurs at the same feedrate as the feeding of the electrode. It can be seen from the trace that during the existing gap control there is slow recovery to machining from a short circuit. Significant amount of short circuit/arcing period is observed as there is a large continuous block of period where discharge/shorting/arcing process was continuing and this is attributed to the feedrate being at 2µm/s. It can also be observed that after retraction the following one second there was no spark which indicated that the Z axis moved forward at 2µm/s and required one second to approach back to the workpiece again.

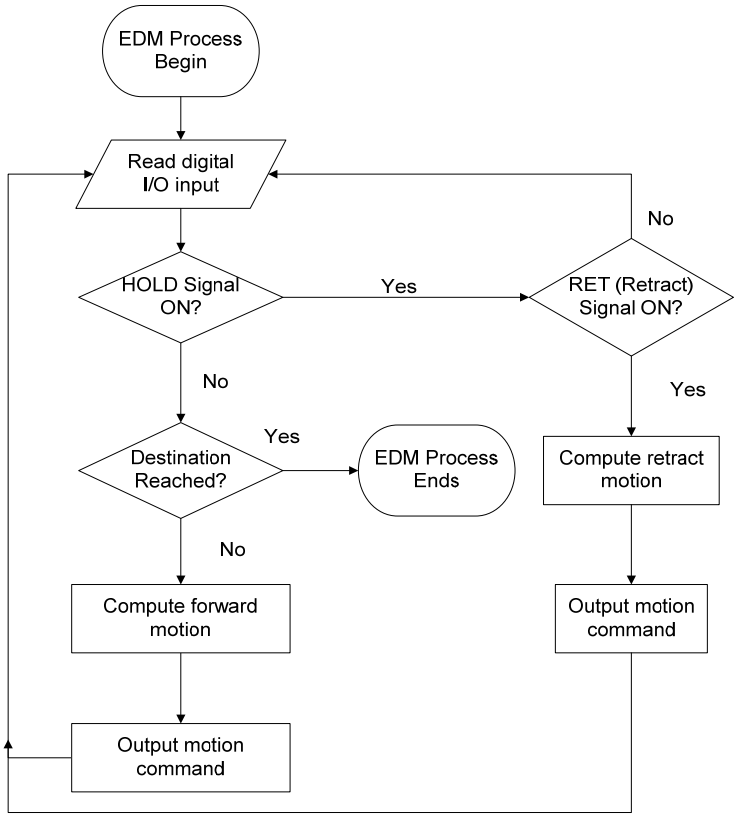

Figure 5.7 Simplified flow chart of the gap control algorithm implemented in the existing code base of the motion controller.

A jump based gap control was implemented which performs by retracting the electrode in the direction opposite to the feed direction at a much higher feedrate and for a larger distance which can be considered as a kind of jump motion after detection of a retract command (Kunieda, et al., 2005, Masaki, et al., 2010b). This was controlled by two input parameters to the controller defined as '*retract feed*' and '*retract distance*'. The electrode also approaches the workpiece at higher feedrate and requires another two input parameters '*approach feed*' and '*approach distance*'. In this new gap control implementation the short circuit/arcing condition can be eliminated very quickly and additionally, it also helps to create a wider gap for efficient flushing

of debris from the gap space. It can be seen in Figure 5.8(b) that the new algorithm does not have long period when current flows through the charging resistor. Additionally the machining seems to be more homogeneously distributed and does not show a long idle period. The decision making for this gap control is implemented inside the compute forward motion and compute retract motion segment of the flowchart shown in Figure 5.7.

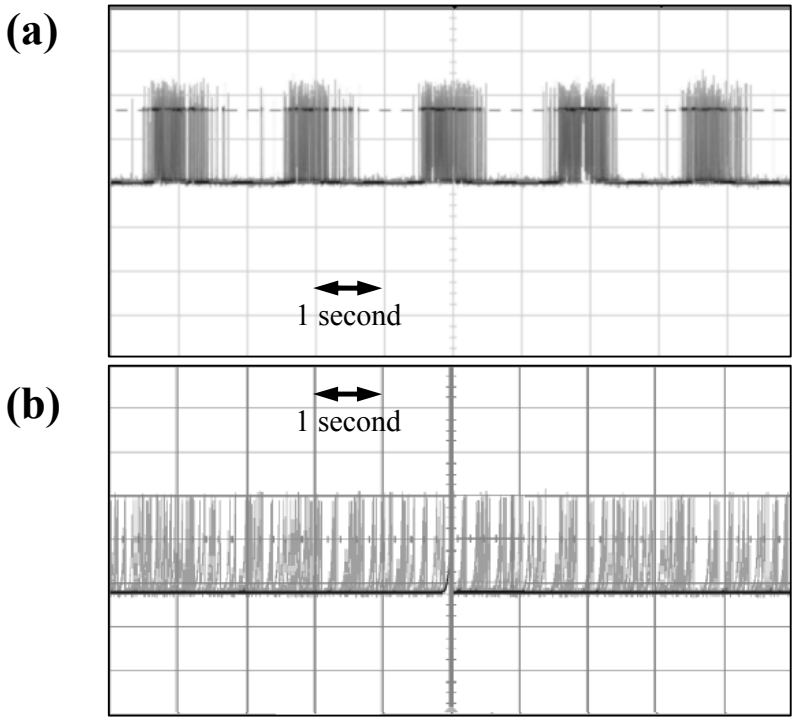

Figure 5.8 Oscilloscope trace across the electrode gap to show machining condition during gap control. (a) The conventional gap control originally implemented on the UMMT suffers slow recovery to machining after retraction and significant amount of short circuit/arcing period is also observed as the retraction was done at 2µm/s. (b) Gap control based on jump algorithm shows quick retraction from short circuit/arcing and also the recovery to machining was very quick.

Experiments were conducted on the UMMT using the RC-based power supply described in section 5.1 of this chapter to observe the machining time improvement

and changes in electrode wear rate with the new gap control strategy. Table 5.2 shows the parameters used for the machining. In Table 4.1 it can be observed that the gap width at both 60V supply voltage and 470 pF capacitance as well as 100V supply voltage with 11pF is around 3.30µm. Therefore, it can be assumed that at 80V and 47pF (Table 5.2) the gap width will be less than 4µm. Hence the '*retract distance*' was set to 5µm in order to guarantee that the electrode has been retracted sufficiently to break any possibility of short circuit/arcing. '*Approach distance*' was set to a slightly smaller value than the '*retract distance*' (4.5µm) to ensure some time and distance for transition from the jump of the tool electrode to gap condition monitoring (as well as to ensure that in case of an overshoot the tool electrode does not initiate short/arcing condition again). The '*retract feed*' and '*approach feed*' was set to 100µm/s which would require approximately 50ms for the retraction to execute. Higher feedrate was not used as it was observed in section 3.4 that the machine requires 10ms to respond to the motion command and requires about 20ms of settling time.

Holes were bored on 50µm and 100µm SUS-304 plate using tungsten electrode and boring of hole was repeated 10 times on each plate for each gap control algorithm. Figure 5.9(a) shows the machining time and Figure 5.9(b) shows the wear on the tool electrode. Even though machining time using the jump based gap control improvement was not considerably faster on 50µm thick SUS-304 plate (80 seconds vs 77 seconds), machining time improvement was observed for boring on 100µm thick plate (207 seconds vs 195 seconds). There was no remarkable difference in observed tool wear rate between the two gap control algorithms. As the primary target of this gap control was to improve machining time of thru and deep holes/features (as machining time was not significantly improved for 50µm deep hole boring), the surface properties of

the workpiece surface and tool electrode surface was not investigated. Furthermore, from this experiment it is evident that the machining time was improved due to reduced arcing. On the other hand it is known that arcing causes surface damage and is not desirable (Kunieda, M. et al., 2005) it was perceived that there was no detrimental effect on the surfaces of the workpiece and electrode if not improvement.

Table 5.2 Parameters for comparing machining time with process feed gap control and jump based gap control

Parameter	Value
Retract Feed	100 µm/s
Retract Distance	5 µm
Approach Feed	100µm/s
Approach Distance	4.5 µm
Machining Feed	2µm/s
Electrode	Tungsten
Workpiece	SUS-304, 50µm and 100µm thick
EDM Oil	Total EDM 3 dielectric oil
Supply voltage	80V
Capacitor	47pF
Electrode dia	~ 45µm
Number of holes machined	10 holes for each group

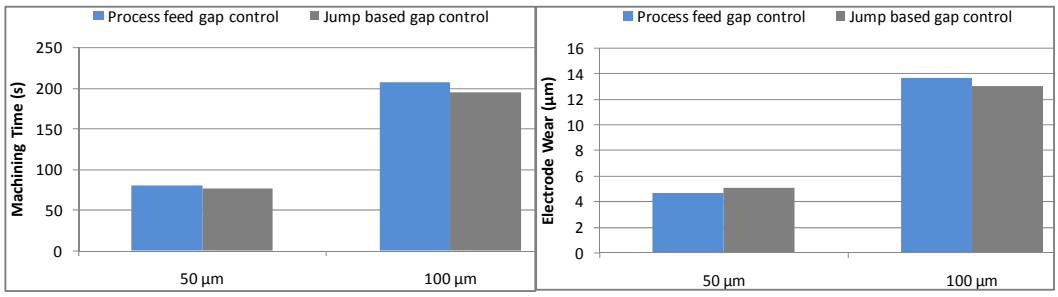

(a) **(b)**

Figure 5.9 Comparison of experimental machining time and electrode wear for machining using process feed rate gap control and jump based gap control on 50µm and 100µm SUS-304 plate.

5.3 Implementation of 3D micro-EDM Milling on UMMT

Commonly used for traditional mold machining, die-sinking EDM process has found wide-spread industrial applications. However, in micro-EDM electrode wear ratio is so large that a fine complex shaped electrode cannot be used because the electrode shape quickly changes. Moreover, it becomes specially a challenge to fabricate such complex electrodes when the feature sizes are below 50μm. These problems can be resolved using a simple cylindrical electrode that moves along a designed 3D tool path to perform non-contact milling like processing by micro-EDM (Yu, Z. Y., et al., 1998). Figure 5.10 illustrates the die-sinking and micro-EDM milling process. There exist serious issues in micro-EDM milling related to tool wear compensation and maintenance of the tool shape, in addition to control of the layer thickness to be machined. Most reports on micro-EDM milling in literature propose a layer-by-layer machining technique (Bleys, P., et al., 2004; Bleys, P., et al., 2002; Hang, G., et al, 2006; Pham, DT., et al., 2004; Yu, Z. Y., et al., 1998). But, the problem with such layer-by-layer machining is that the machining time is significantly longer than die-sinking (Yu, Z. Y., et al., 1998). Lim et al., (Lim, HS., et al., 2003) proposed a method where the X-Y axis moves at a constant speed in one direction and Z axis performs gap control given by the equation 5.1 below:

$$F_Z = k \times \text{sgn}[V_g - V_{th}] \qquad (5.1)$$

where, F_Z is the Z-axis feedrate, V_g the gap voltage between the electrode and workpiece and V_{th} the threshold value for the gap control, and k is a control parameter that determines the speed of the micro-EDM gap control. This process is prone to form

more side wear than bottom wear and therefore, the electrode shape becomes narrower and slot becomes shallower as the process progresses and thus caused the machining failure that they observed during their experiments.

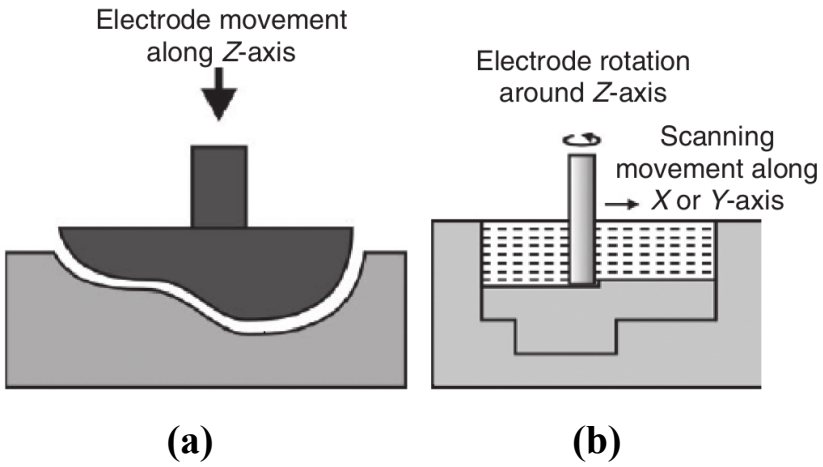

Figure 5.10 Schematic representation of (a) die-sinking micro-EDM, (b) micro-EDM milling (Jahan, MP., et al., 2011).

A new method of micro-EDM milling was proposed by Masaki et al. (2010(b)) which has the capability to perform fast machining while maintaining the electrode shape by having electrode wear only at the bottom of the electrode. On the UMMT this micro-EDM milling algorithm was implemented (Figure 5.11). In this implementation Z axis is programmed to provide up and down motion for the gap control based on the sampled gap voltage status while the X and Y axes are programmed to make linear or circular oscillatory motion simultaneously along the contour to be machined. In order to function properly the most important configuration parameter is the ratio of the feedrate of Z axis for machining and the X-Y axis motion to distribute the sparks over the entire area of the contour which will in turn minimize side wear. The electrode

wear to be distributed at the end of the tool electrode, in order to achieve the ease of machining uniformity and the Z-direction compensation of tool wear. Ideally, the X-Y feedrate is expected to be as fast as possible. But there is a limit to the feedrate because upon motion reversal at very high feedrate there could be higher reversal error from driving axis. From the experiment performed in section 3.3 it was discussed that on the UMMT quadrant reversal could be observed above 80mm/min feedrate and therefore, the practical oscillatory feedrate for X-Y axes is between 30mm/min ~ 60mm/min.

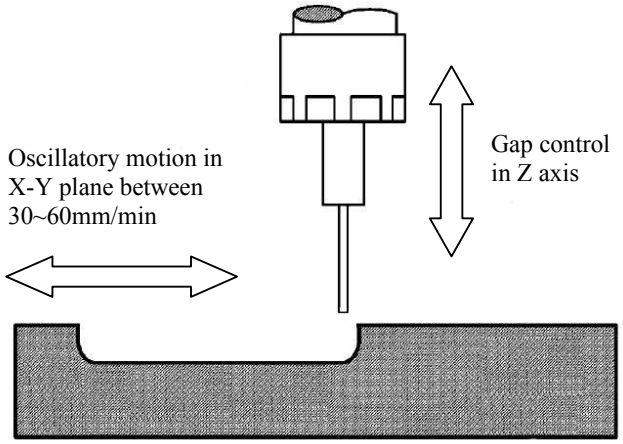

Figure 5.11 Schematic of milling-EDM process with oscillatory motion in X-Y plane and simultaneous gap control in Z axis.

Experiments were conducted to study the achievable average surface roughness of the implemented micro-EDM milling process and to compare the results with conventional die sinking process. Machining was conducted using a 2mm copper tungsten electrode and the machining parameters are shown in Table 5.3. Micro-EDM milling experiments were performed to machine 10μm deep and 2.8mm long slots with flat surfaces were machined by giving 30mm/min XY feedrate. The surface roughness was measured using Taylor Hobson surface profiler (Talysurf Model–120) and the results

are shown in Figure 5.12. It shows the comparison between die-sinking and EDM milling process. It can be observed from the plot that the surface obtained from EDM milling provides slightly better surface than the die-sinking process. This could be attributed to the improved side flushing condition with the moving electrode in EDM milling compared to die-sinking where debris may get trapped which may cause arcing. Further detailed characterization and extensive research on the surface properties between die-sinking and EDM milling was performed by Jahan et al., on the developed setup (Jahan, MP., et al., 2010, Jahan, MP., et al., 2009(b)). They observed traces of surface defects in die-sinking micro-EDM, specially at low voltages due to arcing and short circuit condition occurring. This effect was removed by the tool movement of micro-EDM milling and thus micro-EDM milling has the capability to generate smooth, shiny and defect free surface with lower R_a and R_{max} along with uniform crater distribution. They also concluded that very low discharge energy can be applied more easily in micro-EDM milling without making the machining process unstable due to good inherent flushing conditions. Beyond improvement of surface roughness, the primary advantage of micro-EDM milling is the capability of machining fine features and intricate shapes in 3D using simple cylindrical electrode which is easy to prepare compared to the complexity in electrode preparation for die-sinking operation. In section 5.6 several complex micromachining examples are presented to further demonstrate the capability of micro-EDM milling for micromachining.

Table 5.3 Machining parameters and conditions for studying surface roughness by micro-EDM milling and die sinking.

Parameter	Value
Voltage (V)	140,130,120,110,100
Capacitance (pF)	110
Resistance (Ω)	1000
Dielectric	Total EDM 3 dielectric oil
Tool Electrode	Cu-W (2mm)
Workpiece	Tungsten carbide
Machined Depth	10µm
X-Y motion	2mm (X), 2mm (Y), 30mm/min

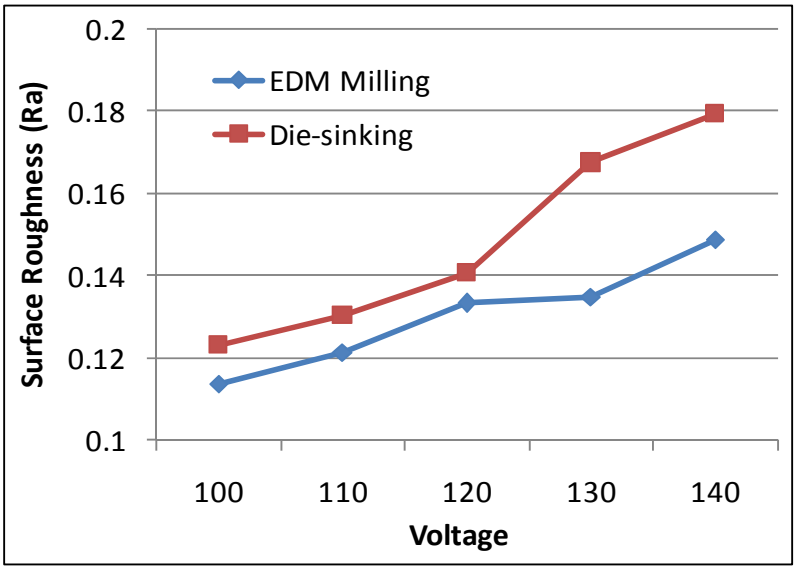

Figure 5.12 Comparison of surface roughness between die-sinking and EDM milling process using Cu-W electrode.

5.4 Straight electrode machining for micro-EDM

The non-contact nature of EDM makes it possible to use a very long and thin electrode for machining tough die material. But electrode wear has to be compensated by changing to a fresh electrode, or by preparing a longer electrode right at the beginning. Another alternative is to fabricate the electrode in-situ for further machining. It is not

recommended to change the micro-electrode during machining, because it incurs inaccuracy due to the change in setup or re-clamping of the micro-electrode.

From an electrode thicker than the required diameter, a cylindrical electrode can be fabricated by the EDG process using a sacrificial electrode (Masuzawa, T., 2000). Different setup and trajectory control of the sacrificial electrode can be used in this process (Fleischer et al., 2004; Kurita et al., 2005), such as using a 'stationary block', 'rotating disk', 'wire EDG (WEDG)', etc. Schematics of these processes are shown in Figure 5.13. In stationary block EDG (BEDG) setup shown in Figure 5.13(a) due to dimensional change in the sacrificial electrode, the diameter of the tool electrode fabricated is usually unpredictable, but provides a smooth surface. The use of a rotating disk involves a rather complicated setup although it provides good shape accuracy (Figure 5.13(b)). The WEDG process (Figure 5.13(c)) has the capability of producing extremely slender rods with good aspect ratio and has received wide industrial acceptance due to the prospect of automation. The advantage of the block electrode method is mainly in its capability to fabricate electrodes that are not cylindrical in shape (for example, triangular or square electrode), in addition to being economical with lower operating cost (Ravi N. et al., 2002). Another important factor is that the diameter precision of commercially available brass wire commonly used for WEDG has a diameter precision of ±1μm (Masaki, T., et al., 2007), which is added to the inaccuracy of micro-EDM process (Kawakami, T., et al., 2005) and therefore in some cases the surface finishing efficiency was not found to be as high as rotating disk method (Lim, HS., et al., 2003).

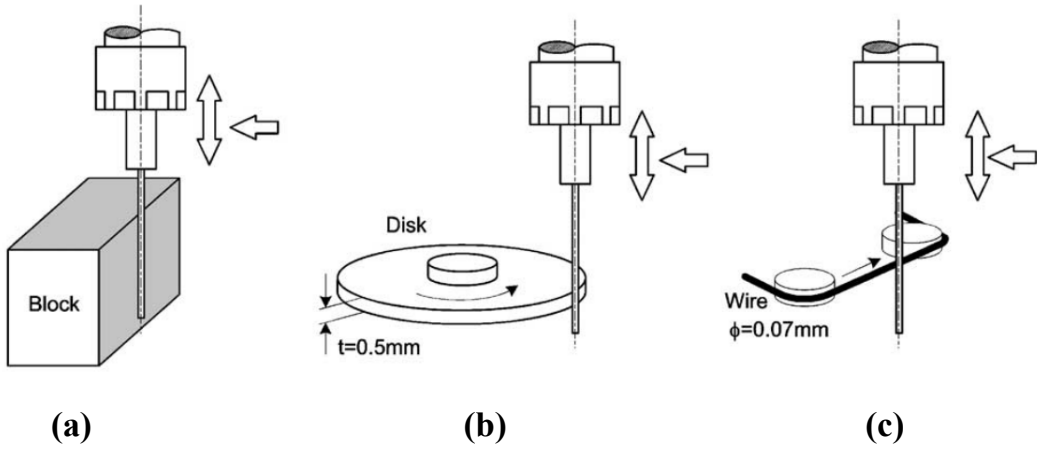

Figure 5.13 On-machine electrode fabrication processes using sacrificial electrode (a) stationary sacrificial block-EDG (BEDG), (b) rotating sacrificial block EDG, (c) wire-EDG (WEDG) (Lim, HS., et al., 2003).

A new process has been developed to combine the advantages of two electrode machining techniques, BEDG process for being economical and simple and for its capability to produce non-cylindrical shape, and 'rotating disk' for providing a smooth surface. In this process, the tool electrode to be prepared is programmed to perform micro-EDM milling process described in section 5.3 to perform moving sacrificial block -EDG (MBEDG). While the tool electrode (Z-axis) controls the spark gap at the top surface of the sacrificial block, a to-and-fro relative translational motion between the block electrode and tool electrode is provided along the longitudinal axis of the block electrode (schematic shown in Figure 5.14). There is erosion on the moving block by electric discharges during machining. However, the erosion is distributed uniformly over a larger area of the block electrode. Most of the sparks are between the gap layer of the top surface of the block electrode and the un-machined part of the tool electrode and there are hardly sparks from the side of the tool. This creates electrodes with a very smooth surface, very good shape accuracy and the fabricated electrodes are not tapered. However, the length of the electrode produced is always slightly smaller

than the target length due to grooves created on the surface of the block electrode. Taking into consideration the machined area between the tool electrode and the sacrificial electrode, the difference between the target length and the actual length is almost negligible. Figure 5.15 shows two shafts fabricated by BEDG and MBEDG process where black arrowhead shows the tapered section of the shaft produced by BEDG and white arrowheads show the straight section produced by MBEDG process. Figure 5.16 shows the erosion marks formed on the tungsten carbide block from BEDG and MBEDG processes. The erosion marks created on the block by the BEDG process (shown in black arrowheads) shows tapered shape of the formed electrode compared to the flat grooves created by the MBEDG process (shown inverted and indicated with white arrowheads).

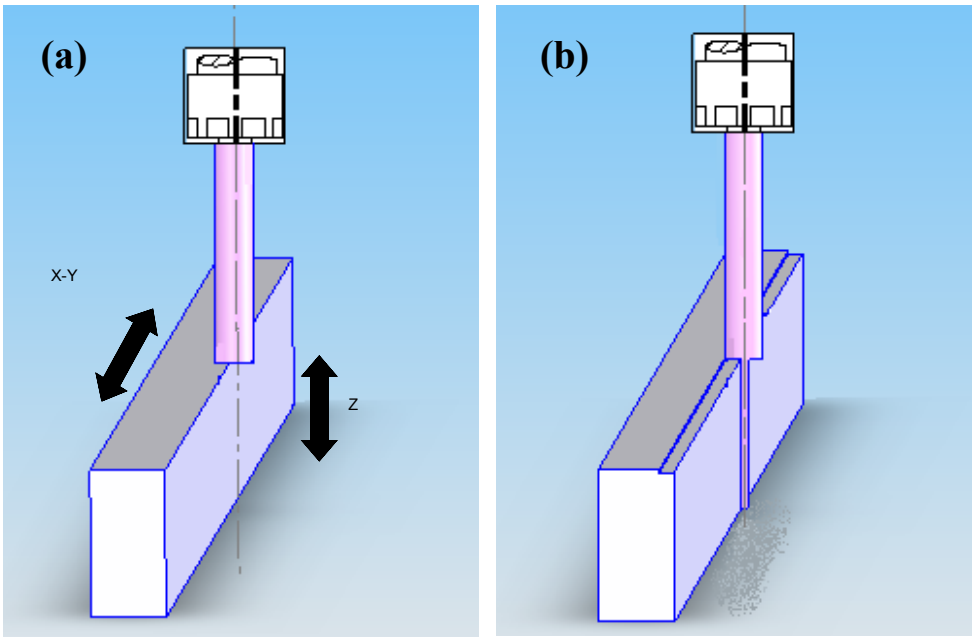

Figure 5.14 Concept of MBEDG process for on-machine tool fabrication. Linear to and fro motion along X-Y axes are performed at 30 mm/min ~ 60 mm/min and Z direction performs gap control (a), and (b) illustrates step created on the block and straight shaft generated.

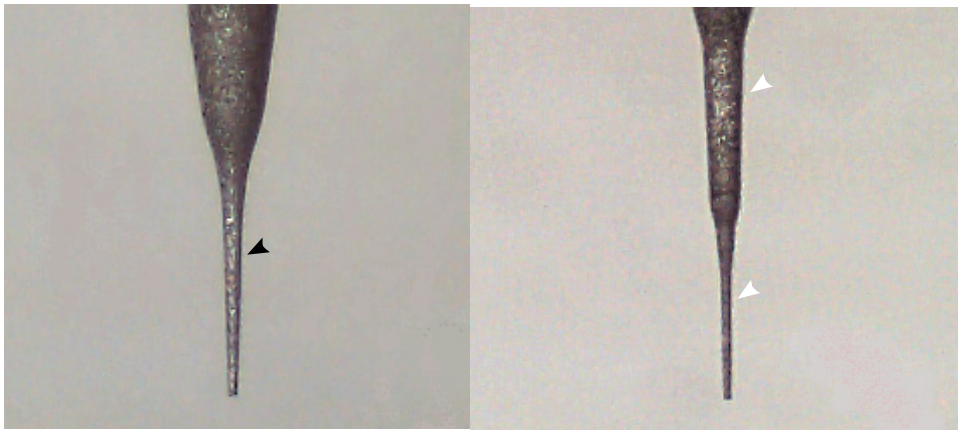

Figure 5.15 Shows shafts fabricated using BEDG process (a) and moving BEDG process (b). Black arrowhead shows the tapered section of the shaft produced by BEDG and white arrowheads show the straight section produced by MBEDG.

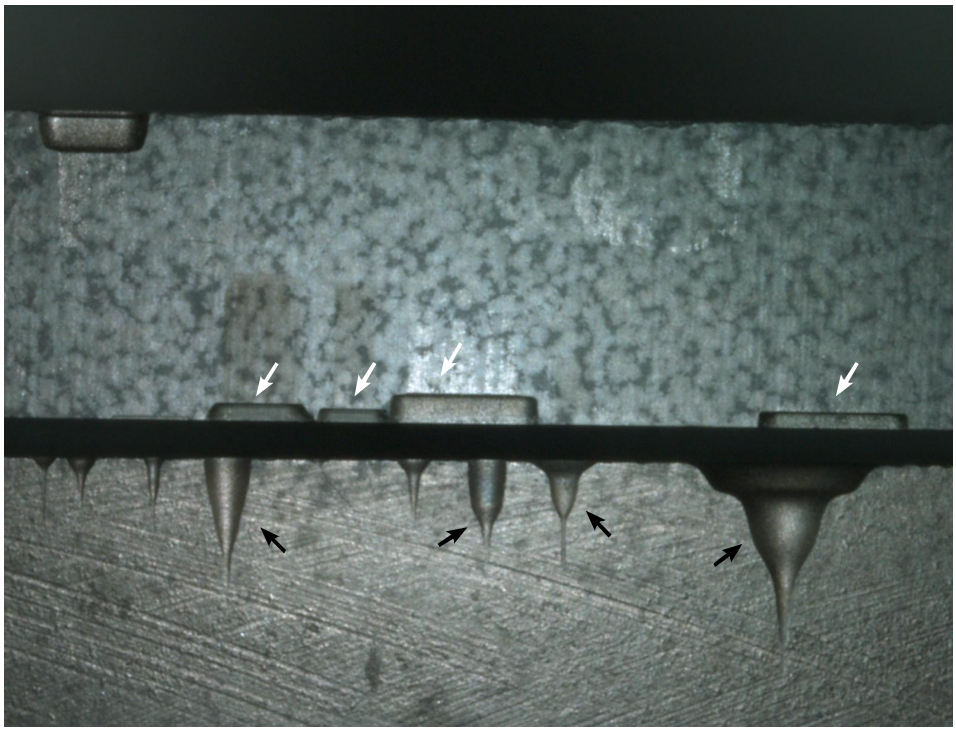

Figure 5.16 Erosion mark created on the tungsten carbide blocks used for BEDG (black arrowheads) and MBEDG process (shown inverted and indicated with white arrowheads).

5.5 Experimental Study of Machining Speed and Tool Wear

For performing micromachining of complex shapes and structures it is necessary to characterize the output parameters like electrode wear ratio (EWR), machining time, material removal rate (MRR) and spark gap in order to be able to compensate for electrode wear and compute expected machining time. Experiments were conducted to study these machining parameters by drilling holes of varying electrode diameters into 50µm thick SUS-304 plate using tungsten and copper-tungsten electrodes. Details of machining conditions are shown in Table 5.4 and experimental results are shown in Figure 5.17. As at 60 V and stray capacitance the discharge energy is considerably low (~37nJ), for machining of most of the 3D features in section 5.6, 80V supply voltage and 47pF capacitance (150nJ discharge energy) have been used). Machining was performed using RC-based power supply described in section 5.1 with jump-based gap control described in section 5.2. Electrodes were fabricated on-machine starting with 0.5mm tungsten electrode which was formed using the MBEDG process described in section 5.4. Three different diameters of tungsten electrode (15.5µm, 33.5µm and 42µm) were compared to provide a range of electrode diameters (from 15µm to 40µm) that will be used in performing complex micromachining in section 5.6. Additionally machining was also performed using Cu-W electrode which is another commonly used electrode material in micro-EDM. Hole drilling was repeated for 10 times in every experimental group to observe variation and repeatability; as statistically significant results are specially important given that micro-EDM is a stochastic process. For drilling holes on 50µm thick plate, an additional 70µm depth was fed into the hole making the total feeding depth to 120µm. This depth was selected based on initial observation on electrode wear being less than 10µm and thus adding an additional

60µm would ensure that a straight electrode portion forms the hole finally to make a straight hole. In the statistical results the first hole was excluded as the machining results of the first hole have shown significant variation MRR and EWR which could be potentially due to the fact that the electrode tip was comparatively smaller in diameter.

Table 5.4 Machining conditions to study machining time, MRR, EWR and spark gap.

Parameter	Value
Supply Voltage	80V
Capacitance	47pF
Workpiece	SUS-304, 50µm thick
Electrode Materials	W (dia 15.5µm ,33.5 µm, 42µm), Cu-W (dia 44.5µm)
Machining Feed	2µm/s
EDM Oil	Total EDM 3 dielectric oil
Gap control	Jump-based (retract feed - 100µm/s, retract distance 5µm, approach feed – 100µm/s and approach distance – 4.5µm)
Electrode Machining	MBEDG
Number of holes machined	9 holes for each group

The mean values of machining time, MRR, spark gap and EWR are shown in Figure 5.17 where the error bar indicates one SD. For micro-EDM with electrode diameter smaller than 50µm it was observed that the machining time did not vary with change in diameter. This resulted in the change in MRR which is potentially misleading as the supplied machining energy was same. This could be due to the fact that with increased surface area the probability of spark increased which led to the increase in MRR. Variation of EWR for tungsten electrode was with ±2µm which indicates that with electrode wear compensation the accuracy of a machined feature may vary ±2µm within one SD. The shape of the electrode was tapered at the bottom of the electrode

due to erosion similar to the observation of Kao et al., (2006). But except the electrode tip the remaining portion that was fed to ensure straight hole machining did not show considerable sign of erosion. Considerable variation in EWR was observed in results for machining with Cu-W electrode (±4µm) which could be due to the higher tool wear of Cu-W which also caused this variation.

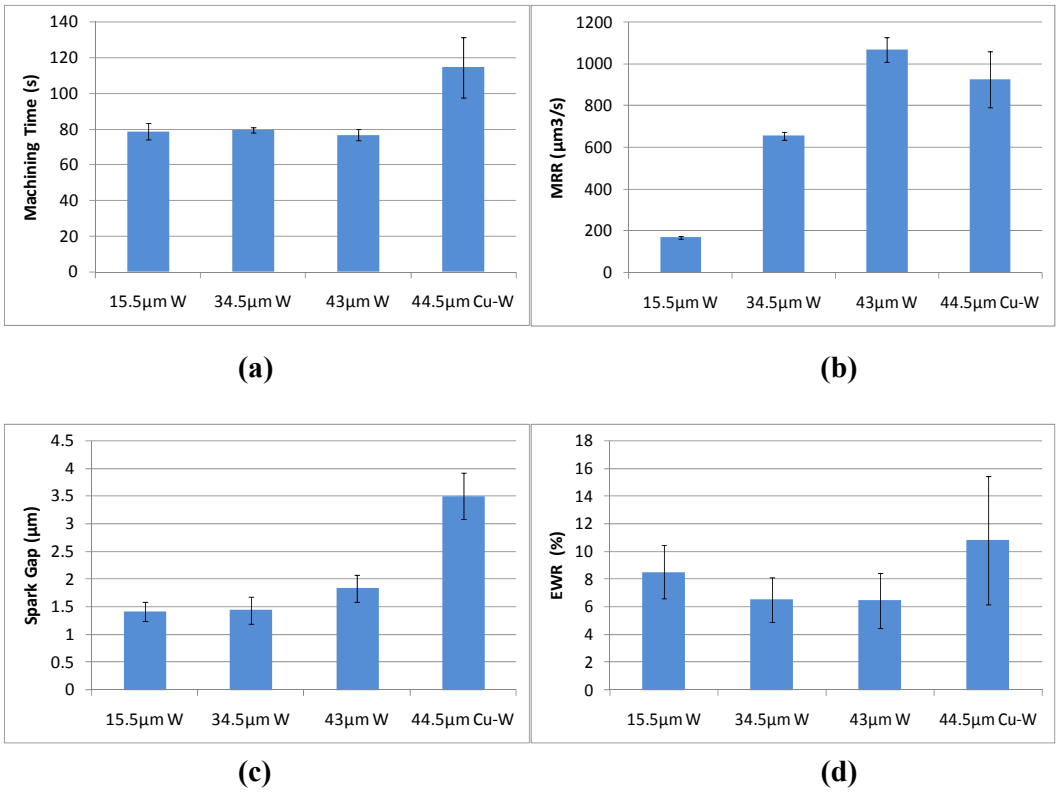

Figure 5.17 Experimental results for studying (a) machining time, (b) MRR, (c) spark gap, (d) EWR.

5.6 Complex Micromachining Using Micro-EDM

Experiments were conducted to explore the capability of the developed system for performing complex micromachining of shapes and features below 50µm dimensional range. The machining conditions for the machining are shown in Table 5.4 and

appropriate diameter tungsten tool electrode was fabricated using MBEDG processes. Figure 5.18 and 5.19 show several micro-EDM samples machined. Tool electrodes, as small as 4µm in diameter, have been fabricated using BEDG process. This electrode was then used for boring holes into 50µm thick SUS-304 plate. Four holes of diameter 6.5µm, 8.5µm, 10.5µm and 12.5µm have been machined as shown in Figure 5.18(a). Figure 5.18(b) shows the close-up of 8.5µm hole and Figure 5.18(c) shows the 6.5µm picture placed next to that showing a red blood cell (Figure 5.18 (d)) for comparison. While machining of electrodes with 4µm diameter is a bit complex and requires careful observation under on-machine scope as well as multiple passes using MBEDG and BEDG process, this shows the capability of micro-EDM process in fabricating shapes at the lower boundary of micromachining domain. It has been mentioned earlier in section 5.1 that the smallest available discharge energy from the developed setup is ~37nJ which, creates a crater of around ~2µm diameter on stainless steel and therefore, this could probably mean the smallest machinable dimension with this setup. Machining of each hole took about 2 minutes to fabricate using machining conditions in Table 5.4 with supply voltage 60V and 33pF capacitor. Figure 5.18(e) shows holes of 10µm diameter on 50µm thick SUS-304 plate forming 'N' – the initial of 'NUS' where each hole was machined in 2 minutes with supply voltage 60V and 33pF capacitor. Figure 5.18(f) shows another array of micro-holes of around 15µm diameter machined using larger spark energy at 100V and 220pF to machine them in ~75 seconds. Figure 5.18(g) shows a simple 35µm deep square trench (25µm wide) machined by micro-EDM milling and a center hole of 25µm diameter drilled by micro-EDM drilling using the sane ekectrode. The hole is separated from the slot with a 5µm wall in 18 minutes. Complex shapes with multiple steps and many layers were also machined to form 3 dimensional structures using micro-EDM milling process. Figure

5.18(h) shows a small pyramid machined using micro-EDM milling process (L: 25µm, W: 25µm, H - 35µm at the top). Each step was machined layer-by-layer to 7µm wide and 7µm deep using an electrode having 15µm diameter and machining took about 150 minutes with 80V and with 33pF capacitance leaving the other machining conditions similar to Table 5.4. Figure 5.19(a) shows 'NUS' (55µm wide and 10µm deep) written by micro-EDM milling process on SUS-304 and machining time was about 25 minutes. Figure 5.19(b) shows the image of a profiled capillary (nozzles) in a spinneret plate for spinning synthetic fibers from a molten or dissolved polymer which has practical industrial application in spinning industry. This spinneret plate with 12µm slot width was machined using an electrode of 8.5µm diameter and machining time was around 90 minutes. Sample on Figure 5.19(c) shows 2 slots (L: 250µm, W: 28.5µm) machined where each slot took 30 minutes to fabricate. Figure 5.19(d) shows adjacent slots of 10µm wide on 50µm thick SUS-304 plate with 2.5µm wall separating them. This shows the minimum achievable feature size as has been mentioned earlier. Figure 5.19(e) shows a central hole with radially distributed slots being machined using similar techniques (L: 100µm, W: 50µm) in 90 minutes which can be used as forming electrode by micro-EDM^n (Masaki, T., et al., 2006) for micro-cavity in micro-fluidic applications. Figure 5.19(f) and close-up in Figure 5.19(g) shows a slot (L: 1000µm, W: 37µm) machined on a hypodermic needle of 200µm thick wall on stainless steel by WEDM process using 30µm tungsten wire for biomedical applications. Figure 5.19 (h) shows a miniature clover shape machined in 50 minutes using an 8µm electrode.

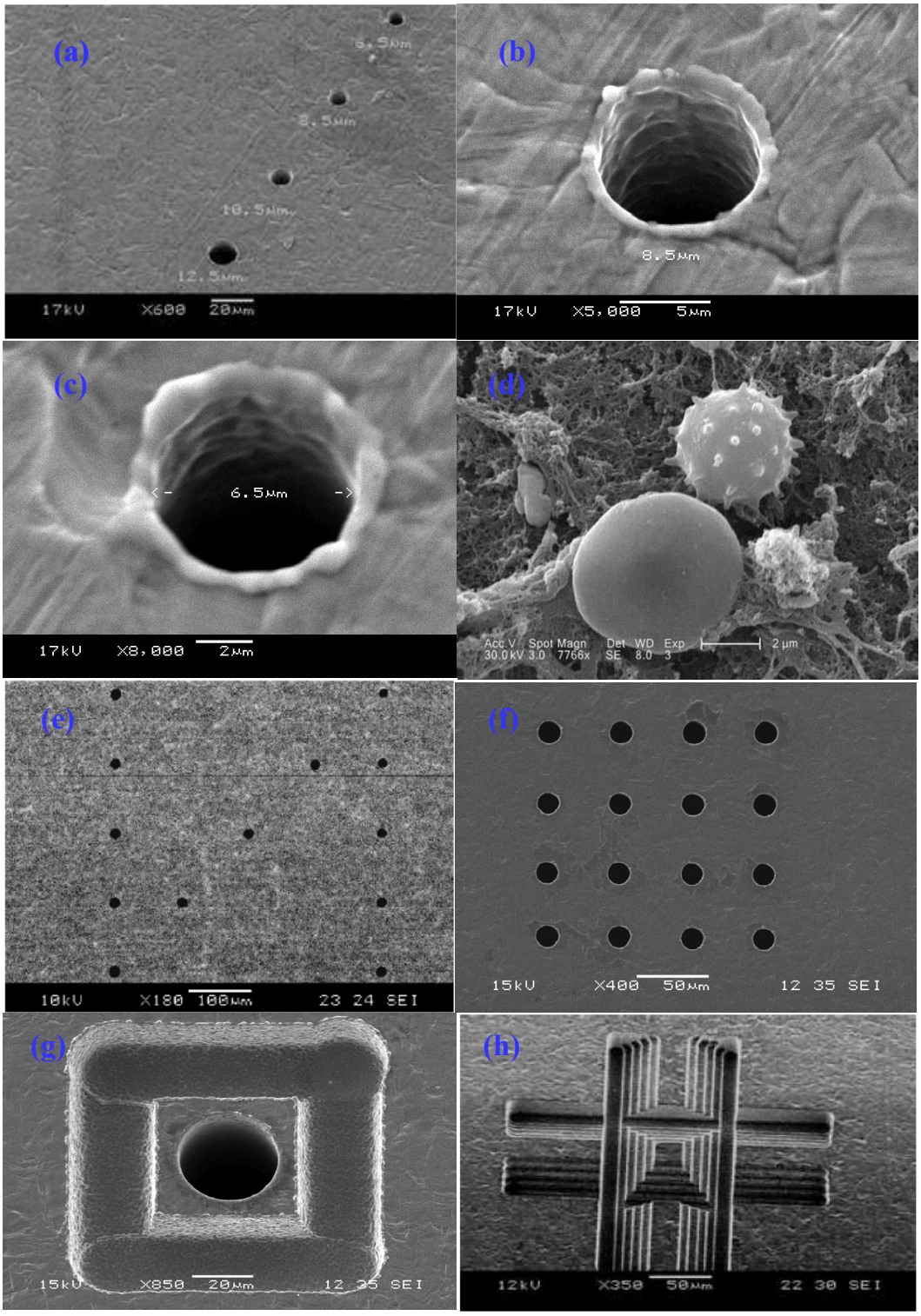

Figure 5.18 Microfabrication by micro-EDM drilling and micro-EDM milling using electrodes fabricated on-machine by BEDG/MBEDG process (1).

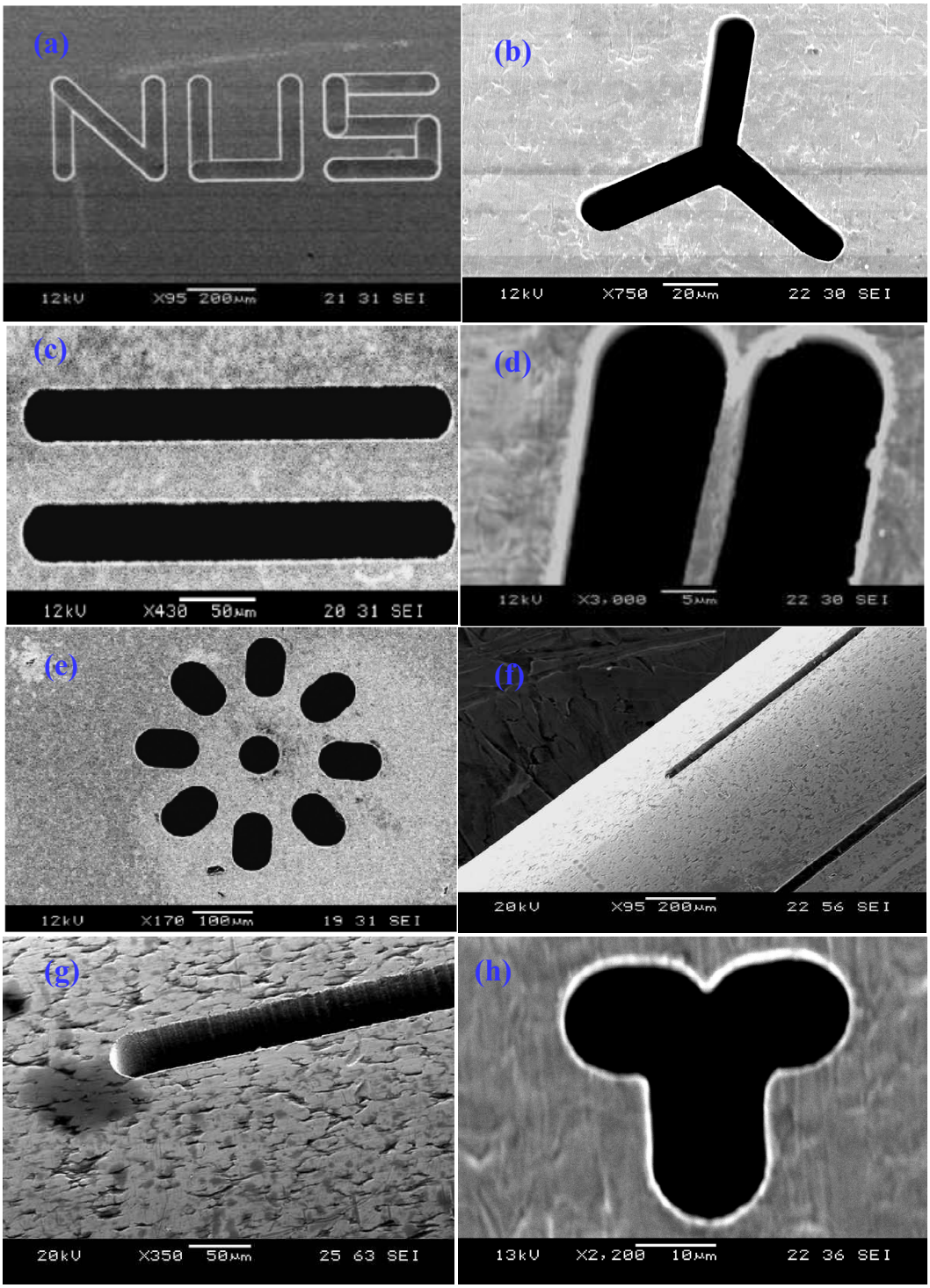

Figure 5.19 Microfabrication by micro-EDM drilling and micro-EDM milling using electrodes fabricated on-machine by BEDG/MBEDG process (2).

5.7 Conclusion

In this chapter the design of an RC relaxation type micro-EDM power supply has been presented. At stray capacitance the smallest available discharge energy ~37nJ at 60V was observed and the stray capacitance was determined to be 20pF~21pF by fitting to the experimentally obtained waveform using the model presented in chapter 4. A jump based gap control was implemented and compared with the earlier implementation of gap control using the process feedrate. Experimental machining time studies demonstrated slight improvement of machining time when boring holes on 50µm thick stainless steel plate, but considerable timing improvement was observed for boring holes on 100µm thick plate; and no considerable difference was observed in electrode wear. A 3D micro-EDM milling process was adopted and used, where simultaneous gap control along Z axis and oscillatory motion along X-Y axes are programmed to make linear or circular oscillatory motion simultaneously along the contour to be machined representing the shape of the feature (either a linear slot of circular arc). With the 3D micro-EDM milling process, improvement of surface roughness was observed compared to direct die-sinking process. Using the 3D micro-EDM milling process, a new electrode machining process capable of making straight electrodes was proposed (MBEDG). Experimental studies were then conducted to characterize the machining time, MRR, spark gap and EWR for micromachining of complex shapes and features of between 5µm~50µm to be machined. Complex micromachining features are presented to demonstrate the capability of the improved UMMT for performing in the lower dimensional range of micromachining domain. The development and studies are necessary for exploration of compound micromachining processes presented in Chapter 6.

6 Compound Micromachining on UMMT

This chapter focuses on the exploration of compound micromachining on the developed UMMT to demonstrate its potential for performing micromachining tasks that are impossible or difficult to achieve using a single process or serially employed processes (using separate setups or machines). The first is a compound micromachining concept where conventional turning tool is in-situ modified using micro-EDM followed by using the modified tool for micro-turning to enable machining of micro-shaft. An application of the micro-shaft is next presented. This involves its use as a tool electrode for performing micro-EDM drilling operation which, being an extension of the earlier compound machining is basically a 3-step compound micromachining (micro-EDM + micro-turning + micro-EDM). This process was experimentally compared with tungsten electrode fabricated using BEDG/MBEDG processes for drilling holes. A third compound micromachining concept is presented using PCD micro-tools shaped in-situ by micro-EDM for micro-grinding and micro-milling.

6.1 Compound Micro-EDM + Micro-turning Process

Micro-turning has the capability to produce 3D structures on micro-scale. The major drawback of the micro-turning process is that the cutting force influences machining accuracy and the limit of machinable size (Rahman, M., et al., 2003; Rahman, M., 2001). Significant work has been done to develop different cutting paths and schemes to reduce the effect of cutting force on the fine shaft (Rahman, A., 2006; Rahman, A.,

2005). A micro-pin of ~350µm diameter with intricate shape and kinks has been fabricated. But, it is very difficult to achieve a straight shaft below 100µm diameter and, in many cases, the tool is either broken, or starts to wobble due to excessive radial cutting force on the micro-shaft as shown in Figure 2.4. In the following a precise tool-setting technique will be presented followed by ultra-sharp tool machining by micro-EDM and finally the cutting scheme of micro-turning process will be presented for machining of micro-shafts around 20µm diameter.

6.1.1 Precise tool-setting technique for micro-turning

To achieve controllable and repeatable dimensions by micro-turning, it is necessary that the tool setting be accurate in the range of 2µm. Just a 5µm error in tool setting along the X direction causes the diameter to be unpredictable by 10µm, which is about 50% for the case of a 20µm diameter target shaft rendering it unacceptable. Such an error is not impossible as commonly tool-setting is performed using tool scope and visual inspection. A precise tool setting technique has been developed to overcome this problem. A rough tool setting is performed first from visual alignment and using tool scope mounted on the UMMT. Using this rough tool setting, three steps of different diameters are turned from the initial cylindrical shaft. In every step, the Y position of the tool is also changed to obtain a different diameter; preferably the shift should be done to keep the clearance angle. The following equations can be solved to find X_0 and Y_0 which are the initial X and Y direction tool setting errors:

$$X^2 = R_0^2 \tag{6.1}$$

$$(X + X_0)^2 + (Y + Y_0)^2 = R_1^2 \tag{6.2}$$

$$(X + X_0 + A_1)^2 + (Y + Y_0 + B_1)^2 = R_2^2 \tag{6.3}$$

$$(X + X_0 + A_2)^2 + (Y + Y_0 + B_2)^2 = R_3^2 \tag{6.4}$$

Equation (6.4) is used for the validation one of the quadratic roots as tool position along the Y axis is symmetrical and provides two roots. Figure 6.1 shows the geometrical relationship between the tool position and the actual turned diameter. For the first step, the turned diameter is R_1 instead of expected diameter R_0. The expected tool position is $P_0(X, Y)$ and the actual tool position is $P_1(X+X_0, Y+Y_0)$, where X_0 and Y_0 are the tool setting errors. For the second step, $X+A_1$ is the expected tool position along X axis and B_1 is the expected tool position along the Y axis, as Y = 0. But, the actual tool position is $P_2(X+X_0+A_1, Y+Y_0+B_1)$ and the turned diameter differs due to the errors in tool centering. Similarly, for the third step, $X+A_2$ are the expected tool position along X axis and B_2 is the expected tool position along the Y axis, where the actual tool position is $P_3(X X_0+A_2, Y+Y_0+B_2)$. In this calculation method, however, the error incurred from spindle runout, clamping error of workpiece as well as straightness have not been considered. Therefore in each iteration there exists slight deviation from the previous tool center; however the value converges within 2μm after 3 iterations of centering as could be seen in Figure 6.2. The new iterative calculation method is vastly more accurate and efficient and this method of tool centering can be automated for industrial applications.

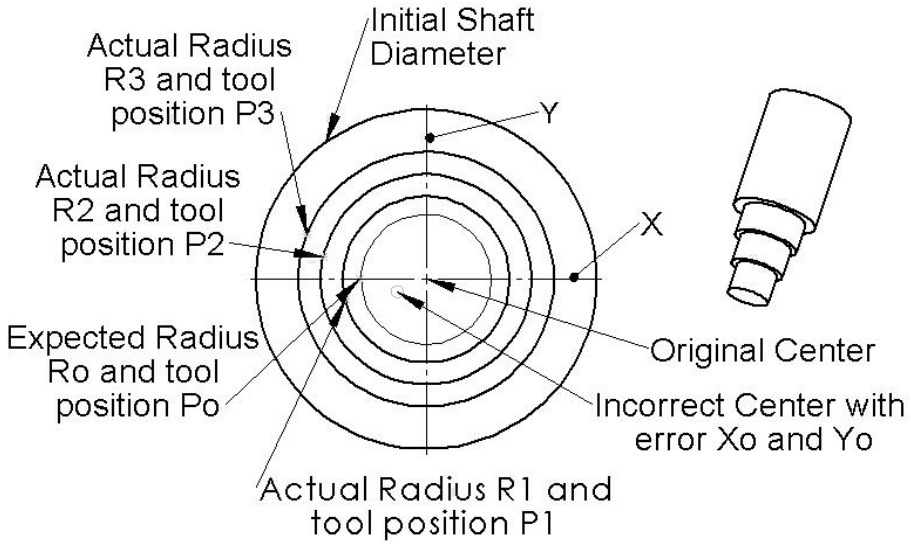

Figure 6.1 Geometrical relationship between tool position and turned diameter

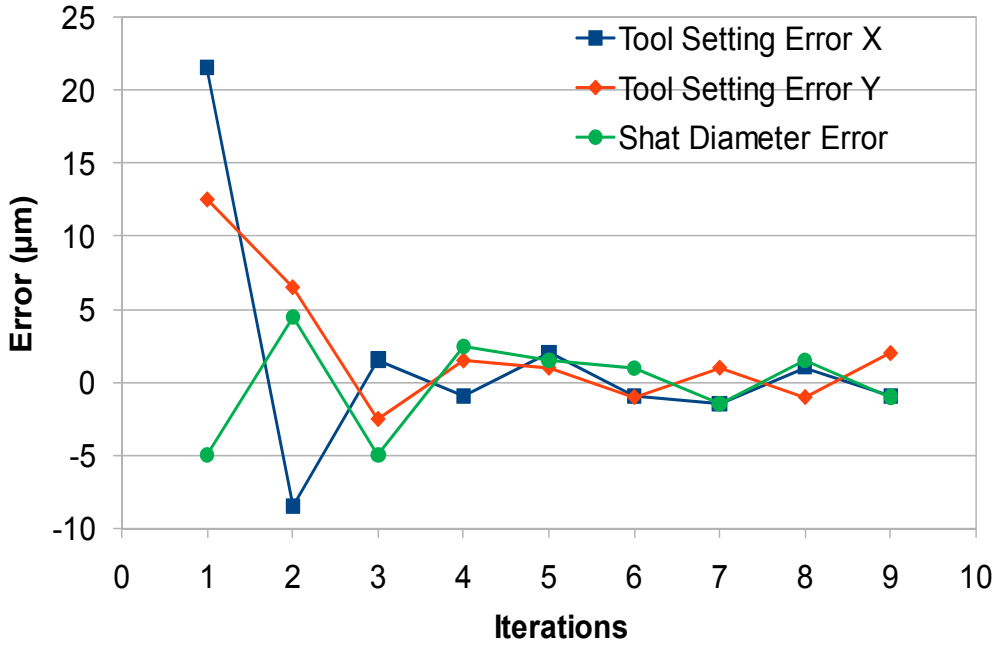

Figure 6.2 Convergence of tool-setting offset and turned diameter error can be observed within 3 iterations.

6.1.2 Ultra sharp micro-turning tool machining by micro-EDM

Commercially available PCD inserts, designed for light finishing cut, have a relatively large tool nose radius e.g., 100μm (Figure 6.3(a)). This tool nose resolves the cutting force on the shaft into two components, namely F_x and F_y, as can be seen in Figure 6.3(b). The F_y component of the cutting force does the actual cutting while the F_x component causes deflection of the micro-shaft. A commercially available PCD insert can be modified to achieve a very sharp cutting edge, such as to reduce the *Fx* component of the cutting force significantly which is illustrated in Figure 6.3(c). Using this process it is possible to achieve a straight shaft of a much smaller diameter. An approach has been developed to produce an ultra sharp edged tool from the commercially available PCD insert using micro-EDM in-situ. A rotating sacrificial electrode is mounted on the spindle and used to perform micro-EDM on the PCD tool edge to produce the very sharp-edge. This is illustrated in Figure 6.4. Table 6.1 shows the parameters that have been used during the machining of the tool tip. Figure 6.5(a) and (b) shows the commercially available PCD insert and the modified PCD tool. The modified PCD tool has less than a 5μm tool nose radius.

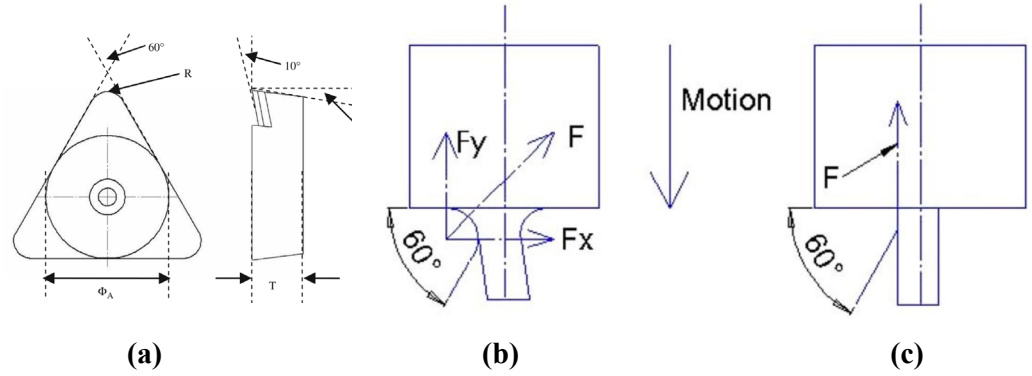

Figure 6.3 (a) Tool geometry of a commercially available PCD insert for finishing light cut, (b) turning with commercial tool, (c) turning with on-machine fabricated sharp tool.

Table 6.1 Parameters for in-situ modification of turning insert

Cutting Conditions	Capacitance (pF)	Voltage(V)	Spindle (rpm)	Machined Depth (µm)
Roughing	4700	120	1000	100
Finishing	100	80	1000	5

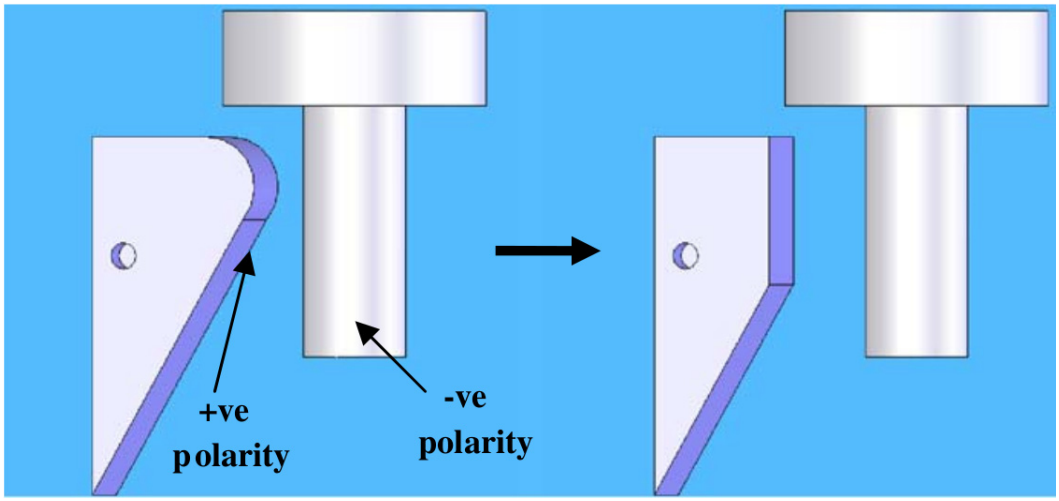

Figure 6.4 Image on the left illustrates the EDG process on the tool tip and the image on the right illustrates modified PCD tool after EDG process.

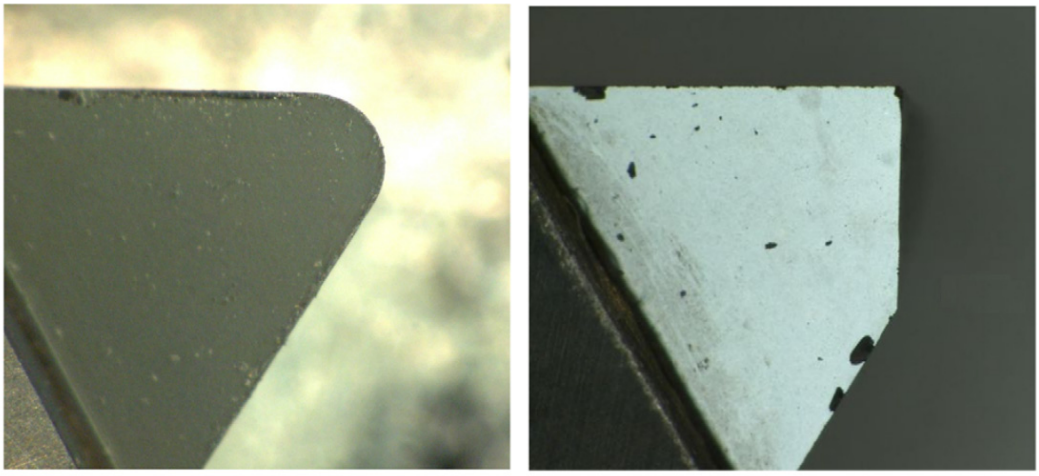

(a) **(b)**

Figure 6.5 (a) commercial PCD tool, (b) and in-situ modified PCD tool by micro-EDM

6.1.3 Machining scheme for fine shafts

The aforementioned tool machining process provides a very sharp tool nose but at the same time the tool tip becomes very weak. Therefore, during the actual machining two cutting tools were used. One of them was a commercially available PCD insert for rough machining to remove the bulk of the material and the second one was the PCD insert modified in-situ by micro-EDM for the final pass to form the micro-shaft. At the beginning of this machining process a PCD insert needs to be modified to form sharp cutting edge. Tool-setting was performed on both the PCD inserts mounted at different locations using the tool-setting technique mentioned in section 6.1.1. The cutting path is also very important, as during the machining process of the micro-shaft it is important that the already fabricated portion of the micro-shaft does not experience any cutting force. Figure 6.6 shows the schematic diagram of the sequential formation of the micro-shaft. Commercial PCD tool was used during step 2 and step 3 of the

machining process where bulk material was removed by turning. In these stages a stronger tool was required for faster machining and since the diameter of the thinnest part of the shaft in this stage was around 0.5mm, the higher radial direction cutting force was not critical to cause deformation to the shaft. In step 4 and step 5, the in-situ modified PCD tool was used which was mounted at a different location. During step 4, the final machining of the micro-shaft was performed in a single pass reducing the diameter from 0.5mm to the expected diameter (around 20μm~10μm). In this stage the sharp tool only removed materials from the stronger base with 0.5mm diameter and the slender fine shaft did not withstand any cutting force. During step 5, a taper at the base of the fine shaft was machined to clear away any uncut chip from the base of micro-shaft.

This has extended the possibility of micro-turning for machining at a much lower dimensional range which is otherwise not possible. Using this technique 2mm long micro-shafts with a diameter as small as 20μm have been machined. The machining process for a 2.0mm long shaft takes less than 2 minutes. Figure 6.7(a) shows a graphite shaft of 0.5mm long and 19μm in diameter that is similarly produced and has been compared to a human hair at the same magnification and scaling as that of the micro-shaft of Figure 6.7(a) for comparison (Figure 6.7(b)). Figure 6.7(c) shows 11μm diameter brass micro-probe with 80μm tip length and Figure 6.7(d) shows another brass micro-shaft of 14μm diameter and 250μm long. The success in this machining arises from the fact that the experiment was performed on a carefully designed UMMT which provides for excellent rigidity and the micro-EDM power supply is capable of providing fine spark discharges for forming very sharp tool nose with nose radius of around 5μm.

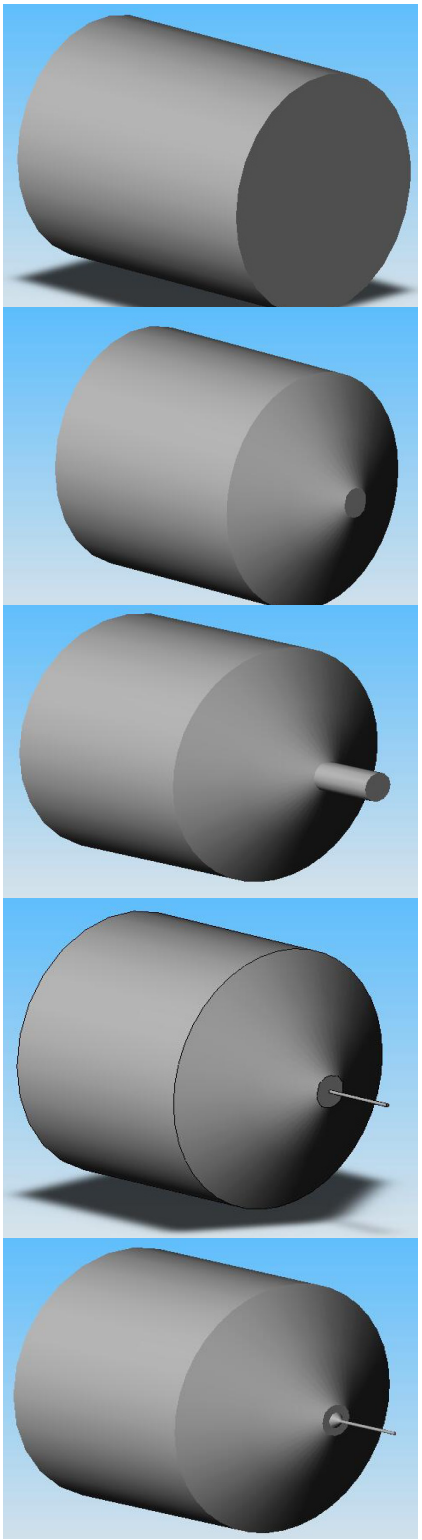

Step 1:
Base material, diameter 4 mm or 6 mm.

Step 2 - Taper Formation:
Tool: Commercial PCD
Depth of Cut: 0.1 mm
Feedrate: 80 mm/min
Tip Dia: 0.50 mm
Spindle: 2000 rpm.

Step 3 – Pencil Shape Formation:
Tool: Commercial PCD
Depth of Cut: 0.1 mm
Feedrate: 80 mm/min
Tip Dia: 0.50 mm
Spindle: 2000 rpm.

Step 4 – Final Shaft Formation:
Tool: In-situ modified PCD
Depth of Cut: Single pass for desired dia
Feedrate: 1~5 mm/min
Tip/Shaft Dia: 10µm ~ 50µm
Spindle: 2000 rpm.

Step 5 – Taper Base of Microshaft
Tool: Modified PCD
Feedrate: 1~5 mm/min
Tip Dia: 0.50 mm
Spindle: 2000 rpm.

Figure 6.6 Different stages of microshaft fabrication process using the ultra sharp tool.

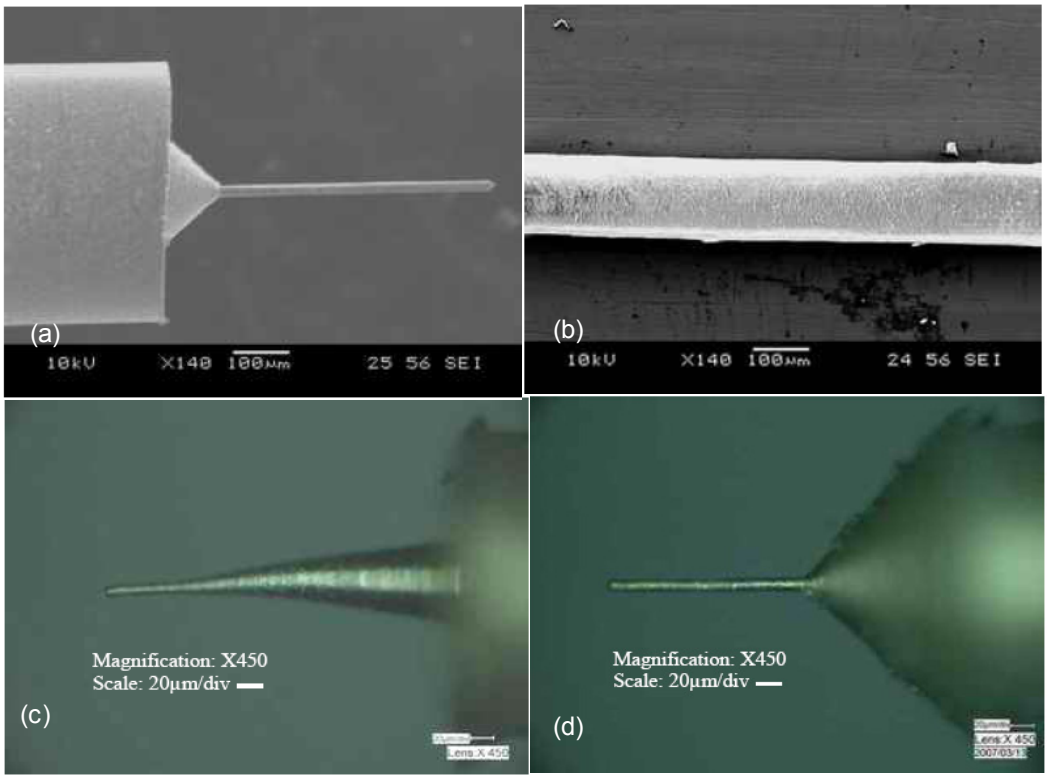

Figure 6.7 (a) 19µm graphite electrode of 0.5mm length fabricated by micro-turning process, (b) SEM image of a human hair for comparison with the shaft of - (a) (same magnification and scaling), (c) 11µm diameter and 80µm long brass microprobe by micro-turning (little bent by accidental touch during measurement), (d) 14µm diameter and 250µm long brass microshaft by micro-turning.

6.2 Compound Micro-turning + Micro-EDM Process

6.2.1 Micro-EDM with electrode fabricated by micro-turning

The electrode machining processes discussed in section 5.4 are very difficult for automation and are error-prone. In most of the cases, an operator is required to monitor the machining process and to perform necessary compensation for the error. Moreover, the electrode machining process can take even close to an hour. Another factor is that when holes with different dimensions are required, the tool electrode machining

becomes the bottleneck of the entire machining process. Potentially, the proposed method of compound process for micro-turning can be used for machining very fine micro-shaft which can then be used as electrodes for micro-EDM; and this practically eliminates the disadvantages of the aforementioned electrode machining processes using sacrificial electrodes.

Figure 6.8 illustrates the concept of the micro-turning-EDM compound machining (Lim, HS., et al., 2002). An electrode of required dimensions is first fabricated by micro-turning prior to performing micro-EDM. Using this compound machining, re-fixturing and clamping error can be avoided and deflection of electrode can be minimized; consequently the accuracy of machining can be improved. Figure 6.9 shows a 22μm brass shaft fabricated by micro-turning process using in-situ fabricated ultra sharp tool mentioned in section 6.1 followed by micro-EDM drilling about 10 holes on stainless steel plate. Electrode wear from EDM process is observable at the tip of the electrode.

This process shows much improvement on the machining time compared to the in-situ tool electrode machining processes described in section 5.4, which takes hours to fabricate as mentioned earlier. Moreover, this compound process does not require much operator's intervention and can mostly be automated due to less likelihood of error. When different diameters of electrode are required for micro-EDM process, micro-turning can significantly reduce the electrode machining time as compared to the conventional sacrificial electrode machining methods.

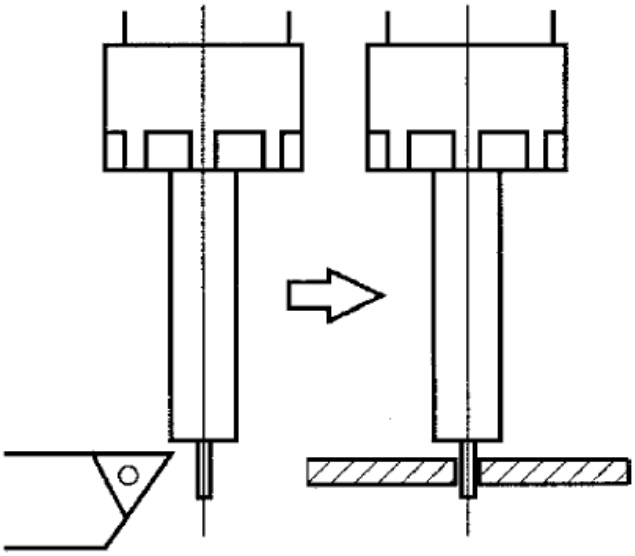

Figure 6.8 Compound process using electrode fabricated by micro-turning (left) for micro-EDM process (right) in the same setup.

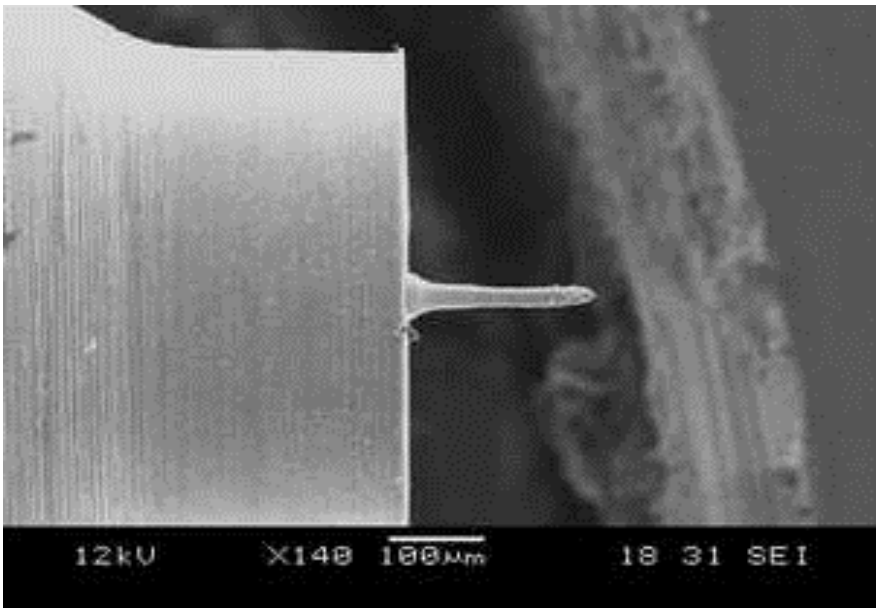

Figure 6.9 A 22µm brass electrode fabricated by micro-turning process and used for machining 10 micro holes on stainless steel plate.

6.2.2 Comparison of repeatability and controllability of electrode fabricated by micro-turning and WEDG

Experiments were conducted to study the repeatability, controllability and electrode wear of the developed micro-turning process and to find out the wear ratio for using the micro-turned brass electrode to machine on 50µm thick SUS-304 workpiece. The purpose of this study is to compare electrode machining by micro-turning to commonly used WEDG process and whether micro-turning can be a viable option for electrode machining in industrial applications. In the first set of experiments 30 holes were machined using electrodes fabricated by micro-turning and WEDG process. The material of the micro-turned electrode is brass and that made by WEDG is tungsten. In WEDG process a single fabricated tungsten electrode (350µm long) was sufficient for boring all 30 holes, but for the micro-turning process the brass electrode had to be re-dressed by micro-turning 3 times due to high electrode wear. It could be observed from the result of Figure 6.10(a) that the holes fabricated using micro-turning process had a roundness error of 3.5µm compared to 2.3µm roundness error from WEDG process. The error bar reflects one SD. The second of experiment was performed to study the diameter controllability of the two electrode machining processes, micro-turning and WEDG. In this experiment, the hole machining was repeated 10 times with each of the three different electrode diameters (50µm, 60µm and 70µm). Machining of each hole started with preparation of a fresh electrode by micro-turning (thus 30 fresh electrodes were prepared) followed by micro-EDM drilling into 50µm SUS-304 plate. For the WEDG process the electrode was fabricated once for each diameter starting from 0.5mm diameter and then machining to the required diameter by WEDG process (thus 3 electrodes with 3 target diameters were machined). In WEDG instead of preparing

30 fresh electrodes only 3 electrodes were machined, as that would be a practical comparison due to low tool wear of W compared to the high tool wear of the brass electrodes (which requires more frequent machining of brass electrodes). Variance of the machined hole diameters by the turning process found from the experiments is 3.4μm compared to the variance of 1.3μm observed from WEDG process, shown in Figure 6.10(b).

The results suggest that holes machined using brass electrode fabricated by micro-turning are less accurate than those by the tungsten electrode fabricated by WEDG. The degradation in accuracy is mainly caused by the high wear rate of the brass electrode which results in more debris formation from discharge sparks in the electrode gap space and thus causes uncontrolled arcing. Electrode wear ratio of the holes machined was compared and it can be observed from Figure 6.10(c) that the electrode wear ratio of brass electrode (65%) was significantly higher compared to the tungsten electrode (9%) machined by WEDG. Thus brass electrode is not suitable for machining of complex 3D shapes by micro-EDM milling demonstrated in section 5.6.

However, brass electrode can be suitable for micro-EDM hole drilling process if the expected accuracy can be compromised. Using a 1.0 mm long and 50 μm diameter electrode it is possible to drill about 20 holes on a 50μm SUS plate. This issue of extremely high electrode wear could be overcome by selecting an electrode with low wear, for example Cu-W or graphite, which will also improve the machining accuracy in turn. The wear ratio of Cu-W was observed to be around 11%~12% (Figure 5.17) which indicates that micro-turning can be a viable option even for 3D micro-EDM milling of complex features if Cu-W or graphite electrodes are used. In the processes

compared, the main advantage of the micro-turning based process is the significant reduction in electrode machining time (even considering that the micro-turned electrodes had to be prepared 3 times which took only 6 minutes compared to around 30 minutes of electrode machining time for WEDG process) as well as the capability of automation when different electrode diameter is required for machining holes and slots of different dimension.

6.3 Micro-grinding and Micro-milling using PCD Tool

Micro-tools made of PCD offer new promise for micromachining of hard and brittle materials. PCD consists of micrometer-sized diamond grains sintered under high temperature and pressure with metallic cobalt and the cobalt fills the interstices between the diamond particles and forms an electrically conductive network adequate for micro-EDM (Kozak J., et al., 1994, Liu, YH., et al., 1997). After shaping, the surface of a PCD tool contains protruding diamond grains that are randomly distributed, which act as hard and tough cutting edges for micromachining. The first demonstration of the micro-EDM shaped PCD tools in machining tungsten carbide, electroless plated nickel and silicon was performed by Wada et al. (Wada, T., et al., 2002). The feasibility of ductile mode micromachining of brittle glass materials with PCD micro-tools that are prepared in a variety of shapes using non-contact micro-EDM process was demonstrated by Morgan et el. (2004).

(a)

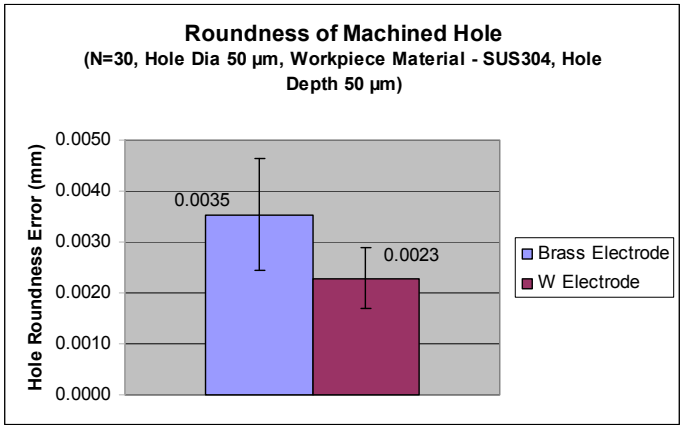

(b)

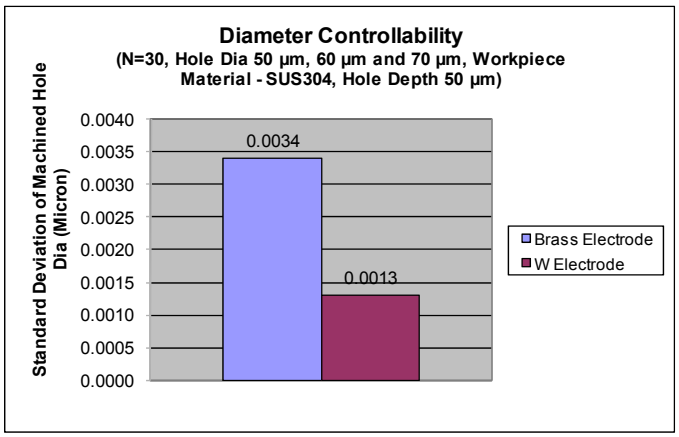

(c)

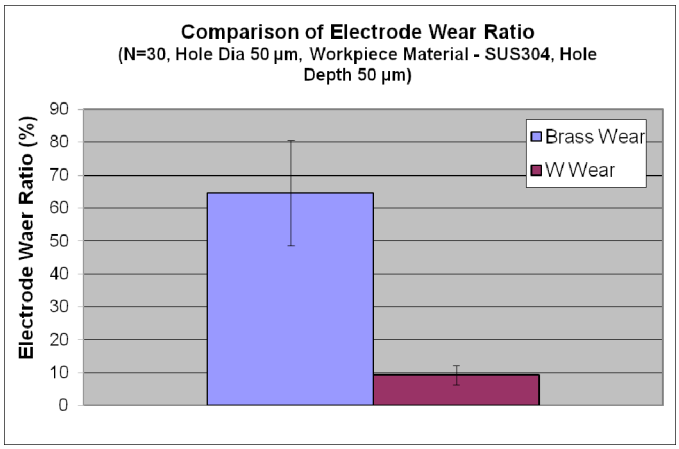

Figure 6.10 Comparison between machining with electrode fabricated by micro-turning and electrode fabricated by WEDG process; (a) repeatability of micro hole boring process, (b) controllability of micro hole boring process and (c) comparison of electrode wear ratio.

6.3.1 Compound micro-grinding with PCD tool fabricated by Micro-EDM

Difficulty in micro-grinding process is the machining of the grinding tool and the accuracy of the ground feature size. For example, while fabricating a 50μm slot on glass, it is difficult to find such tool which can be used for grinding. In the feasibility study of Morgan et al., 2004, a PCD bonded tool was fabricated using WEDG/BEDG process to provide cylindrical cutting edge. As the tool was fabricated on the same machine, there was no error involved due to re-clamping of the tool. It not only improved the accuracy of the machined slot, but also eliminated the wobbling of the grinding tool and thereby reduces the cutting force on the micro-sized tool.

During the experiments performed by Morgan et al. (2004) the tool was fabricated on a commercial micro-EDM machine (Panasonic MG-ED82W). But, the cutting experiments were conducted on the three axis micro-EDM machine that has an additional nanopositioning stage (Polytee PI Nanocube) to provide for fine positioning and depth of cut. A micro-milling machine has the fine control capability and the rigidity required but such capability was not incorporated in the micro-EDM machine that they used. Therefore, to further demonstrate the capability of the UMMT as a ready platform for compound micromachining and to explore the feasibility of performing micro-grinding on the UMMT, experiments have been conducted on the UMMT for shaping PCD micro-tools for micro-grinding.

The PCD micro-tool was shaped using the MBEDG process mentioned in section 5.4. Figure 6.11 shows the cylindrical PCD bonded tool at each machining step starting

from 1.0mm diameter to finally 30µm diameter for machining of slots on glass. Using larger discharge energy during micro-EDM creates larger craters on the PCD tool and using smaller energy during EDM creates smaller craters. The size of the crater can be compared to the grit size. Bigger craters remove material faster at the expense of surface roughness, while smaller craters give a slower material removal rate and provide a better surface finish. Table 6.2 shows the machining conditions for forming the PCD micro-tools. The observed peak-to-valley height on the surface of the formed tool was 8.28µm for the parameters used for rough shaping of the tool (Morgan et al., 2004). During the final pass of the tool shaping supply voltage was set to 80V and 110pF capacitor was installed to obtain an average peak-to-valley height of 3.71µm which can be considered as the grit size on the surface of grinding wheel used for very fine grinding operation (grit size #4000). Using micro-tools fabricated using the process mentioned above, micro-grinding was performed on BK-7 glass. Figure 6.12(a) shows 'NUS' written using micro-grinding process with a 150µm diameter PCD micro-tool and the depth of the slots were 50µm. The depth of cut in every feed for the grinding was 1µm with 20µm/s feedrate. Figure 6.12(b), (c) and (d) shows the magnified view of such a surface machined. The surface roughness was measured to be 0.0339µm using Taylor-Hobson surface profiler (Figure 6.13). Fabricated slot shows very smooth surface which is comparable to the surface obtained from ductile mode cutting of glass in macro scale.

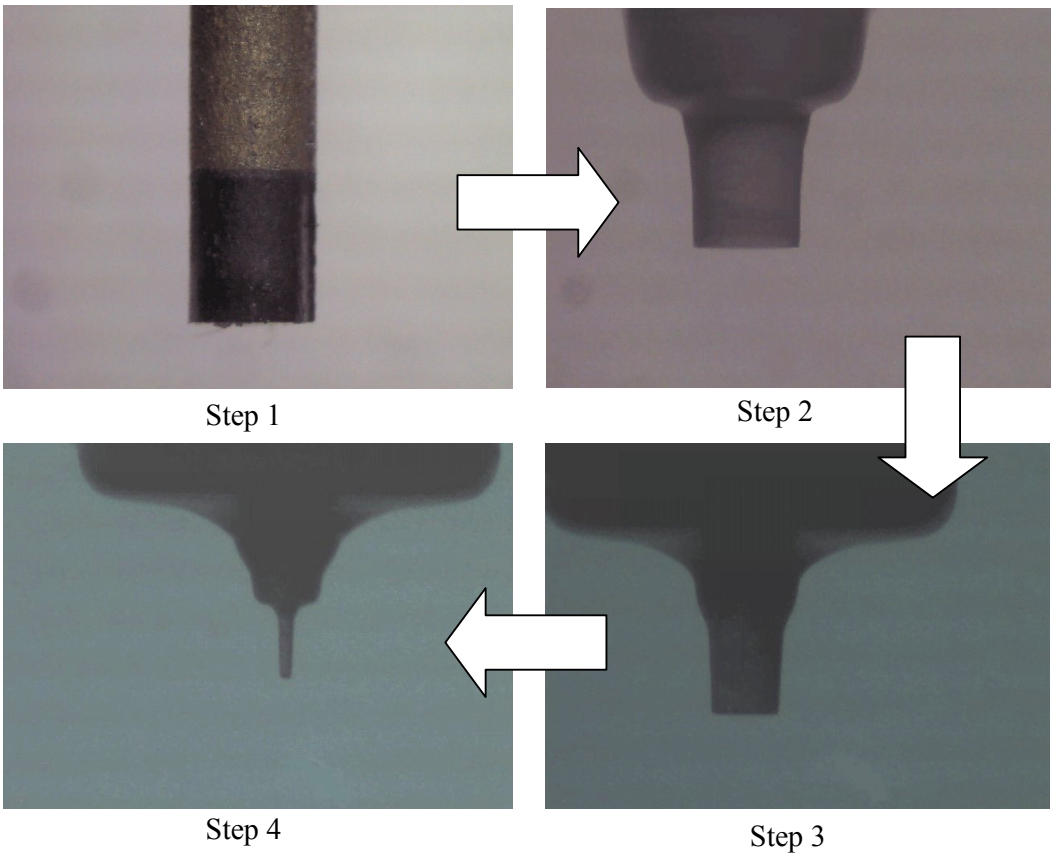

Figure 6.11 Different stages of a micro-grinding tool in-situ fabrication process by MBEDG process. Step 1 reduces the 1.0mm PCD tool to 500µm, followed by reduction to 150µm and finally ~30µm diameter straight PCD micro tool is formed in step 4.

Table 6.2 Machining conditions for PCD micro-tools machining.

Cutting Conditions	Capacitance (pF)	Voltage(V)	Spindle (rpm)
Rough Shaping	3300	110	2500
Fine Shaping	110	80	2500

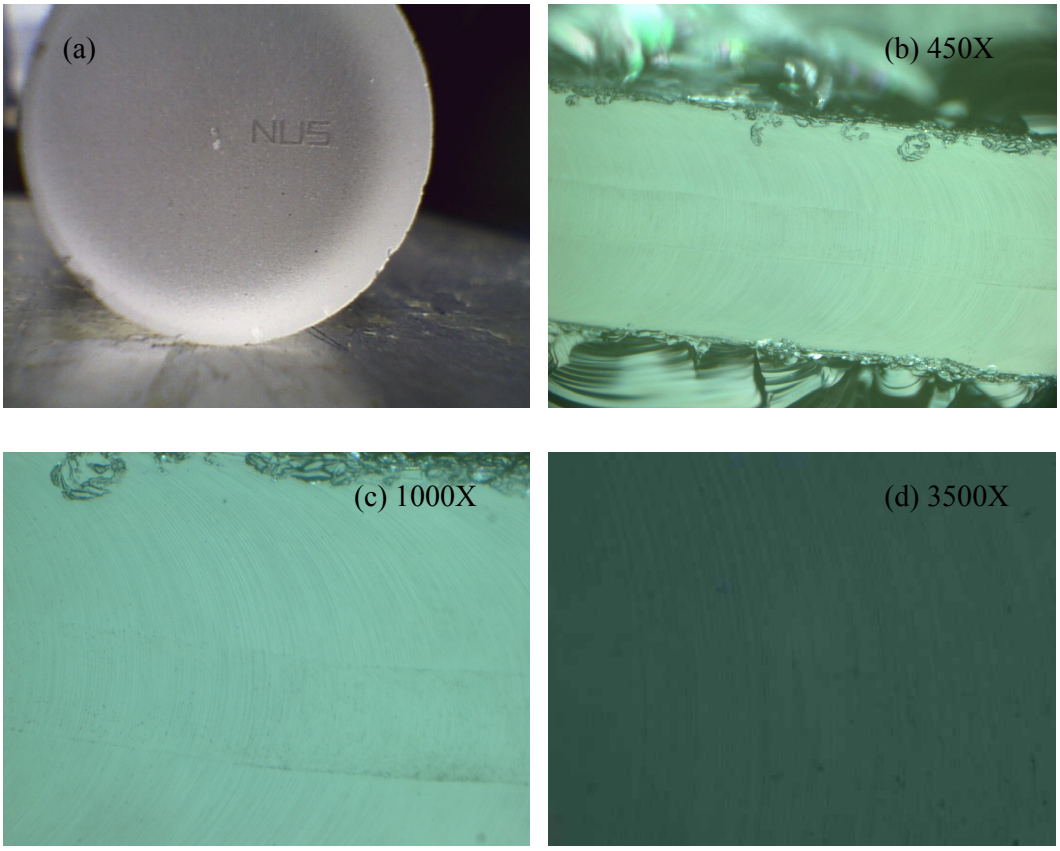

Figure 6.12 (a) 'NUS' (slot width 150 µm x depth 50 µm) machined on BK-7 glass by micro-grinding, (b) surface at 450X magnification, (c) surface at 1000X magnification and (d) smooth surface shown at 3500X magnification.

6.3.2 Compound micro-milling with PCD tool

Compared to the micro-grinding process mentioned in section 6.3.1 where cutting is realized by means of the interaction of micrometer sized abrasive grains of PCD tool with the micro-grains of workpiece surface; in micro-milling cutting operation is performed by defined cutting edge on the tool (e.g., face milling where the cutting edges are located at the face of the cutter and in peripheral milling the cutting edges are located on the circumference of the milling cutter) (Grote, KH., and Antosson, EK., 2009). In this experiment a D shaped milling tool was machined in-situ using the

PCD tool shaping technique described in section 6.3.1 for micro-milling of fine slots. The tool shaping was performed as the steps shown in Figure 6.11 to fabricate a cylindrical tool of 32~34µm diameter. After the fine shaping of the tool, another pass of MBEDG was performed on the tool without any spindle rotation with an offset of 7µm to form a D-shape that enables the PCD to operate as a milling tool in-situ. Micro-milling experiment was then conducted on a PZT substrate coated with Ag (Figure 6.14). The depth of cut used for the micro-milling in every pass was 2µm with spindle speed 2500rpm and the feedrate was varied at 8mm/min, 20mm/min, 40mm/min, 60mm/min, 80mm/min and 100mm/min. Each 15µm deep by 5mm width slot was repeated 3 times at the same feedrate with 100µm slot pitch. Figure 6.15(a) shows a slot machined at 8mm/min feedrate and the cutter mark was observable, but for machining at 60mm/min and above feedrate, the silver layer was plastically pushed instead of machining, as could be seen in Figure 6.15(b). This could probably be due to the presence of a single cutting edge on the in-situ fabricated milling cutter where the feed per revolution was considerably higher above 60mm/.min. Thus the thrust force on the silver workpiece, when the cutting edge was not engaged, was considerably higher than the maximum cutting force the silver layer could withstand. This successfully demonstrated the capability of performing micro-milling using in-situ fabricated milling tool for micromachining of features between 20µm to 50µm on the UMMT.

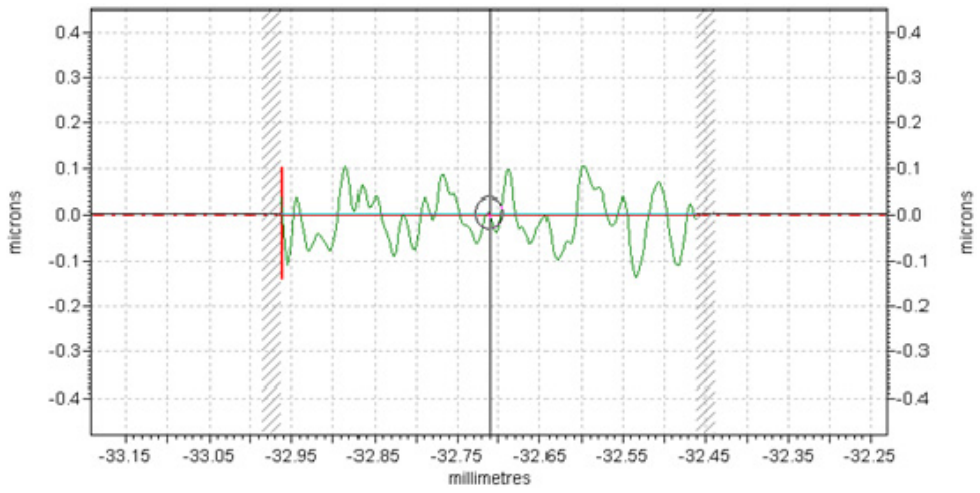

Figure 6.13 Surface Roughness (R_a) 0.0339µm of the micro ground slot observed from Taylor-Hobson surface profiler.

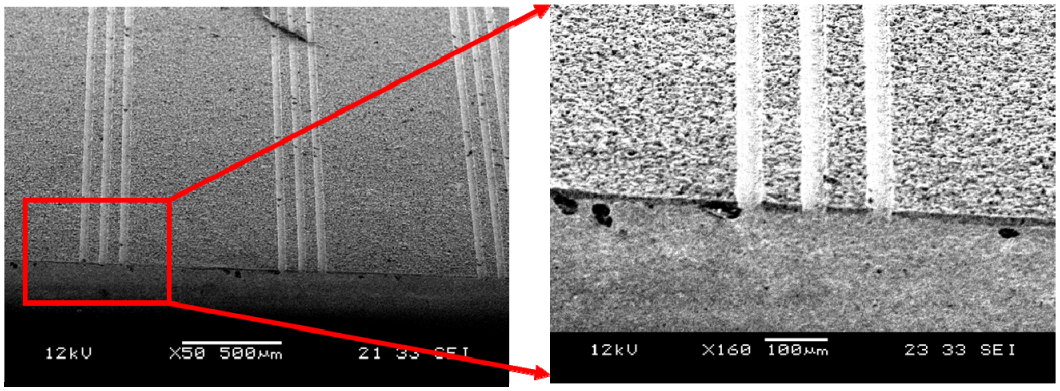

Figure 6.14 15µm deep and 35µm wide slots machined by micro-milling using PCD micro tool on PZT substrate coated with Ag.

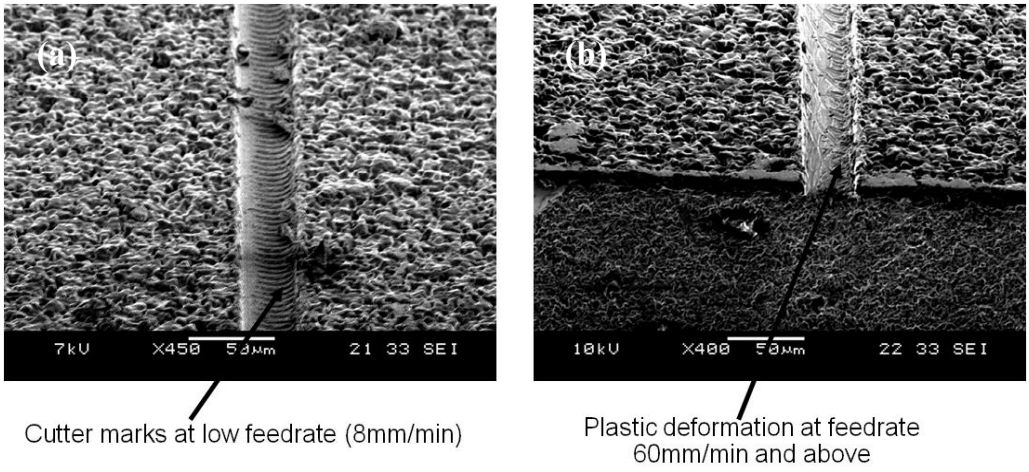

Figure 6.15 Close up view of the slots machined with PCD micro tools. (a) slot machined at 8mm/min feedrate, (b) slot machined at 60mm/min feedrate.

Using this technique demonstrated in section 6.3, further detailed study on micromachining of various brittle and difficult-to-cut glasses and cutting tools with different geometries were conducted by Perveen et al. (2012a, 2012b) using the same setup. They concluded that the micro-EDM parameters have significant influence on the surface roughness and performance of the fabricated PCD tool during glass micromachining. They also concluded that better surface roughness could be achieved by forming the tool with very low discharge energy. During the machining of PCD tool using micro-EDM, lower discharge energy produces smooth surface on the PCD tool. This generates smaller chips on the glass surface during micro-grinding and eventually generates better surface finish. Thus the improvement on the micro-EDM setup and availability of very low discharge energy was extremely instrumental for advanced application of compound micromachining.

6.4 Conclusion

In this chapter different tool-based compound micromachining techniques have been explored and the suitability and effectiveness of the UMMT to serve as a platform for compound micromachining were demonstrated. Micro-turning for machining of micro-shaft as small as 10μm was performed using a PCD turning insert modified by performing micro-EDM to fabricate an ultra sharp tool nose. Using this technique further compound process has been demonstrated by performing micro-EDM drilling. The experiment was repeated and statistical results indicate electrode machining by micro-turning can be a feasible industrial alternative to commonly used WEDG process where the electrodes can be fabricated much faster. Micro-grinding and micro-milling was also performed using cylindrical PCD tool modified using micro-EDM. The obtainable surface roughness from micro-grinding and demonstrated dimensional range for performing micro-milling indicates high potential for industrial applications of compound micromachining.

7 Conclusions and Future Work

7.1 Conclusions

The focus of the research work presented in this thesis is on the development and study of micro-EDM based tool-based compound micromachining (TCMMP) using a specially developed universal multi-process machine tool (UMMT). This also involved the preparation of the UMMT as a ready platform for industrial applications of TCMMP. The primary objective of this project is to demonstrate micromachining capabilities for machining of shapes and features in the lower dimensional range of between 5μm ~ 50μm in micromachining domain. The research work also aims to contribute to the fundamental understanding of the process physics of micro-EDM process and interaction of micro-EDM plasma with micro-EDM power supply. Following are some of the important contributions and conclusions that can be drawn from this research work:

TCMMP concept on UMMT: The concept of compound micromachining is a new area of significant research interest that is practically a step forward from multi-process micromachining on a single platform. Even though there exists enormous industrial demand for compound micromachining to meet the requirements of MEMS/Bio-MEMS industry, there has not been much successful demonstration of the machining capability below 100μm feature size prior to this research work. The research work presented in this thesis is first of its kind to the best knowledge of author that demonstrated a holistic approach in developing micro-EDM based compound

micromachining starting with identifying the required criteria and evaluating the machine tool for performing micromachining at the stated dimensional range; through theoretical analysis and development stages; and finally demonstrating the capabilities of multiple compound micromachining processes. This contribution is a significant step forward in the field of compound micromachining.

Evaluation of UMMT: An earlier developed UMMT was evaluated for performing TCMMPs around the lower dimensional bound of micromachining range for machining of 5µm~50µm features. The research work contributed to the theoretical analysis of required discharge energy to be 30nJ~50nJ for 2µm hemispheric crater and indicated that an RC power supply is more appropriate for such small discharge energy range.

Analysis of Micro-EDM Electric Characteristics: A model for the RLC network of RC power supply was proposed employing micro-EDM plasma properties. This proposed model bridges a crucial gap in the present theoretical understanding on the interaction of micro-EDM plasma with different circuit elements as well as micro-EDM power supply. It also provides significant insight for realizing changes in current waveform due to changes in process parameters, such as, input voltage, capacitance and inductance and the resistance *R*. Furthermore, by employing this proposed model the determination of inductance and stray capacitance using non-linear least square fitting was demonstrated. This theoretical analysis is novel and unique as per the existing literature and a significant leap forward for micro-EDM technology.

Micro-EDM Setup for Complex Micromachining: An RC relaxation type micro-EDM power supply was developed which is capable of providing discharge energy as small as ~37nJ. A jump based gap control strategy was implemented which showed less erratic machining and improved machining time. 3D micro-EDM milling process was implemented on the UMMT and a new electrode machining process capable of making straight electrodes was proposed (MBEDG). This holistic development work resulted in the successful demonstration of micromachining of feature size as small as 3μm ~ 5μm using micro-EDM process which has not been demonstrated earlier. This marked contribution will enable new industrial micromachining processes to be proposed using tool-based micromachining techniques.

Compound Micromachining based on Micro-EDM and Micro-turning Process: A new TCMMP for machining of ultra sharp tool for micro-turning was developed where the radial force has been removed considerably. This TCMMP resulted in successful machining of micro-shafts as small as 11μm in diameter by micro-turning. This proposed technique is a significant contribution to the concept of TCMMP that has extended the promise of micro-turning for machining at a much lower dimensional range which is otherwise not possible.

Compound Micromachining based on Micro-turning and Micro-EDM Process: Experiments were conducted to establish the possibility of using micro-turning as the electrode machining process for micro-EDM. This process demonstrated the potential of reducing the electrode machining time to 2 minutes compared to more than 30 minutes of machining time using sacrificial electrode method by WEDG. This resulted

in the successful development of another compound process having much promise and potential.

Compound Micromachining based on Micro-EDM and Micro-grinding/Micro-milling: Exploration of TCMMP included machining of micro-slots with excellent surface roughness on glass and micro-milling of 35µm micro-slots on PZT substrate for MEMS application using a D-shaped PCD tool. In these processes, the concept of *in situ* micro-milling and micro-grinding tool fabrication employing TCMMP was demonstrated and further substantiated the promise of TCMMP for micromachining between 5µm~50µm dimensional range.

Overall, the research work significantly contributed to the demonstration of the potential of TCMMPs for micromachining applications. These processes can be used for machining of components for MEMS, micro-molds, micro-fluidic channels, micro-probes and patterns in glass substrates for lab-on-chip devices or biomedical arrays and such machining can be performed around the lower dimensional bound of micromachining range.

7.2 Recommendations for the Future Work

1. The exploration of micro-EDM based TCMMP opens up an entirely new research field using the UMMT as an example of platform suitable for such operations. Implementation of micro-ECM process on the UMMT and exploration of micro-ECM based TCMMP in combination with micro-EDM process will potentially make the platform even more universal. The advantage of high machining speed and smooth surface generation capability of micro-ECM can be leveraged for

exploration of compound micromachining processes tailored for specific manufacturing need.

2. It was observed from the proposed model of micro-EDM power supply that the assumption of electrode plasma interface diameter is very crucial input parameter for the model and requires to be recomputed for different discharge energy range. Further development on the proposed model integrating the electrode plasma interface diameter will allow the model to obtain electrode plasma interface diameter based on discharge energy setting alone and will serve as a unified model for power supply network employing plasma properties.
3. Presence of inductance in the power supply network has been observed to minimize the peak height and increase pulse width of the current waveform which results in shallower and flatter craters and improves surface roughness. Developing a circuit with switchable inductance will allow improvement of surface roughness during the finishing operation of very fine micro-features and thin-walled structures.
4. Further research work can be done on the proposed micro-turning process to understand the cutting force on the ultra sharp tool edge and to study rake angle, clearance angle and relief angle formation on-machine using simple carbide block grinding in addition to using PCD tool. Exploration in micro-turning of Cu and graphite for machining of micro-electrode and performing complex 3D micromachining is an area with immense research potential. Machining of complex micro-milling tools and performing micro-milling on SUS-304 will substantially increase the material removal rate that can be obtained from micro-EDM.
5. For machining of complex fine-featured micro-parts, the tool compensation and tool path generation becomes more complex. It is recommended to focus the

research activity towards the development of CAM system for generation of tool path, selection of appropriate process parameters, e.g., voltage, capacitance and integration of automated tool wear compensation which is essential for industrially scalable applications of TCMMPs

Bibliography

Adams DP., et al., 2001, Micromilling of Metal Alloys with Focused Ion Beam Fabricated Tools, Precision Engineering, Vol 25, page 107-113.

Adams, DP., et al., 2000, Microgrooving and microthreading tools for fabricating curvilinear features. Journal of the International Societies for Precision Engineering and Nanotechnology, Vol 24, page 347 – 356

Alting, L., et al., 2003, Micro Engineering. Annals of the CIRP, 52/2, pages 635-658.

Ansel, Y., et al., 2002, Development of tools for handling and assembling microcomponents. J of Micromechanics and Microengineering, Vol. 12, pages 430 – 437.

Aspinwall, DK., 2001, Hybrid high speed machining (HSM): system design and experimental results for grinding/HSM and EDM/HSM. Annals of the CIRP, Vol – 50/1, pages 145–148.

Bao, W. Y., et al, 2000, Modeling micro-end-milling operations. Part – II: Tool Run-out. International Journal of Machine Tools and Manufacture, vol 40, pp 2175-2192.

Bleys, P., et al., 2004, Sensing and compensation of tool wear in milling EDM, Journal of Materials Processing Technology, Vol - 149, pp 139 – 146.

Bleys, P., et al., 2002, Real-time Tool Wear Compensation in Milling EDM, Annals of the CIRP, Vol 51/1, pp 157 – 160.

Brinksmeier, E., et al., 2001, Machining of Precision Parts and Microstructures. Initiatives of Precision Engineering at the Beginning of a Millennium, 10th International Conference on Precision Engineering (ICPE), July 18-20, 2001, Yokohama, Japan.

Chae, J., et al., 2005, Investigation of micro-cutting operations, International Journal of Machine Tools and Manufacture, Vol. 20, 1-20.

Chen, ST., et al., 2009, Development of a micro diamond grinding tool by compound process. Journal of Materials Processing Technology, Vol – 209/10, pp 4698–4703.

Chern, G. L., et al., 2007, Study on burr formation in micro-machining using micro-tools fabricated by micro-EDM. Precision Engineering, vol 31, page 122–129.

Cheng, X., et al., 2008, Development of ultra-precision machining system with unique wire EDM tool fabrication system for micro/nano-machining. Annals of the CIRP, Vol – 57, pages 415 – 420.

Chyan, H. C., et al., 1998, Development of curved helical micro-drill point technology for micro-hole drilling. Mechatronics 8, page 337-358.

Corbett, P.A., et al., 2000, Nanotechnology: international developments and emerging products, Annals of CIRP 49, 523–546.

Descoeudres, A., et al., 2008, Time- and spatially-resolved characterization of electrical discharge machining plasma, Plasma Sources Sci. Technology, 17 (2008) 024008, doi:10.1088/0963-0252/17/2/024008

Descoeudres, A., 2006, Characterization of Electrical Discharge Machining Plasmas, PhD Thesis, Swiss Federal Institute of Technology Lausanne (EPFL).

Descoeudres, A., et al., 2004, Optical emission spectroscopy of electrical discharge machining plasma, Journal of Materials Processing Technology 149, pp 184–190.

Dhanik, S., Joshi, SS., 2005, Modeling of a Single Resistance Capacitance Pulse Discharge in Micro-Electro Discharge Machining, Journal of Manufacturing Science and Engineering, Vol. 127, pp 759 – 767.

Dibitonto, DD., et al., 1989, Theoretical models of the electrical discharge machining process. I. A simple cathode erosion model, Journal of Applied Physics 66 (9), pp 4095–4103.

Dornfeld, D., et al., 2006, Recent Advances in Mechanical Micromachining, Annals of the CIRP Vol 55/2, 745 – 768.

Egashira, K., 2002, Micro-drilling of Monocrystalline Silicon Using a Cutting Tool. Precision Engineering, Vol – 26, page 263–268.

El-Giar EM, et al., 2000, Localized electrochemical deposition of copper microstructures. Journal of Electrochemical Society, Vol – 147, pages 586 – 591.

El-Giar EM, et al., 1997, Localized electrochemical plating of interconnectors for microelectronics, Proceedings of IEEE Conference on Communications, Power and Computing, WESCANEX 97, pages 327–332.

Fang, F. Z., et al., 2006, Tool-based Micromachining and Applications in MEMS, MEMS/NEMS Handbook Techniques and Applications, Springer US, Volume 3 - Manufacturing Methods, 678 – 740.

Fang F. Z., et al., 2003, Tool Geometry Study in Micromachining, Journal of Micromechanics and Microengineering, vol 13, page 726-731.

Fleischer, J., et al., 2004, New applications for micro-EDM. Journal of Materials Processing Technology , Vol – 149, pages 246 – 249.

Friedrich, C. R., 2002, Micromechanical Machining of High Aspect Ratio Prototypes. Microsystem Technologies, Vol 8, pp 343-347.

Friedrich, C. R., et al., 1997, Micromilling Development and Applications for Microfabrication. Microelectronic Engineering, Vol 35, pp 367-372.

Gao, W. et al., 2003, Precision Nano-fabrication and Evaluation of a Large Area Sinusoidal Grid Surface for a Surface Encoder. Precision Engineering, Vol – 27, page 289 – 298.

Gianchandani et al., 2006, A Micromachining Process for Die-Scale Pattern Transfers in Ceramics and Its Application to Bulk Piezoelectric Actuators, Journal of Microelectromechanical Sys., Vol. 15, No. 3, pp. 605-612.

Grote, KH., and Antosson, EK., 2009, Springer Handbook of Mechanical Engineering, Manufacturing Engineering, Applications in Mechanical Engineering (Part B), ISBN 9783540491316, pp 523 – 785.

Grover, FW., 2004, Inductance Calculations, Dover Phoenix Edition, ISBN: 0 486 49577 9.

Han, F., et al., 2006, Experimental attempts of sub-micrometer order size machining using micro-EDM, Precision Engineering 30, pp 123-131.

Han, F., et al., 2004. Improvement of machining characteristics of micro-EDM using transistor type isopulse generator and servo feed control. Precision Engineering, Vol – 28, pages 378–385.

Hang, G., et al, 2006, Micro-EDM Milling of Micro Platinum Hemisphere, Proceedings of the 1st IEEE International Conference on Nano/Micro Engineered and Molecular Systems, Jan 18 - 21, Zhuhai, China, pages 579 – 584.

Hara, S., 2001, Ultra-high Speed Discharge Control for Micro Electric Discharge Machining. Initiatives of Precision Engineering of a Millenium, Kluwer Academic Publisher, 194 – 198.

Ho, KH., et al., 2003, State of the art electrical discharge machining (EDM). International Journal of Machine Tools and Manufacture, Vol 43, page 1287–1300.

Hung, JC., et al., 2006, Micro-hole machining using micro-EDM combined with electropolishing. Journal of Micromechanics and Microengineering, Vol – 16, pages 1480 – 1486.

Hunter, IW., et al., 1997, Three-dimensional microfabrication by localized electrochemical deposition and etching. US Patent Specification 5, 641, 391.

Ikawa, N., et al., 1992, Minimum thickness of cut in micromachining. Nanotechnology, Vol 3, page 6 – 9.

Imai, Y., et al., 2004, Local actuator module for highly accurate micro-EDM. Journal of Materials Processing Technology, Vol – 149, pp 328 – 333.

ISO 230 – 1, 1996 – Test Code for machine Tools – Part 1: Geometric accuracy of machines operating under no-load or finishing conditions. International Standards for Business, Government and Society, International Organization for Standardization.

ISO 230 – 2, 2006 Test Code for machine Tools – Part 2:Determination of accuracy and repeatability of positioning numerically controlled axes. International Standards for Business, Government and Society, International Organization for Standardization.

Jia, ZX., et al., 1997, Study on a new kind of combined machining technology of ultrasonic machining and electrical discharge machining, International Journal of Machine Tools and Manufacture, Vol 37/2, pages 193 – 199.

Jahan, MP., et al., 2011, MICRO-ELECTRO DISCHARGE MACHINING (μEDM), Micro-Manufacturing: Design and Manufacturing of Micro-Products, John Wiley and Sons.

Jahan, MP., et al., 2010, A Comparative Study on the Performance of Sinking and Milling micro-EDM for Nanofinishing of Tungsten Carbide, International Journal of Nanomanufacturing, Vol 6, pp 190 – 206.

Jahan, MP., et al., 2009(a), A study on the quality micro-hole machining of Tungsten Carbide by micro-EDM process using Transistor and RC-type pulse Generator, Journal of Materials Processing Technology, Vol. 209, Issue 4, pp. 1706-1716.

Jahan, MP., et al., 2009(b), An experimental investigation on the surface characteristics of Tungsten Carbide for the fine-finish Die-sinking and Scanning micro-EDM, International Journal of Abrasive Technology, Vol. 2/3, pp. 223-244.

Jahan, MP., et al., 2008, A Comparative Study of Transistor and RC Pulse Generators for Micro-EDM of Tungsten Carbide, International Journal of Precision Engineering and Manufacturing, Vol. 9, No. 4, pp. 3-10, 2008.

Kao, CC. and Shih, AJ., 2006, Sub-nanosecond monitoring of micro-hole electrical discharge machining pulses and modeling of discharge ringing, International Journal of Machine Tools and manufacture, Vol 46, pp 1996–2008.

Kawakami, T., et al., 2005, Study on Factors Determining Limits of Minimum Machinable Size in Micro EDM. Annals of the CIRP, Vol 54/1, pp 167-170.

Kitagawa, T., et al., 1990, Plasma Hot Machining for New Engineering Materials. Wear, Vol – 139 , pages 251 – 267.

Koshy, P., et al., 1996, Mechanism of material removal in electrical discharge diamond grinding. International Journal of Machine Tools and Manufacture, Vol – 36/10, pages 1173 – 1185.

Kozak J., et al., 1994, Material removal in wire EDM of PCD blanks Journal of Engineering for Industry, Vol – 116, pp 363–369.

Kunieda, M. et al., 2005, Advancing EDM through Fundamental Insight into the Process, Annals of the CIRP, 54/2, pp 599–622.

Kunieda, M., et al., 2004, Improvement of Dry EDM Characteristics Using Piezoelectric Actuator, Annals of the CIRP, 53/1, pages 183 – 186.

Kuo, CL., et al., 2004, Fabrication of series-pattern micro-disk electrode and its application in machining micro-slit of less than 10 μm. International Journal of Machine Tools and Manufacture, Vol. 44, pages 545–553.

Kuo, C. L., et al., 2003, Fabrication of 3D Metal Microstructures Using a Hybrid Process of Micro-EDM and Laser Assembly, Int J Adv Manufacturing Technology, 21, pp. 796-800.

Kurafuji, H. and Masuzawa, T., 1968, Micro-EDM of cemented carbide alloys. Japan Society of Electrical-Machining Engineers, Vol. 2/3, pages 1–16.

Kurita, T., et al., 2001, Development of Hybrid Micro Machine Tool, Proceedings of Second International Symposium on Environmentally Conscious Design and Inverse Manufacturing, pages 797 – 802.

Kurita, T., et al., 2005, Development of new-concept desk top size machine tool. International Journal of Machine Tools and Manufacture, Vol – 45, pages 959 – 965.

Kurita, T., et al., 2006, A study of EDM and ECM/ECM-lapping complex machining technology. International Journal of Machine Tools and Manufacture, Vol – 46, pages 1804 – 1810.

Lang, W., 1999, Reflexions on the future of microsystems, Sensor and Actuators 72, 1–15.

Langen, HH., et al., 1995, Modular Method for Microparts Machining and Assembly with Self-Alignment. Annals of the CIRP, Vol – 44/1, pages 173 – 176.

Lee DG, et al., 2003, Micro-drilling of alumina green bodies with diamond grit abrasive micro-drills. International Journal of Machine Tools and Manufacture, Vol 43, page 551–558.

Lieberman, MA., Lichtenberg, AJ., 2005, Principles of Plasma Discharges and Materials Processing, Second Edition, John Wiley and Sons, ISBN 0-471-72001-1.

Lim, HS., et al., 2003, A Study on the machining of high-aspect-ratio micro-structures using micro EDM, Journal of Materials Processing Technology, 140, pp. 318-325.

Lim, HS., et al., 2002, Improvement of Form Accuracy in Hybrid Machining of Microstructures, Journal of Electronic Materials, Vol – 31/10, pages 1032 – 1038.

Liu. K, et al, 2006, Effect of plastic side flow on surface roughness in micro-turning process, Int J of Machine Tools and Manufacture, Vol 46, pp. 1778 – 1785.

Liu, X, et al., 2004, The mechanics of machining at the micro scale: assessment of the current state of the science. Journal of Manufacturing Science and Engineering, Vol 126, pp 666-678.

Liu, YH., et al., 1997, Electric discharge milling of polycrystalline diamond. Proceedings of Institution of Mechanical Engineers, Part B: Journal of Engineering Manufacture, Vol – 211(8), pp 643–647.

Lsqcurvefit, R2012a, Optimization toolbox 6.0, Matlab, MathWorks Inc, http://www.mathworks.com/help/toolbox/optim/ug/lsqcurvefit.html.

Madou, M.J., 1997, Fundamentals of Microfabrication, CRC Press, Boca Raton.

Maluf, N., 2002, An Introduction to Microelectromechanical Systems Engineering, Measurement Science and Technology, Vol-13/2.

Masahiro, M., Masaki, T., et al., 1995, Electric Discharge Machine and Method. European Patent Specification, Number – 95116174.4.

Masaki, T., Kuriyagawa, T., 2010(a), Study of precision micro-electro-discharge machining (1st report), International Journal of Electrical Machining, Vol 15.

Masaki, T., Kuriyagawa, T., 2010(b), Study of precision micro-electro-discharge machining (2nd report), International Journal of Electrical Machining, Vol 15.

Masaki, T., et al., 2007, Study on shaping spherical Poly Crystalline Diamond tool by Micro-electro-Discharge Machining and micro-grinding with the tool. International Journal of Surface Science and Engineering, Vol – 1/4, pages 344 – 359.

Masaki, T., et al., 2006, Repetitive Pattern Transfer Process of Micro EDM. International Journal of Electro Machining, Vol – 11, page 33 – 34.

Masaki, T et al., 1990(a), Electric Discharge Machining Method and Apparatus for Machining a Microshaft, United States Patent, Number – 4,900,890.

Masaki, T., et al., 1990(b), Micro electro-discharge machining and its applications. Micro Electro Mechanical Systems - IEEE, pp 21 – 26.

Masaki, T et al., 1989, Micro Electro-Discharge Machining. Proceedings of International Symposium for Electro-Machining 1989, pp 26-29.

Mahardika, M., et al., 2008, A new method for monitoring micro-electric discharge machining processes. International Journal of Machine Tools and Manufacture, Vol – 48, pages 446 – 458.

Masuzawa, T., et al., 2005, Surface Finishing of Micropins Produced by WEDG. Annals of the CIRP, Vol – 54/1, pages 171 – 174.

Masuzawa, T., 2000, State of the Art of Micromachining. Annals of the CIRP, 49/2, pp 473-488.

Masuzawa, T., et al., 1997, Three-Dimensional Micromachining by Machine Tools. Annals of the CIRP, Vol – 46/2, pp 621 – 628.

Masuzawa, T., et al., 1994, A combined electrical machining process for micronozzle fabrication, Annals of the CIRP, Vol. 43/1, pages 189–192.

Masuzawa, T et al., 1985, Wire Electro-Discharge Grinding for Micro-Machining. Annals of the CIRP, Vol 34/1, pp 431-434.

Meeusen, W., et al, 2003, Micro-Electro-Discharge Machining as Microsensor Fabrication Technology, IEEE Sensors Journal, Vol 3/5, pp 632-639.

Michel, F., et al., 2000, EDM for micro fabrication-technology and applications. Proceedings of International Seminar on Precision Engineering and Micro Technology (Aachen), pages 127–139.

Morgan, JC., et al., 2006, Micro-machining and micro-grinding with tools fabricated by micro electro-discharge machining. International Journal of Nanomanufacturing, Vol 1 / 2, pages 242 – 258.

Morgan, JC., et al., 2004, Micro machining glass with polycrystalline diamond tools shaped by micro electro discharge machining. Journal of Micromechanics and Microengineering, Vol 14, page 1687–1692.

Moylan, SP., 2006, High-Speed micro-electro-discharge machining, PhD Thesis, Purdue University - West Lafayette, UMI Number – 3232216.

Nagahanumaiaha et al., (2009), Characterization of plasma in micro-EDM discharge using optical spectroscopy, Journal of Manufacturing Processes, V–11, pp 82–87.

Ohmori, H., et al., 2003, Improvement of Mechanical Strength of Micro Tools by Controlling Surface Characteristics. Annals of the CIRP, 52/1, page 467 – 470.

Okuyama, H., et al, 1998, Micromachining with SR and FEL, Nuclear Instruments and Methods in Physical Research B, vol.144, pp.58-65.

Onikura, H., et al., 2000, Fabrication of Micro Carbide Tools by Ultrasonic Vibration Grinding. Annals of the ClRP Vol. 49/1, pp 257 – 260.

Perveen, A., et al., 2012a, Fabrication of different geometry cutting tools and their effect on the vertical micro-grinding of BK7 glass, International Journal of Advanced Manufacturing Technology, Vol 61, pp 101 – 115.

Perveen, A., et al., 2012b, A study on microgrinding of brittle and difficult-to-cut glasses using on-machine fabricated poly crystalline diamond (PCD) tool, Journal of Materials Processing Technology, Vol 212, pp 580 – 593.

Pham, DT., et al., 2004, Micro-EDM - recent developments and research issues. Journal of Materials Processing Technology, 149, pages 50-57.

Piel, Alexander, 2010, Plasma Physics: An Introduction to Laboratory, Space, and Fusion Plasmas, Springer-Verlag Berlin Heidelberg 2010, DOI 10.1007/978-3-642-10491-6.

Pramanik, A., et al., 2003, Cutting performance of diamond tools during ultra-precision turning of electroless-nickel plated die materials. Journal of Materials Processing Technology, Vol 140, page 308–313.

Picard, YN, et al., 2003, Focused Ion Beam-Shaped Microtools for Ultra-precision Machining of Cylindrical Components. Precision Engineering, Vol 27, page 59 – 69.

Rahman, A., et al, 2006, Development of Micropin Fabrication Process using Tool Based Micromachining, Int J of Adv. Manuf. Tech, Vol 27 (9 -10), pp. 939 – 944.

Rahman, A., et al., 2005, CNC microturning: an application to miniaturization. International Journal of Machine Tools and Manufacture, Vol – 45, pp 631 – 639.

Rahman, M., et al., 2007(a), Integrated Hybrid Micro/Nano-Machining, ASME Conference on Proceedings of the 2007 International Manufacturing Science and Engineering Conference (MSEC 2007 – 31009), Georgia, Utlanta, USA.

Rahman, M, et al., 2007(b), Tool-based nanofinishing and micromachining. Journal of Materials Processing Technology, Vol 185, Issue 1 -3 , pp 2 – 16.

Rahman, M., et al., 2003, Compound fabrication process and apparatus. United States Patent, Number – 10/377,140.

Raizer, YP., et al., 1991, Gas discharge physics, Springer-Verlag, Berlin.

Rajurkar KP., et al., 2006, Micro and nano machining by electro-physical and chemical processes. Ann CIRP 55(2):643–666.

Rajurkar, et al., 2000, 3D Micro-EDM Using CAD/CAM, Annals of the CIRP, 49/1, pp 127-130.

Ravi N. et al., 2002, The effects of electro-discharge machining block electrode method for microelectrode machining. Journal of Micromechanics and Microengineering, Vol – 12, pages 532 – 535.

Rizzoni, G., 2005, Principles and Applications of Electrical Engineering, 5th edition, McGraw-Hill, 978-0073220338.

Rosa, EB., 1908, The self and Mutual Inductance of Linear Conductors, Bulletin of the Bureau of Standards 4(2): pp 301–344.

Roth, RJ., 1995, Industrial Plasma Engineering – Volume 1: Principles, Institute of Physics Publishing, Reprint – 2000, ISBN 0-7503-0317-4.

Sato, T et al., 1985, Electro-Discharge Machine for Micro Hole Boring. National Technical Report (Japan), Vol 81/Oct, pp 105 – 113.

Sato, T., et al., 1989, Application of WEDG for Microdrilling and Microendmilling, Proceedings of Annual Spring Assembly of JSPE, page 1091-1092 (in Japanese).

Schaller, T., et al., 1999, Microstructure grooves with a width of less than 50m cut with ground hard metal micro end mills. Precision Engineering, vol – 23, page 229–235.

Schoth, A., et al, 2005, Micro wire EDM for high aspect ratio 3D microstructuring of ceramics and metals, Microsystem Technologies 11, pp 250-253.

Shimada, S., 2001, Molecular Dynamics Simulation of the Atomic Processes in Microcutting. Micromachining of Engineering Materials, CRC Press, page 63 – 83.

Shimada, S., et al., 1993, Feasibility Study on Ultimate Accuracy in Microcutting Using Molecular Dynamics Simulation. Annals of the CIRP, 42/1, page 91 – 94.

Son, S.M., et al., 2007, Influences of pulsed power condition on the machining properties in micro EDM. J. Mater. Process. Technol. 190, 73–76.

Takahata, K et al., 2002, Batch Mode Micro-Electro-Discharge Machining. Journal of Microelectromechanical Systems, Vol 11/2, Apr – 2002, pp 102-110.

Tansel, I., et al., 1998, Micro-end-milling – I. International Journal of Machine Tools and Manufacture, Vol 38, pp 1419-1436.

Vasile, MJ., et al., 1999, Microfabrication techniques using focused ion beams and emergent applications. Micron, Vol 30, page 235–244.

Vasile MJ., et al., 1996, Micrometer-scale machining: tool fabrication and initial results. Precision Engineering, vol 19(2–3), page 180–186.

Wada, T., et al., 2002, Development of micro grinding process using micro EDM trued diamond tools, Proceedings of Annual Meeting of the American Society for Precision Engineering (St Louis, MO, 2002/10), pp 16–19.

Watanabe, H., et al., 2008, Microdrilling for printed circuit boards (PCBs) - Influence of radial run-out of microdrills on hole quality. Precision Engineering 32, page 329–335.

Weck, M., et al., 1997, Fabrication of micro components using ultra precision machine tools, Nanotechnology 8 (1997) 145–148

Wong, YS., 2003, Investigation of micro-EDM material removal characteristics using single RC-pulse discharges. Journal of Materials Processing Technology, Vol – 140, pages 303 – 307.

Xuan F Zha, et al., 2006, Web-Enabled Database System Development for Design and Manufacturing of Micro-Electro-Mechanical Systems (MEMS), MEMS/NEMS Handbook Techniques and Applications, Springer US, Volume 1 – Design Methods, 73-109.

Yang, Z., et al., 2002, Principle of precision micro-drilling with axial vibration of low frequency. International Journal of Production Research, Vol – 40/6, page 1421 – 1427.

Yeo SH., et al., 2008, Critical assessment and numerical comparison of electro-thermal models in EDM. Journal of Materials Processing Technology, Vol – 203, pp 241–251.

Yu, Z. Y., et al., 1998, Micro-EDM for three-Dimensional cavities – Development of Uniform Wear Method, Annals of the CIRP, 47/1, 169-172.

Zaman, M. T., et al., 2006, A three-dimensional analytical cutting force model for micro end milling operation. International Journal of Machine Tools and Manufacture, Vol 46, pp 353 – 366.

Zhao, W., et al, 2004, A CAD/CAM system for micro-ED-milling of small 3D freeform cavity, Journal of Materials Processing Technology, 149, pp. 573-578.

List of Publications

Journal Paper:

1. ABMA Asad, T Masaki, M Rahman, Lim HS, YS Wong, 2007, Tool based Micro-machining. Journal of Materials Processing Technology, Vol 192 – 193, P 204-211.

2. M Rahman, Takeshi Masaki, ABMA Asad, YS Wong, Lim HS. Miniaturized Universal Machine Tool for Hybrid Micromachining Processes. International Journal of Electro Machining, Vol – 12, Feb - 2007.

3. M Rahman, ABMA Asad, Takeshi Masaki, YS Wong, HS Lim, 2007, Integrated Hybrid Micro/Nano-Machining, Proceedings of the ASME International Manufacturing Science and Engineering Conference, MSEC2007, pp 197 – 210.

4. MP Jahan, YS Wong, M Rahman, ABMA Asad, 2009, An Experimental Investigation on the Surface Characteristics of Tungsten Carbide for the Fine Finish Die-Sinking and Scanning Micro-EDM. International Journal of Abrasive Technology, Vol – 2 / 3, pages 233 – 244.

5. M Rahman, ABMA Asad, Takeshi Masaki, YS Wong, HS Lim, 2010, A Multi-process Machine Tool for Compound Micromachining. International Journal of Machine Tools and Manufacture, Vol 50/4, pages 344 – 356.

6. M Rahman, ABMA Asad, Takeshi Masaki, YS Wong, AS Kumar, 2010, Compound Micro/Nano Machining – A Tool-Based Invovative and Integrated Approach, Key Engineering Materials, Vol 447 – 448, pages 9 – 15.

7. ABMA Asad, T Masaki, YS Wong, M Rahman, Analysis of Micro-EDM Electrical Characteristics in RC Circuit Employing Plasma Properties (under review).

Book Chapter:

1. MP Jahan, ABMA Asad, T Masaki, M Rahman, YS Wong, 2011, Chapter 12 – Micro-EDM, Micro-Manufacturing: Design and Manufacturing of Micro-Products, Edited by M. Koc and T. Ozel , John Wiley and Sons.

Appendix A – Measuring Instruments

S/N	Instrument	Manufacturer	Model	Specifications
1	Digital Micrometer	Mitutoyo	293-761-30	Range: 0-25mm, Resolution: 0.001mm, Accuracy: +/- 0.001mm, Quantizing Error: 1 count
2	Dial Indicator	Mitutoyo	2109S-10	Resolution: 0.001mm , Range: 1mm , Accuracy: 3 micron, Measuring force: 1.5 Newton or less,
3	Digital Indicator	Mitutoyo	ID-F125 / 543-551-1	Range: 0-25mm, Resolution: 0.001mm/0.01mm, Accuracy: +/-0.003mm, Quantizing Error: 1 count,
4	Data Collection and Processor	Mitutoyo	(DP-1VR)	Can be used with any Mitutoyo digital instrument for printing data
5	Engineering Square	Helios	EIM0076/MT81	
6	Granite Straight Block/Parallel Blocks	TRU-Stone Technologies		Grade: laboratory grade AA (.000025" per 6"), 305mm X 50mm X 25mm
7	Stainless Steel Straight Block	Tsugami Corporation, Japan	PTW / 02044	Length: 200 mm, Grade: 0,
8	Granite Angle Block	TRU-Stone Technologies		Grade: laboratory grade AA (.000025" per 6"), 230mm X 150 mm X 75 mm
9	Slip Gauges			
10	KGM Grid Encoder	Heidenhain	KGM-182	Range: φ 230mm, Accuracy Grade: ±2µm
11	LASER Interferometer	Hewlett Packard	5519B Laser Head	He-Ne Laser, Beam Dia: 6 mm, Wavelength Accuracy: ±0.1 ppm,
12	SEM	Jeol Ltd	JSM-5500	Maximum Magnification 50,000X
13	Digital Optical Microscope	Keyence	VH-Z450	Maximum Magnification 3,000X

Appendix B – Performance Evaluation Details

B.1 Straightness of X Axis:

Travel Length: 200mm

Measuring Instrument: Dial Indicator and Granite Straight Block

Measurement Setup: Figure B.1 (a)

Measurement Results: X dz: 2 μm; X dy : 1 μm

B.2 Straightness of Y Axis:

Travel Length: 100mm

Measuring Instrument: Dial Indicator and Granite Straight Block

Measurement Setup: Figure B.1 (b)

Measurement Results: Y dx: 1 μm; Y dz : 2 μm

B.3 Straightness of Z Axis:

Travel Length: 100mm

Measuring Instrument: Dial Indicator and Granite Straight Block

Measurement Setup: Figure B.1 (c)

Measurement Results: Z dx: 1 μm; Z dy : 2 μm

B.4 Squareness of X-Y axis:

Travel Length: 200mm

Measuring Instrument: Dial Indicator and Granite Angle Block

Measurement Setup: Figure B.1 (d)

Measurement Results: 1 μm

B.5 Squareness of Y-Z axis:

Travel Length: 100mm

Measuring Instrument: Dial Indicator and Granite Angle Block

Measurement Setup: Figure B.1 (e)

Measurement Results: 4 μm

B.6 Squareness of X-Z axis:

Travel Length: 100mm

Measuring Instrument: Dial Indicator and Granite Angle Block

Measurement Setup: Figure B.1 (f)

Measurement Results: 3 μm

B.7 Radial runout in Spindle taper:

Measuring Instrument: Dial Indicator

Measurement Setup: Figure B.2 (a)

Measurement Results: 2 μm

B.8 Spindle axis straightness in X direction

Measured Length: 30mm

Measuring Instrument: Dial Indicator

Measurement Setup: Figure B.2 (b)

Measurement Results: 4 μm

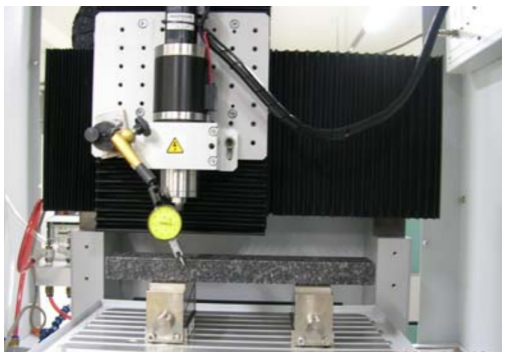

(a) Straightness of X-axis

(b) Straightness of Y-axis

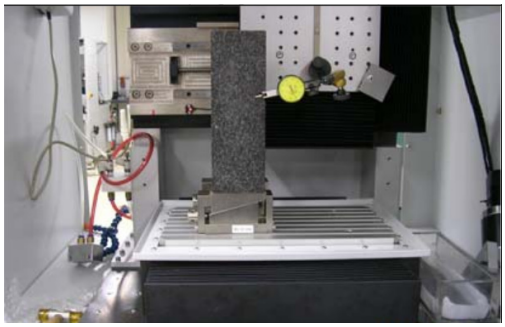

(c) Straightness of Z-axis

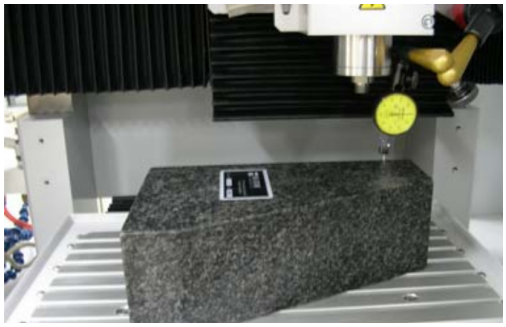

(d) Squareness of X-Y axis

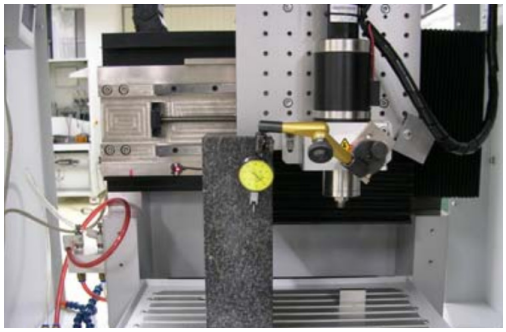

(e) Squareness of Y-Z axis

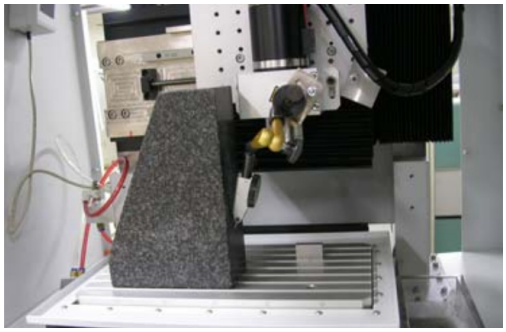

(f) Squareness of Z-X axis

Figure B. 1 Showing the setup used for measure straightness and squareness of the UMMT

B.9 Spindle axis straightness in Y direction

Measured Length: 30mm

Measuring Instrument: Dial Indicator

Measurement Setup: Figure B.2 (c)

Measurement Results: 4 μm

(a) Radial runout in spindle taper

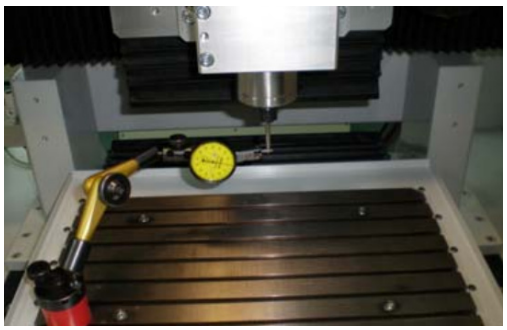

(b) Spindle axis straightness in X direction

(c) Spindle axis straightness in Y direction

Figure B. 2 Showing the setup used for measuring spindle runout and spindle axis straightness of the UMMT

B.10 Accuracy and Repeatability of X axis

Measured length: 200 mm

No of target position: 21

No of total data run: 6

Travel mode: Bidirectional

Ave air temp: 23.72˚C

Ave air pressure: 758.81 mm Hg

Measurement equipment: Laser Interferometer

Compensation table used: Table B.1

Measurement setup and results: Figure B.3

B.11 Accuracy and Repeatability of Y axis

Measured length: 100 mm

No of target position: 11

No of total data run: 6

Travel mode: Bidirectional

Ave air temp: 24.01˚C

Ave air pressure: 759.37 mm Hg

Measurement equipment: Laser Interferometer

Compensation table used: Table B.2

Measurement setup and results: Figure B.4

B.12 Accuracy and Repeatability of Y axis

Measured length: 100 mm

No of target position: 11

No of total data run: 6

Travel mode: Bidirectional

Ave air temp: 23.44˚C

Ave air pressure: 757.57 mm Hg

Measurement equipment: Laser Interferometer

Compensation table used: Table B.3

Measurement setup and results: Figure B.5

Table B. 1 Compensation table for X-axis

Position (mm)	0	10	20	30	40	50	60	70	80	90	100
Compensation (μm)	0	1.599	1.105	0. 519	1.855	4.564	5.466	6.155	7.217	8.845	11.086
Position (mm)	110	120	130	140	150	160	170	180	190	200	
Compensation Value (μm)	13.931	15.272	16.871	18.603	20.155	22.595	25.912	27.648	27.962	27.143	

Table B. 2 Compensation table for Y-axis

Position (mm)	0	10	20	30	40	50	60	70	80	90	100
Compensation Value (μm)	0	-0.599	-0.132	2.757	5.669	6.304	6.095	5.932	6.815	8.668	10.506

Table B. 3 Compensation table for Z-axis

Position (mm)	0	10	20	30	40	50	60	70	80	90	100
Compensation Value (μm)	0	0.539	1.619	1.690	1.963	3.032	5.282	6.630	7.535	8.196	9.012

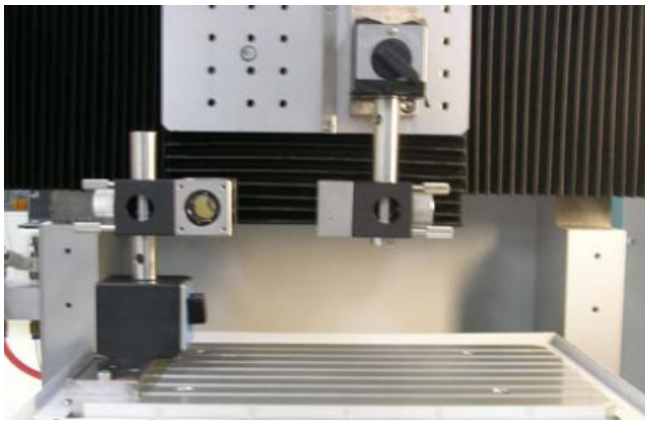

(a) X axis accuracy and repeatability measurement setup

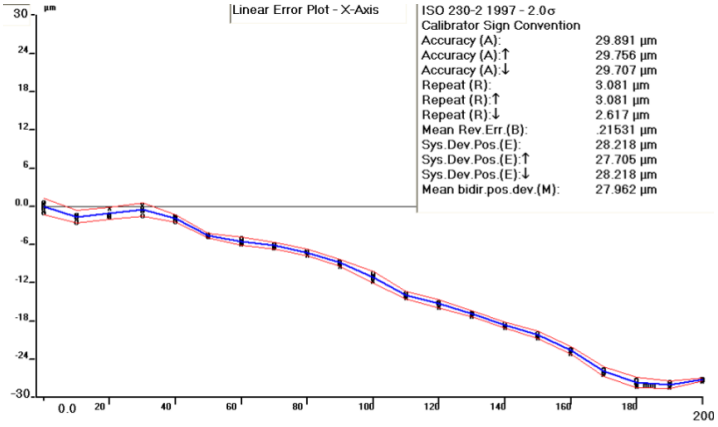

(b) X axis accuracy and repeatability measurement result (without compensation)

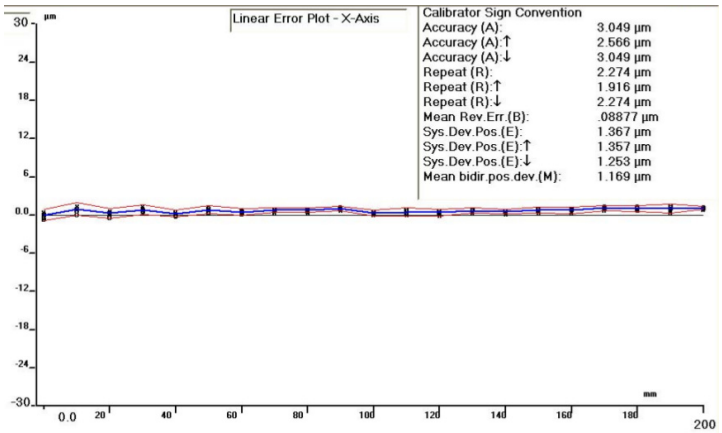

(c) X axis accuracy and repeatability measurement result (with compensation)

Figure B. 3 X-axis accuracy and reputability measurement

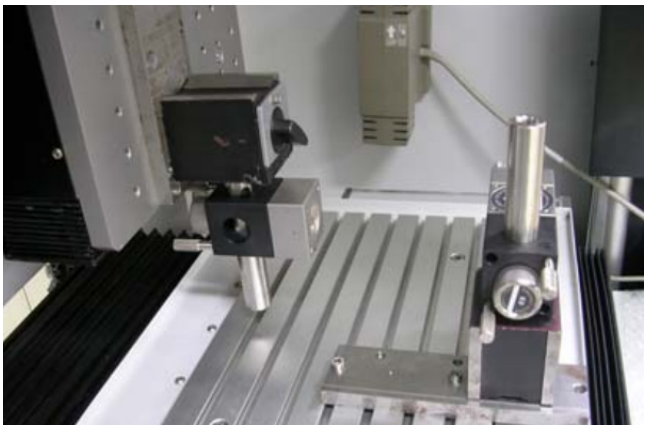

(a) Y axis accuracy and repeatability measurement setup

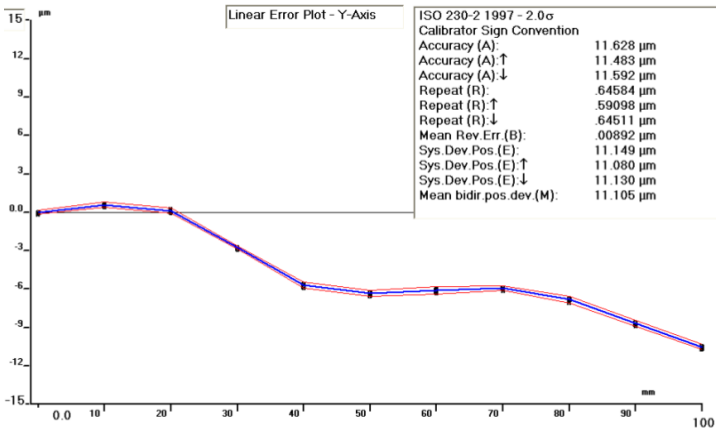

(b) Y axis accuracy and repeatability measurement result (without compensation)

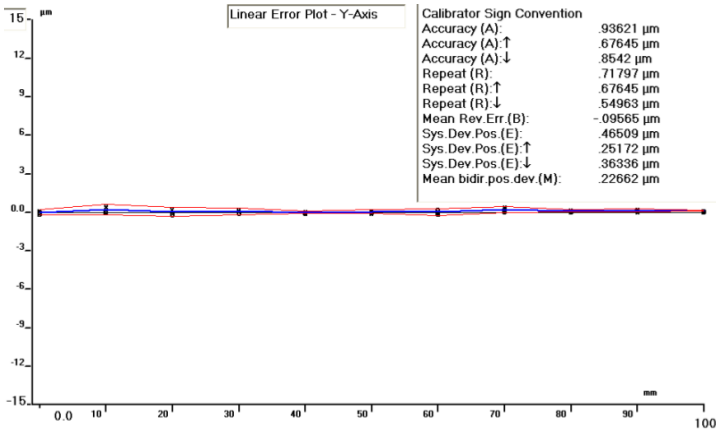

(c) Y axis accuracy and repeatability measurement result (with compensation)

Figure B. 4 Y-axis accuracy and reputability measurement

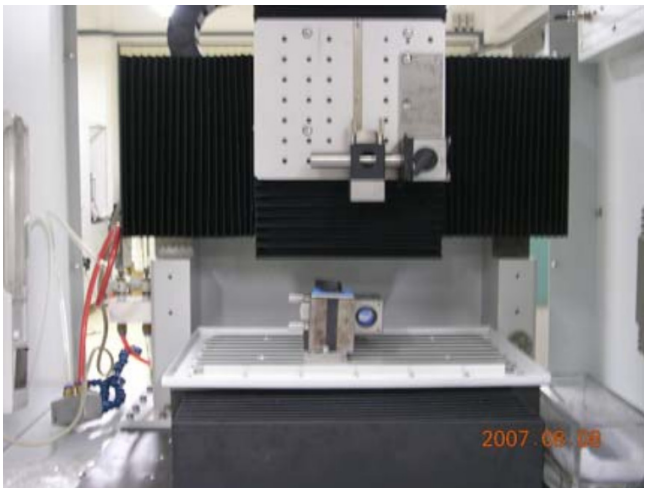

(a) Z axis accuracy and repeatability measurement setup

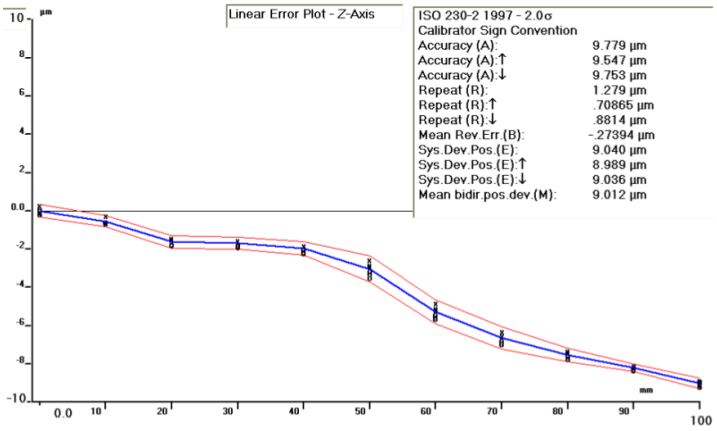

(b) Z axis accuracy and repeatability measurement result (without compensation)

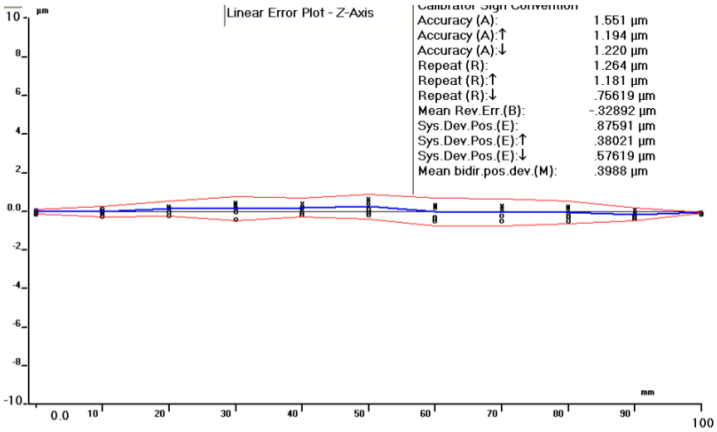

(c) Z axis accuracy and repeatability measurement result (with compensation)

Figure B. 5 Z-axis accuracy and reputability measurement